People's Democratic Republic of Algeria

Ministry of Higher Education and Scientific Research

University Mohamed El Bachir El Ibrahimi of Bordj Bou Arreridj

Faculty of Sciences and Technology

Department of Electronics

Doctoral Thesis

Submitted in fulfillment of the

requirements for the degree of

Doctor in Telecommunications

Presented by

Rachid CHELGHOUM

Theme

Elaboration and Experimental Characterization of New Low-loss Dielectric Composite Materials for Application in Dielectric Resonator Antennas

Thesis defended on 26/11/2025, in front of the jury composed of:

Mrs. Zoubeida MESSALI	Pr.	NPS of Constantine	President
Mr. Farid BOUTTOUT	Pr.	University of Bordj Bou Arreridj	Supervisor
Mr. Khaled ROUABAH	Pr.	University of M'Sila	Examiner
Mr. Salah MOKHNACHE	MCA	Setif 1 University	Examiner
Mr. Abderrahim YOUSFI	MCA	University of Bordj Bou Arreridj	Examiner
Mr. Abdelhalim BRAHIMI	MCB	University of Bordj Bou Arreridj	Invited

2025-2026

Acknowledgements

In the name of ALLAH (God), most gracious, most merciful, who guided me on my path to success and gave me the will, the health, the courage, and above all, the patience during these long years of study to accomplish and complete this work and to overcome all difficulties.

This work was carried out at the Laboratory of Electronics and Advanced Telecommunications, University Mohamed El Bachir El Ibrahimi of Bordj Bou Arreridj, in collaboration with the Laboratory of Scientific Instrumentation, Setif 1 University-Ferhat ABBAS, and the Laboratory of Electromagnetic Characterization, University of Zaragoza, Spain.

I would like to express my deep gratitude, appreciation, and sincere thanks to my previous supervisor, Mr. ***Zitouni MESSAI****, Professor at the University Mohamed El Bachir El Ibrahimi of Bordj Bou Arreridj, for proposing and supervising this thesis, and for his availability, support, and guidance during these years.*

As fate would have it, he left us forever at the end of this work. Gone from our sight, but never from our hearts. We pray to Allah (God) to grant him a spacious place in paradise.

I wish to express my sincere gratitude and thanks to Mr. ***Abdelhalim BRAHIMI,*** *Doctor at the University Mohamed El Bachir El Ibrahimi of Bordj Bou Arreridj, for his great help and for all his efforts to make this work a success and for his good advice at all times. I have benefited from his scientific experience, especially in the first part of the characterization of dielectric materials. I thank him for kindly agreeing to be an invited member of the jury of this thesis.*

I would also like to thank Mr. ***Nacerdine BOUROUBA****, Professor at Setif 1 University-Ferhat ABBAS, for his valuable help and advice.*

I would also like to thank Mr. ***JUAN PABLO Martínez Jimenez****, Professor and Director of the Laboratory of Electromagnetic Characterization at the Department of Applied Physics, University of Zaragoza, Spain, for his precious help and advice.*

I would like to express my deep and sincere gratitude to Mr. ***Farid BOUTTOUT****, Professor at the University Mohamed El Bachir El Ibrahimi of Bordj Bou Arreridj, for his warm encouragement, valuable help and advice, and especially for the valuable remarks, he provided to help me finalize my article.*

I also thank him for kindly agreeing to take on the role of my supervisor after

Acknowledgements

the previous supervisor passed away.

I would also like to extend my sincere thanks to Mr. ***Idris MESSAOUDENE*** *and Mr.* ***Massinissa BELAZZOUG****, Associate Professors at the University Mohamed El Bachir El Ibrahimi of Bordj Bou Arreridj, for their help, encouragement, and valuable advice, particularly in the field of dielectric resonator antennas.*

I would like to express my gratitude to the members of the jury who devoted their valuable time and expertise to evaluate this doctoral thesis, each by name:

Mrs. ***Zoubeida MESSALI,*** *Professor at the University Mohamed El Bachir El Ibrahimi of Bordj Bou Arreridj, for the honor she bestowed upon me by agreeing to chair the defense jury of this thesis.*

Mr. ***Khaled ROUABAH,*** *Professor at the University of M'Sila, for the honor he bestowed upon me by agreeing to examine this thesis.*

Mr. ***Salah MOKHNACHE,*** *Associate Professor at Setif 1 University-Ferhat ABBAS, for the honor he bestowed upon me by agreeing to examine this thesis.*

Mr. ***Abderrahim YOUSFI,*** *Associate Professor at the University Mohamed El Bachir El Ibrahimi of Bordj Bou Arreridj, for the honor he bestowed upon me by agreeing to examine this thesis.*

This work would never have been possible without the help of the many people who have supported me over the years, and so this thesis is a tribute to them. It is also a tribute to my family, whose unwavering support has sustained me all these years.

I would also like to thank all the members of the Laboratory of Fundamental and Numerical Mathematics at Setif 1 University-Ferhat ABBAS, where I work, for the good times we have spent together.

Finally, a very special thank you to all those who have encouraged me through thick and thin, as well as to everyone who has contributed directly or indirectly to my development at all levels.

Rachid CHELGHOUM

Dedication

Dedicated to:

My dear parents

My supportive wife

My daughters, Maria, Assil, and Sara

My brothers and sisters

My family

My friends and colleagues

«The memory of my supervisor, Prof. Zitouni MESSAI»

Abstract

Dielectric resonator antennas (DRAs) offer promising solutions for many advanced wireless communication systems due to their attractive features, including compact size, multiple feeding mechanisms, low loss, low cost, wide bandwidth, and high radiation efficiency.

This thesis presents the design and investigation of several dielectric resonator antennas fabricated from binary composite materials consisting of epoxy resin (RE) and barium titanate ($BaTiO_3$).

The first part is devoted to the characterization of the dielectric behavior of the binary composite. We studied the influence of barium titanate on the dielectric behavior of the binary composite with different volume fractions of epoxy resin (from 50% to 100% in steps of 5%), which were prepared at room temperature and under atmospheric pressure. The dielectric properties of composites were assessed using the time domain spectroscopy (TDS) technique to extract the dielectric properties of all samples. The experimentally obtained properties are suitable for meeting the practical requirements of manufacturing high-performance dielectric resonator antennas.

The second part focuses on the design and study of dielectric resonator antennas using the dielectric properties of materials obtained experimentally. These antennas are designed, simulated, and optimized using the electromagnetic software Ansys HFSS. In total, four types of antennas are investigated.

The first type of antennas is based on the effect of the dielectric properties on the performance parameters of cylindrical dielectric resonator antennas, using all the composite material samples. Three sets of antennas are obtained and classified according to the number of frequency bands: single-band, dual-band, and triple-band.

For the second type of antennas, we studied the influence of compound structures on the performance parameters of dielectric resonator antennas. The structure consists of a combination of four dielectric resonator shapes: three identical rectangular joined with one cylindrical, all having the same height. A single sample containing 60% of RE and 40% of $BaTiO_3$ was used. The proposed antenna gives a dual-band frequency, with one of the bands being wide.

For the third type of antennas, we investigated the effect of multiple structures using two composite material samples on the performance parameters of the dielectric resonator antennas. The structure consists of four identical adjacent rectangular resonators, made from two samples: one with 60% RE and 40% of $BaTiO_3$, and another with 50% of RE and 50% of $BaTiO_3$. The suggested antenna provides three frequency bands.

In the fourth type of antennas, we studied the effect of combining multiple dielectric resonator shapes (a hybrid structure), coupled through an aperture formed by two large rectangular slots and their offset positions. A composite material sample consisting of 60% of RE and 40% of $BaTiO_3$ was used. The antenna offers an ultra-wideband with a relative bandwidth of 97% and two circularly polarized bands.

The resulting antennas are suitable for use in frequency bands corresponding to centimeter wavelengths.

Key words: Dielectric Material, Binary Composite, Time Domain Spectroscopy, Dielectric Resonator Antenna, Aperture Coupling, Multiband, Wideband, Circular Polarization.

ملخص

توفر هوائيات الرنان العازل (DRAs) حلولاً واعدة للعديد من أنظمة الاتصالات اللاسلكية المتقدمة بفضل ميزاتها الجذابة، بما في ذلك حجمها الصغير، وآليات التغذية المتعددة، والخسارة المنخفضة، وتكلفتها المنخفضة ونطاق ترددي واسع وكفاءتها الإشعاعية العالية.

تُقدم هذه الأطروحة تصميم ودراسة لعدة هوائيات الرنان العازل مصنوعة من مواد مركبة ثنائية تتكون من راتنج الإيبوكسي (RE) وتيتانات الباريوم $(BaTiO_3)$.

الجزء الأول مخصص لتوصيف سلوك العازل للمركب الثنائي، حيث درسنا تأثير تيتانات الباريوم على سلوك العازل للمركب الثنائي مع نسب حجمية مختلفة من راتنج الإيبوكسي (من 50% إلى 100% بزيادات مقدارها 5%)، والتي تم تحضيرها في درجة حرارة الغرفة وتحت الضغط الجوي، تم تقييم خصائص العازل للمركبات باستخدام تقنية التحليل الطيفي في المجال الزمني (TDS) لاستخلاص خصائص جميع العينات، تعتبر الخصائص التي تم الحصول عليها تجريبياً مناسبة لتلبية المتطلبات العملية لتصنيع هوائيات الرنان العازل عالية الأداء.

يركز الجزء الثاني على تصميم ودراسة هوائيات الرنان العازل باستخدام الخواص العازلة للمواد التي تم الحصول عليها تجريبيا، تم تصميم هذه الهوائيات ومحاكاتها وتحسينها باستخدام البرنامج الكهرومغناطيسي (Ansys HFSS)، حيث تمت دراسة أربعة أنواع من الهوائيات في المجموع.

يعتمد النوع الأول من الهوائيات على تأثير الخواص العازلة على خصائص أداء هوائيات الرنان العازل الأسطوانية، باستخدام جميع عينات المواد المركبة، اين تم الحصول على ثلاث مجموعات من الهوائيات، وتصنيفها وفقًا لعدد نطاقات التردد: أحادي النطاق، وثنائي النطاق، وثلاثي النطاق.

بالنسبة للنوع الثاني من الهوائيات، درسنا تأثير الهياكل المركبة على خصائص أداء هوائيات الرنان العازل، حيث يتكون الهيكل من مزيج من أربعة أشكال الرنان العازل ، ثلاثة أشكال مستطيلة متطابقة متصلة مع أسطوانة جميعها لها نفس الارتفاع، تم استخدام عينة واحدة تحتوي على 60% من راتنجات الإيبوكسي و40% من تيتانات الباريوم. يوفر الهوائي المقترح ترددًا ثنائي النطاق، حيث ان أحد النطاقين عريض.

بالنسبة للنوع الثالث من الهوائيات، درسنا تأثير الهيكل المتعدد باستخدام عينتين من المواد المركبة على خصائص أداء هوائيات الرنان العازل، ويتكون الهيكل من أربعة مستطيلات من الرنان العازل متجاورة متطابقة، مصنوعة من عينتين: واحدة تحتوي على 60% من راتنجات الإيبوكسي (RE) و40% من تيتانات الباريوم، والعينة الأخرى تحتوي على 50% من راتنجات الإيبوكسي و50% من تيتانات الباريوم، يوفر الهوائي المقترح ثلاثة نطاقات تردد.

في النوع الرابع من الهوائيات، درسنا تأثير الجمع بين عدة أشكال من الرنان العازل (هيكل هجين) ومقترن بفتحة مكونة من فتحتان مستطيلتان كبيرتان وموضع إزاحتهما، تم استخدام عينة واحدة من المواد المركبة تتكون من 60% من راتنجات الإيبوكسي و40% من تيتانات الباريوم. يوفر الهوائي نطاقًا عريضًا جدًا، مع عرض نطاق نسبي يبلغ 97%، وهو هوائي مستقطب دائريًا ذات نطاقين.

الهوائيات المتحصل عليها مناسبة للاستخدام في نطاقات التردد التي توافق الطول الموجي السنتيمتري.

كلمات مفتاحية: العازل، مركب ثنائي، التحليل الطيفي للمجال الزمني، هوائي الرنان العازل، اقتران بفتحة، متعدد النطاقات، نطاق عريض، إستقطاب دائريً.

Résumé

Les antennes à résonateur diélectrique (DRAs) offrent des solutions prometteuses pour nombreux systèmes de communication sans fil avancés en raison de leurs caractéristiques attrayantes, notamment leur taille compacte, leurs mécanismes d'alimentation multiples, leurs faibles pertes, leur faible coût, leur large bande passante et leur efficacité de rayonnement élevée.

Cette thèse présente la conception et l'étude de plusieurs antennes à résonateur diélectrique fabriquées à partir de matériaux composites binaires constitués de résine époxy (RE) et de titanate de baryum ($BaTiO_3$).

La première partie est consacrée à la caractérisation du comportement diélectrique du composite binaire. Nous avons étudié l'influence du titanate de baryum sur le comportement diélectrique du composite binaire avec différentes fractions volumiques de résine époxy (de 50% à 100% par étapes de 5%), qui ont été préparées à la température ambiante et sous pression atmosphérique. Les propriétés diélectriques des composites ont été évaluées en utilisant la technique de spectroscopie dans le domaine temporel (TDS) pour extraire les propriétés diélectriques de tous les échantillons. Les propriétés que nous avons obtenues expérimentalement sont adaptées pour répondre aux exigences pratiques de fabrication des antennes à résonateur diélectrique à haute performance.

La deuxième partie se concentre sur la conception et l'étude des antennes à résonateurs diélectriques en utilisant les propriétés diélectriques des matériaux obtenus expérimentalement. Ces antennes sont conçues, simulées et optimisées à l'aide du logiciel électromagnétique Ansys HFSS, au total, quatre types d'antennes sont étudiés : Le premier type d'antennes est basé sur l'effet des propriétés diélectriques sur les paramètres de performance des antennes à résonateur diélectrique cylindrique, en utilisant tous les échantillons de matériaux composites, trois ensembles des antennes sont obtenus et classées selon le nombre de bandes de fréquences : simple bande, double bande et triple bande.

Pour le deuxième type d'antennes, nous avons étudié l'influence des structures composées sur les paramètres de performance des antennes à résonateur diélectrique. La structure est une combinaison de quatre formes de résonateurs diélectriques : trois rectangulaires identiques joints à un cylindre, tous ayant la même hauteur, un seul échantillon contenant 60% de RE et 40% de $BaTiO_3$ a été utilisé, l'antenne proposée donne une fréquence double bande, avec une des bandes étant large.

Pour le troisième type d'antennes, nous avons étudié l'effet de la structure multiple en utilisant deux échantillons de matériaux composites sur les paramètres de performance des antennes à résonateur diélectrique. La structure est composée de quatre rectangles adjacents identiques, fabriqués à partir de deux échantillons: un avec 60% de RE et 40% de $BaTiO_3$ et un autre avec 50% de RE et 50% de $BaTiO_3$, l'antenne proposée fournit trois bandes de fréquences.

Dans le quatrième type d'antennes, nous avons étudié l'effet de la combinaison de plusieurs formes de resonateurs diélectriques (une structure hybride), couplées par une ouvertures formée par deux

Résumé

grandes fentes rectangulaires et leur position décalées, un échantillon de matériau composite composé de 60% de RE et 40% de $BaTiO_3$ a été utilisé, l'antenne offre une bande ultra-large avec une largeur de bande relative de 97% et deux bandes à polarisation circulaire.

Les antennes résultantes sont adaptées pour une utilisation dans des bandes de fréquences correspondant à des longueurs d'onde centimétriques.

Mots clés : Matériau Diélectrique, Composite Binaire, Spectroscopie en Domaine Temporel, Antenne à Résonateur Diélectrique, Couplage par Ouverture, Multi bande, Large Bande, Polarisation Circulaire.

Table of Contents

List of Figures

Chapter 1: Theoretical concepts of dielectric materials

Chapter 2: Manufacturing method and experimental characterization results

Chapter 3: Basic principles of dielectric resonator antennas

Chapter 4: Study and design of dielectric resonator antennas

List of Tables

Chapter 2: Manufacturing method and experimental characterization results

Chapter 4: Study and design of dielectric resonator antennas

List of Abbreviations

2D	Two Dimension
3D	Three Dimension
ADAS	Advanced Driver Assistance System
ADS	Advanced Design System
AR	Axial Ratio
$BaTiO_3$ (BT)	Barium Titanate
BW	Bandwidth
CDRA	Cylindrical Dielectric Resonator Antenna
CST	Computer Simulation Technology
DR	Dielectric Resonator
DRA	Dielectric Resonator Antenna
FBW	Fractional bandwidth
FCC	Federal Communications Commission
FDTD	Finite Difference Time Domain
FEM	Finite Element Method
FIT	Finite Integration Technique
FSS	Fixed Satellite Service
GPS	Global Positioning System
HEM	Hybrid Electromagnetic
HFSS	High Frequency Structure Simulator
HSDRA	Hybrid Shaped Dielectric Resonator Antenna
IEEE	Institute of Electrical and Electronics Engineers
IoT	Internet of Think
LHCP	Left-Hand Circular Polarization
MLC	Multi Layer Capacitor
PCB	Printed Circuit Board
PTC	Positive Temperature Coefficient
PRS	Partially Reflecting Surface
RCA	Resonant Cavity Antenna

RDRA	Rectangular Dielectric Resonator Antenna
RE	Epoxy Resin
RFID	Radio Frequency Identification
RHCP	Right-Hand Circular Polarization
SLL	Side Lobe Level
SNR	Signal to Noise Ratio
SUT	Sample Under Test
TDS	Time Domain Spectroscopy
TDR	Time Domain Reflectometry
TE	Transverse Electric
TM	Transverse Magnetic
USA	United States of America
USSR	Union of Soviet Socialist Republics
UWB	Ultra Wide Band
VSWR	Voltage Standing Wave Ratio
WLAN	Wireless Local Area Network

Introduction

Introduction

Wireless communications technology has evolved rapidly over the past century, leading to an increasing demand for high-performance antennas capable of meeting the requirements of emerging applications. Modern antennas must support wider frequency bands, higher data rates, improved efficiency, and compact designs to keep pace with the rapid growth of wireless services such as fifth-generation (5G) networks, the Internet of Things (IoT), and future communication systems. In this context, dielectric resonator antennas (DRAs) have emerged as strong candidates owing to their superior performance characteristics and design flexibility. In parallel, materials science has also progressed significantly, with the global research community playing a pivotal role in advancing novel manufacturing techniques and developing innovative materials that directly contribute to the realization of high-performance DRAs. Microwave dielectric materials have a significant impact across various domains, particularly in microelectronic components used in telecommunications systems, such as ultrasonic transducers, cavities, filters, substrates, wave absorbers, antennas, sensors, and resonators [1-4]. They are widely used as insulators in power transmission and distribution networks, especially as cable sheathing and electrical insulation [5]. An ideal dielectric material is perfectly non-conductive, as it contains no free charges within its structure. In practice, however, real dielectric materials contain a certain amount of free charge due to the presence of impurities, which cause slight conduction, especially at low frequencies. These materials can store electrical energy, a property quantified by their relative permittivity, also known as the dielectric constant. The movement of charges caused by polarization when the dielectric material is subjected to an external electric field results in dielectric loss [6].

The growing demands of society require miniaturization, operational stability, and enhanced performance of electronic devices. In this context, composite materials play a key role in the development of future materials for industrial applications. These composites are formed by combining two or more constituents to achieve improved or desirable properties that the individual materials do not possess. [7].

In the first part of this thesis, we examine the dielectric behavior of binary composites composed of epoxy resin (RE) and barium titanate ($BaTiO_3$). Each sample contains X% (volume fraction) of epoxy resin, while the barium titanate loading ratios represent Y% (Y=100-X) of the composite, and their components vary complementarily in increments of 5% up to X=50%. The dielectric properties of samples are extracted using the time-domain spectroscopy (TDS) technique.

Barium titanate ($BaTiO_3$or BT) has a long and distinguished history since its first appearance in the 1940s. It has been the subject of extensive research and remains of great interest to many

researchers, as it was the first ferroelectric ceramic and is a good candidate for a wide range of applications. Barium titanate is widely used due to its remarkable dielectric properties, which make it a valuable material for piezoelectric applications. It belongs to the perovskite family, characterized by the general formula ABO_3. Barium titanate can be tailored to meet the diverse requirements of various electronic components [8].

Time domain spectroscopy (TDS) is a well-established method for detecting and modeling discontinuities in transmission lines. This technique is based on observing the reflections caused by discontinuities that occur from a launched pulse. These reflections provide information about the characteristics and positions of the discontinuities. Beginning with the Fellner-Feldegg publication, TDS has emerged as a crucial instrument for studying the dielectric properties of various materials. The utilization of time domain spectroscopy can be observed in various fields, including industry, medicine, and agriculture. Initially, it was utilized to identify discontinuities in cables, but today, the same technique enables the measurement of groundwater pressure [9, 10].

Traditionally, dielectric materials have been used as passive microwave components in the design of filters and oscillators since the 1960s [11, 12]. Later, McAllister et al. were the first to propose their use as radiating elements. In 1983, they introduced the first dielectric resonator antenna (DRA) [13]. Since then, numerous researchers have focused on the study of DRAs.

The second part deals with dielectric resonant antennas, which offer several attractive features such as compact size, multiple feeding mechanisms, low loss, low cost, and high radiation efficiency [14, 15]. Furthermore, DRAs are made entirely of dielectric materials, allowing them to maintain very low losses even in the millimeter-wave frequency spectrum. All of these characteristics make DRA highly suitable for use in mm-wave applications [16, 17]. The resonant frequency of a DRA depends mainly on its size, shape, and the dielectric material properties.

Modern devices rely on wireless communication, including mobile phones, WLAN, Wi-Fi, radar, satellites, Bluetooth, sensors, sonar, airplanes, automobiles, walkie-talkies, and wireless computer networks. Most of these technologies use antennas to transmit or receive data, and their widespread use has become an essential part of modern life [18]. The need to transmit large amounts of data in a short time has driven the development of advanced wireless communication technologies. Wideband antennas and multiband antennas with specific polarizations are key components of these systems. Ultra-wideband (UWB) technology offers several benefits, including high data rates, low power consumption, and high-accuracy systems [19]. Moreover, the bandwidth of the dielectric resonator antenna is inversely related to its dielectric constant [20].

Introduction

Multiband antennas are of growing interest, especially to reduce the number of antennas by combining multiple applications on the same antenna. Circular polarization provides an additional advantage, as it enhances the robustness of transmitted signals, helping to mitigate noise and multipath fading [21, 22].

Multiple modes can be excited within a single element of dielectric resonator antenna. The excitation of these modes contributes to bandwidth enhancement and enables the DRA to support operation across multiple frequency bands, thereby making it a strong candidate for multifunctional applications.

This thesis presents the design and investigation of several dielectric resonator antennas using the properties of composite dielectric materials obtained experimentally. We use the electromagnetic simulation software Ansys HFSS to design, simulate, and optimize the antenna structures.

The work presented in this thesis comprises the following four chapters:

The first chapter describes the theoretical basis for understanding the mechanisms and processes that determine the properties of dielectric materials and their main aspects. It provides a detailed description of the interaction between the electric field and the dielectric material, leading to polarization phenomena and local field theory derived from Maxwell's equations. In addition, we discuss the specific dielectric properties of materials and the factors that influence them.

The second chapter provides an overview of composite materials, the different materials used, and the techniques and procedures for preparing samples of binary mixtures based on epoxy resin (RE) and barium titanate ($BaTiO_3$). Moreover, it discusses the techniques employed for experimental measurements and the methodology for extracting dielectric properties in order to obtain numerical results.

The third chapter focuses on the theoretical study of dielectric resonator antennas. It begins with a brief introduction, followed by a review of fundamental antenna parameters, a description of the advantages of dielectric resonator antennas, an overview of the shapes used in DRA design, and the different feeding mechanisms. The study emphasizes two shapes: rectangular and cylindrical, with an analysis of their main resonant modes and resonance frequencies. Finally, some techniques used to improve bandwidth, gain, and methods for achieving multiband operation are presented.

The fourth chapter is devoted to the design and study of four types of dielectric resonator antennas, classified according to their structures. The first type concerns cylindrical dielectric resonator antennas. The dielectric properties of each sample of binary composite (RE- $BaTiO_3$) are successively applied to a cylindrical dielectric resonator until the final sample.

Introduction

Numerical results are presented in terms of the reflection coefficient, radiation pattern, gain, and the three fundamental modes of the cylindrical dielectric resonator antenna.

The second type is a composite structure consisting of four dielectric resonator shapes: three rectangular and one cylindrical, all with the same height, using a single sample of the binary mixture. The proposed antenna parameters are presented in terms of the reflection coefficient, radiation pattern, and gain.

The third type of antenna structure consists of four identical adjacent rectangular shapes, using two samples of the binary mixture. The proposed antenna parameters are presented in terms of the reflection coefficient, radiation pattern, gain, and electric field distributions.

The fourth type consists of two identical, adjacent structures, each composed of a cylindrical resonator and a rectangular resonator of equal height. The results are presented in terms of the reflection coefficient, radiation pattern, gain, and axial ratio.

Finally, this work finalizes with a conclusion that highlights the main contributions, summarizes the results obtained, and discusses their importance.

References

[1] Mailadil. T. Sebastian, *"Dielectric Materials for Wireless Communication"*, Elsevier, Amsterdam, 2008.

[2] R. Delfouf, N. Bouzit, N. Bourouba, A. Brahimi, and J. P. Martinez Jiménez, "Dielectric behavior investigation of composite materials based on epoxy resin/Fe3O4/CaTiO3, SrTiO3 using mixture laws", *ECS Journal Solid State Science Technology*, vol. 11, 093003, 2022.

[3] A. Ashery, S. A. Gad, A. H. Gaballah, and G. M. Turky, "Fabrication, electrical and dielectric characterization of Au/CNT/TiO2/SiO2/p-Si/Al with high dielectric constant, low loss dielectric tangent", *ECS Journal Solid State Science Technology*, vol. 10, 051003, 2021.

[4] A. Ashery, S. A. Gad, G. M. Turky, and F. A. Maged, "Carbon nanotubes/N-Si heterojunction with high dielectric constant and rectification ratio, low dielectric loss tangent", *ECS Journal Solid State Science Technology*, vol. 11, 021003, 2022.

[5] Matiullah Ahsan, Md Nor Ramdon Bahrom, Zainab Zainal, Azrul Mohd Ariffin, Muhammad Saufi, Mohd Fairouz Mohd Yousof, Nor Aira Zambri, Farahiyah Mustafa, Faridah Hanim Mohd Noh, Aimi Syammi Ab Ghafar, Mehmood Ahmed, "Comprehensive Analysis of Insulator Performance in High Voltage Transmission Systems: Implications for Efficient Power Transfer", *Journal of Advanced Research in Applied Mechanics,* vol. 115, no. 1, pp. 117-130, 2024.

[6] Sabina Orlowska, "*Conception et prédiction des caractéristiques diélectriques des matériaux composites à deux et trois phases par la modélisation et la validation expérimentale*", thèse doctorat, Ecole Centrale de Lyon -France, 2003.

[7] Perambur. S. Neelakanta, "*Handbook of Electromagnetic Materials*", *CRC-Press*, 1995.

[8] M. M. Vijatović, J. D. Bobić, B. D. Stojanović, "History and Challenges of Barium Titanate: Part I", *Science of Sintering*, vol. 40, pp. 155-165, 2008.

[9] Y. Dobrincu, S. B. Balmus, G. N. Pascariu, and D. D. Sandu, "Characterization of dielectric mixtures by the time domain reflectometry (TDR) ", *Journal of Optoelectronics and Advanced Materials*, vol. 8, no. 3, pp. 956-961, 2006.

[10] Vasilica Pascariu, G.N. Pascariu, Paul Gasner, "Characterization of dielectric mixtures TCA/RE and TBA/RE by the time domain reflectometry (T.D.R)", *Journal of Optoelectronics and Advanced Materials*, vol. 10, no. 7, pp. 1857-1860, 2008.

[11] A. Okaya, and L.F. Barash "The dielectric microwave resonator", *proceeding of the IRE*, vol. 50, no. 10, pp. 2081-2092, 1962.

[12] S.B. Cohn, "Microwave Bandpass Filters Containing High-Q Dielectric Resonators", *IEEE Transactions on Microwave Theory and Techniques,* vol. MTT-16, no. 4, pp. 218-227, 1968.

[13] S. Long, M. McAllister, and L. Shen, "The resonant cylindrical dielectric cavity antenna", *IEEE Transactions on Antennas and Propagation,* vol. AP-31, no. 3, pp. 406-412, 1983.

[14] A. Petosa, A. Ittipiboon, Y. M. M. Antar, D. Roscoe, and M. Cuhaci, "Recent advances in dielectric-resonator antenna technology", *IEEE Antennas Propagation Magasine*, vol. 40, no. 3, pp. 35-48, 1998.

[15] S. Keyrouz and D. Caratelli, "Dielectric resonator antennas: basic concepts, design guidelines, and recent developments at millimeter-wave frequencies", *International Journal of Antennas and Propagation,* ID: 6075680, pp. 1-20, 2016.

[16] S. K. K. Dash, T. Khan, and A. De, "Dielectric resonator antennas: an application oriented survey", *International Journal of RF Microwave Computer-Aided Engineering*, vol. 27, no. 3, pp. 1-22, 2016.

[17] C. Du, M.S. Fu, H. W. Liu, H. H. Guo1, H.T. Chen, J. Zhang, J. P. Wang, S. F. Wang, H. W. Liu, W. F. Liu, Long Li and Zhuo Xu, "Dielectric resonator antenna with Y3Al5O12 transparent dielectric ceramics for 5G millimeter-wave applications" *Journal of the American Ceramic Society*, vol. 104, no. 9, pp. 4659-4668, 2021.

[18] R. S. Yaduvanshi and G. Varshney, "*Nano Dielectric Resonator Antennas for 5G Applications*", CRC Press, Taylor & Francis, Boca Raton, 2020.

[19] S. Huda, A. Saha, and A. Karmakar, "Ultra wideband (UWB) dielectric resonator antenna using fractal-inspired feeding mechanism", *International Journal of Communication Systems*, vol. 36, no. 13, e5519, 2023.

[20] A. Petosa and A. Ittipiboon, "Dielectric resonator antennas: a historical review and the current state of the art", *IEEE Antennas and Propagation Magasine*, vol. 52, no. 5, pp. 91-116, 2010.

[21] J. Iqbal, U. Illahi, M. A. Khan, A. Rauf, E. M. Ali, I. Bari, H. Ali, M. A. Khan, M. Alibakhshikenari, and M. Dalarsson, "A novel single-fed dual-band dual circularly polarized dielectric resonator antenna for 5G Sub-6 GHz applications", *Applied Sciences*, vol. 12, no. 10, pp. 5222-5240, 2022.

[22] R. Kumar and R. Kumar Chaudhary, "A dual-band dual-polarized cubical DRA coupled with new modified cross-shaped slot for ISM (2.4 GHz) and Wi-MAX (3.3-3.6 GHz) band applications", *International Journal of RF Microwave Computer-Aided Engineering*, vol. 29, no. 1, e21449, 2019.

Chapter 1

Theoretical Concepts of Dielectric Materials

Chapter 1: Theoretical concepts of dielectric materials

1.1 Introduction

Research on dielectric materials, technology development, and new device innovation have experienced extraordinary growth over the past century. Understanding the science and technology of dielectric materials has been essential to meeting societal needs by enabling the development of a diverse range of high-performance electronic devices utilized in fields such as automotive, communications, military, and medical applications.

Today, the need for integration and miniaturization of devices in advanced electronics and telecommunications systems is driving the rapid development of new dielectric materials. These materials are very promising for the future due to their specific properties, such as permittivity, low dielectric loss, low conductivity, and high-quality factor. The term "dielectric" refers to a material that can store electrical energy and acts as an electrical insulator capable of being polarized by an applied electric field.

In this chapter, we describe the theoretical basis for understanding the different mechanisms and processes that determine the properties of dielectric materials and their main aspects. First, we provide a brief definition of dielectric materials, based on their behavior under an applied electric field. We then explain the phenomenon of polarization in dielectric materials, including its different types and the dipole moment. Next, we discuss the interaction between electromagnetic fields and dielectric materials using Maxwell's equations, and finally, we explain the various aspects that influence the properties of dielectric materials, such as dielectric constant, dielectric loss, conductivity, and dielectric strength.

1.2 Dielectric materials

Relatively little attention was paid to the properties of the insulating material until 1837, when Michael Faraday published the first numerical results of measurements of this material, which he called the dielectrics [1].

A dielectric material is a poor conductor of electricity and has an energy gap of 3 eV or more. This wide energy gap prevents the thermal excitation of electrons from the valence band to the conduction band [2]. In other words, a dielectric material has no free electrical charges that can move macroscopically. It is sometimes referred to as an electrical insulator [3]. The atoms in dielectric materials are ionized to some degree and carry either a positive or negative charge.

Theoretical concepts of dielectric materials

A material is classified as a dielectric when, under the influence of an electric field, the equilibrium positions of its charges are altered, leading to a deformation of the electron cloud around the atom. This displacement represents a microscopic electrical shift: positive charges move in the direction of the field, while negative charges move in the opposite direction, creating a dielectric polarization within the material. Moreover, electric dipoles become oriented and aligned with the direction of the applied electric field. The total electric field in a dielectric material is the sum of the applied electric field and the induced electric field resulting from the polarization [3]. When the external electric field is removed, the charges return to their equilibrium position, and the polarization disappears.

The ideal or perfect dielectric material refers to a theoretical concept that exhibits no electrical conductivity ($\sigma=0$) and its permittivity ε is purely real number. Materials such as wood, glass, chalk, plastics, rubber, paper, quartz, and distilled water are considered close to perfect dielectrics. In practice, real dielectric materials possess an imaginary component associated with dielectric losses when subjected to an external electric field. This phenomenon results in very low conductivity, as indicated by the imaginary part of the complex permittivity [4-6]. For this reason, the interaction of a dielectric material with an electric field is characterized by two fundamental parameters: the dielectric constant and the dielectric loss, which are expressed through the complex permittivity, also denoted as ε_r^* [7, 8].

$$\varepsilon_r^* = \varepsilon_r' + \mathrm{i}\varepsilon_r'' \tag{1.1}$$

The real part (ε_r') represents the dielectric constant or relative permittivity, while the imaginary part (ε_r'') represents the dielectric loss, and $\mathrm{i}^2 = -1$.

Dielectric materials exist in liquid, gaseous, and solid states. Solid dielectric materials are the most widely used, with many of them being excellent electrical insulators. Examples include porcelain (ceramics), mica, glass, and plastics, among others. Thus, while a good dielectric is necessarily an excellent insulator, the reverse is not always true [9]. Unlike ordinary insulators, dielectric materials can be used to store electrical energy.

Dielectric materials are essential in numerous applications, such as capacitors, electrical insulators, oscillators, filters, antennas, electronic components, etc.

The main characteristics of dielectric materials are as follows:

- The energy gap of dielectric materials is very wide.
- The thermal stability is excellent, and the insulation resistance is high.
- The dielectric materials have high electrical resistivity.
- The attraction between the electrons and the parent nucleus is very strong.
- The electrical conductivity of these materials is very low because there are no free electrons to carry current.

1.3 Electric dipoles

A dielectric material, like any other material, is composed of ions with positive and negative charges that are balanced for a supposedly perfect solid to ensure electrical neutrality [10]. Atoms consist of electrons, which carry negative charges, and protons, which carry positive charges. In the absence of an electric field, the positive and negative electric charges in a dielectric medium remain bound to specific atoms or molecules. However, when an electric field is applied, the distribution of these charges is altered, leading to the formation of electric dipoles [11].

An electric dipole is a system consisting of two electric charges of equal magnitude but opposite signs, one positive $(+q)$ and the other negative $(-q)$, separated by a distance d, as shown in Figure 1.1.

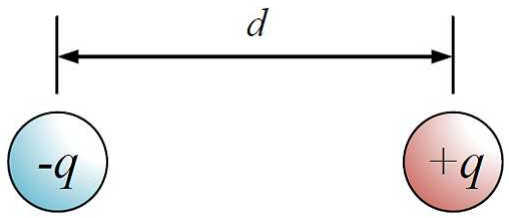

Figure 1.1: An electric dipole.

An electric field affects an electric dipole, generating a dipole moment. This results in a pair of equal and opposite forces (F_1 and F_2) that drive the electric dipole to align with the direction of the external electric field (see Figure 1.2). The force F acting on a charge q is related to the electric field E by the following equation:

$$\vec{F} = q \cdot \vec{E} \tag{1.2}$$

Each electric dipole is characterized by its dipole moment m, given by:

$$\vec{m} = q \cdot d \cdot \vec{r} \quad (1.3)$$

q: The charge carried by an atom (c).

d: The distance between two charges (m).

$\vec{r}$: Unit vector representing the displacement vector pointing from the negative to the positive charge.

The dipole moment is the product of a charge by a distance. It is measured in coulomb-meters $(c.m)$. The Debye unit is commonly used [10].

$[m] = D(1\ Debye = 1/3 \times 10^{-29} c.m = e \times 2.08 \times 10^{-11} c.m)$

where e is the charge of the electron.

$e = 1.602 \times 10^{-19} c.$

The polarization is then identical with the dipole moment density, and is also denoted by P [1].

Polarization P is defined as total dipole moments in a dielectric per unit volume: $P = \sum m/V$

where V is the overall volume of the sample, and $\sum m$ represents the vector sum of dipole moments.

The torque τ acts on the rigid body of the dipolar molecule according to the following equation:

$$\tau = (F \sin\theta) d \quad (1.4)$$

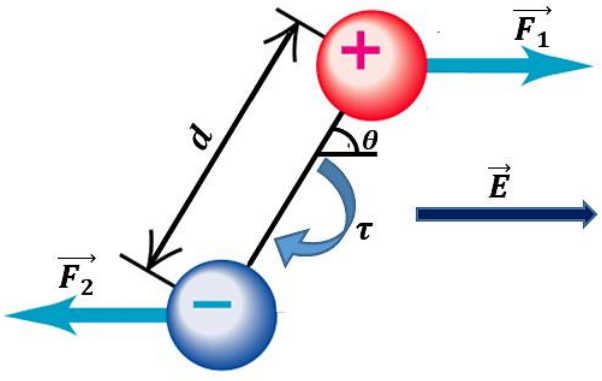

Figure 1.2: Dipole moment.

The reorientation of polar molecules in an alternating electric field is not instantaneous. Thus, in

a uniform electric field, the electric dipole experiences only a single moment.

1.4 Mechanisms of polarization

The first step in studying dielectrics is to understand the different types of polarization. It is important to distinguish between polar solids and non-polar solids [4, 10].

- **Non-polar solids:** In non-polar solids, the centers of gravity of the positive and negative charges coincide. The distribution of charges is symmetrical, and therefore the dipole moment is zero in the absence of an external electric field.
- **Polar solids:** Polar solids are composed of polar molecules in which the centers of gravity of the positive and negative charges do not coincide (for example, a water molecule). This is called molecular polarization, and the distribution of charges is asymmetrical. Most molecular solids and ferroelectric solids, which exhibit spontaneous polarization. For example, the structure of barium titanate.

When an electric field is applied to a dielectric material, the atoms or molecules within it undergo a change in the distribution of charges, creating electric dipoles, a phenomenon known as polarization. The degree of polarization depends on the atomic structure of the dielectric material as well as the strength of the applied electric field. Michael Faraday first discovered the effect of dielectric polarization in 1837 [1]. The polarization mechanism describes how atoms or molecules respond to an external electric field, resulting in a dipole orientation. Several types of polarization can occur in a dielectric material. The four fundamental types of polarization are electronic polarization (P_e), ionic or atomic polarization (P_i), dipolar or orientation polarization (P_d), and space charge or interface polarization (P_s). These mechanisms do not occur simultaneously but depend on the excitation frequency of the applied external field. The polarization mechanisms are illustrated in Figure 1.3 and are commonly classified into two regimes: the relaxation regime (space charge and dipolar polarization) and the resonance regime (ionic and electronic polarization) [10, 12-15].

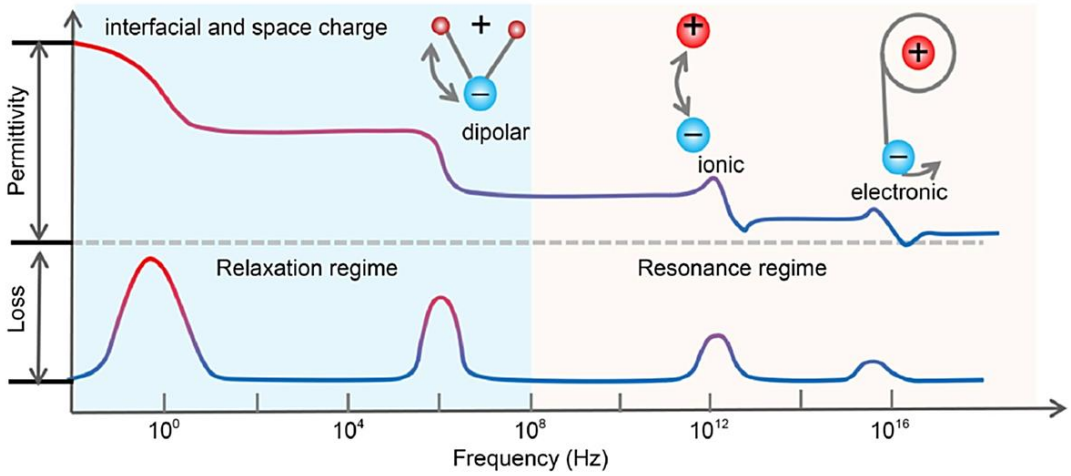

Figure 1.3: Dielectric polarization mechanisms and dielectric response (permittivity (ε') and dielectric loss (ε'')) with different frequencies [14].

The total polarization in a dielectric material is the sum of four types:

$$\overrightarrow{P_t} = \overrightarrow{P_e} + \overrightarrow{P_i} + \overrightarrow{P_d} + \overrightarrow{P_s} \tag{1.5}$$

1.4.1 Electronic polarization

Electronic polarization (P_e) refers to the displacement of the center of the electron cloud in an atom relative to the center of its nucleus. This results in microscopic shifts of the positive nucleus and negative electrons in opposite directions within the same atom when a dielectric material is subjected to an electric field, as illustrated in Figure 1.4. This phenomenon occurs in all dielectric materials, regardless of their atomic structure. The electronic orbits are distorted with extremely fast kinetics (10^{-15} seconds), and the response typically falls within the ultraviolet range, around 10^{15} Hz. When the electric field is removed, the electronic polarization and the induced dipoles vanish [10, 12-15].

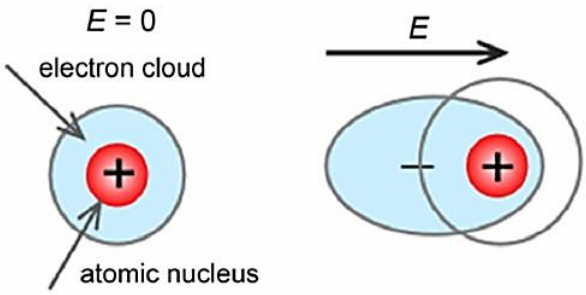

Figure 1.4: Schematic of the mechanism of electronic polarization.

1.4.2 Ionic (or atomic) polarization

Atomic polarization (P_i) occurs in solid materials with ionic bonds when an external electric field is applied, causing the positive and negative ions in the material to shift slightly in opposite directions, as illustrated in Figure 1.5. Under the influence of the external electric field, cations and anions are slightly displaced from their equilibrium positions, creating a dipole moment. Ionic polarization is established in approximately 10^{-13} seconds, which is slower than electronic polarization.

Ionic polarization and the molecular distortion polarization occur in the infrared frequency range, typically between 10^{12} and 10^{14} Hz [10, 12-15].

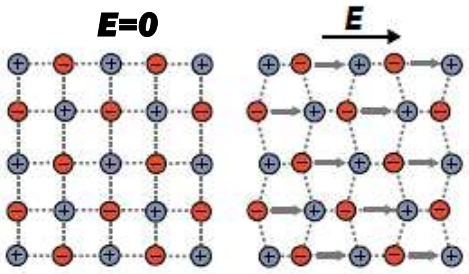

Figure 1.5: Schematic of the mechanism of ionic polarization.

1.4.3 Dipolar (or orientation) polarization

Dipolar polarization (P_d) occurs in polar molecules, such as water molecules. The molecular dipoles align with the direction of the applied electric field, as illustrated in Figure 1.6. The time required to establish polarization depends on both the frequency of the applied field and the viscosity of the medium. Dipolar polarization is most significant at lower frequencies, as the molecules need time to reorient. This type of polarization typically occurs in the microwave frequency range, between 10^8 and 10^{11} Hz [10, 12-15].

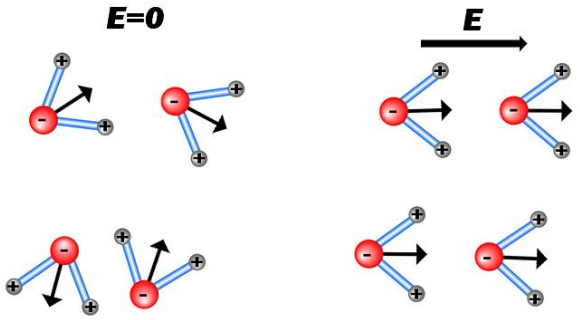

Figure 1.6: Schematic of the mechanism of dipolar polarization.

1.4.4 Space charge (or interface) polarization

This type of polarization (P_s) is associated with mobile and trapped charges. In materials composed of more than one phase (heterogeneous materials), charges can move under the influence of an external electric field. Their displacement eventually leads to accumulation at the interfaces between the different phases, as shown in Figure 1.7. Space charge polarization occurs at low frequencies, typically ranging from 10^{-1} to 10^{2} Hz [10, 12-15].

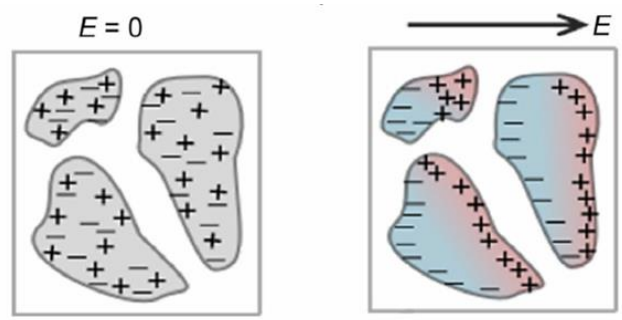

Figure 1.7: Schematic of the mechanism of interfacial polarization.

1.5 Properties of the dielectric materials

The dielectric properties of a material are determined by the ability of charges to move within it in response to an external electric field. These properties also refer to the ability of a material to store electrical energy, become polarized under an applied electric field, and its dissipation factor. Dielectric properties are important for predicting the behavior of materials and essential for many applications. They are discussed in detail below:

1.5.1 Dielectric constant (relative permittivity)

The dielectric constant (ε_r) of a dielectric material is defined as the ratio of the capacitance (c) of a capacitor measured with the dielectric material placed between its parallel plates to the capacitance (c_0) of the same capacitor measured in a vacuum (without the dielectric material). The distance separating the parallel plates is L, as illustrated in Figure 1.8. The increase in capacitance is due to the polarization of the dielectric material when a voltage is briefly applied. The movement of charges is the source of the stored energy. Increasing the capacitance in this way is desirable because it allows more electrical energy to be stored for a given field strength [4, 10, 16].

$$c = q/v = \varepsilon_r \varepsilon_0 A/L \tag{1.6}$$

$$\varepsilon_r = \varepsilon/\varepsilon_0 = c/c_0 \quad (1.7)$$

In practice, the complex permittivity introduced in relationship (1.1) is used instead of the relative permittivity mentioned in relationship (1.7) because it also has an imaginary component that is associated with dielectric loss.

$$\varepsilon_r^* = \varepsilon_r' + \mathrm{i}\varepsilon_r''$$

The real part (ε_r') is the dielectric constant, also known as relative permittivity, which represents the ability of a dielectric material to store electrical energy, which is quantified by its permittivity. This permittivity indicates how easily a material can be polarized when an electric field is applied. Higher permittivity corresponds to a greater ability to store energy. The imaginary part (ε_r'') represents the energy dissipation or dielectric loss.

The dielectric constant is a unitless quantity that represents the ratio of two similar quantities.

The following physical values are:

- ε_r: Dielectric constant or relative permittivity (unitless quantity)
- ε: Absolute permittivity (F/m)
- ε_0: Free space permittivity (F/m)
- ε_r' or ε': Real part of the complex permittivity or dielectric constant (unitless quantity)
- ε_r'' or ε'': Imaginary part of the complex permittivity (unitless quantity)
- c: Capacitance with the dielectric material (F)
- c_0: Capacitance with vacuum (F)
- q: Charge carried by an atom (c)
- v: The difference in potential (or voltage) between two plates (v)
- A: Area of the plate (or cross section area of the sample) (m^2)
- L: Distance between parallel plates (m)

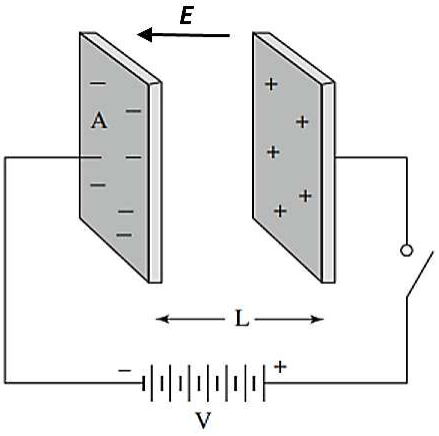

Figure 1.8: Two metal plates, separated by a distance L, can store electric energy after being briefly charged by a battery.

Dielectric permittivity (ε) represents an important physical property. It is defined as the ratio between electric displacement ($\vec{D}$) to the electric field ($\vec{E}$).

$$\vec{D} = \varepsilon \vec{E} \tag{1.8}$$

1.5.2 Electrical susceptibility

Electrical susceptibility (χ_e) of a dielectric material, also called the polarization coefficient, is a measure of how easily the material becomes polarized when exposed to an electric field. It determines the dielectric constant of the material and therefore influences many other phenomena in that medium. Electrical susceptibility is defined as the proportionality constant that relates the electric field E to the induced dielectric polarization density P, such that:

$$P = \varepsilon_0 \chi_e E \tag{1.9}$$

where ε_0 is the free space permittivity.

The susceptibility of a medium is related to its relative permittivity (ε_r), which is expressed by the following equation:

$$\chi_e = \varepsilon_r - 1 \tag{1.10}$$

Therefore, by definition, if $\varepsilon_r = 1$ in a vacuum (free space), then the susceptibility is $\chi_e = 0$. This means that no polarization occurs [17].

1.5.3 Dielectric loss

An efficient dielectric supports fluctuating of charges with minimal energy dissipation in the form of heat. Energy losses in dielectric materials generally arise from two mechanisms. Conduction loss occurs when charges flow through the material, causing energy dissipation. Dielectric loss, on the other hand, results from the polarization response to an alternating electromagnetic field. The movement of charges causes energy dissipation as the polarization changes direction [15].

The dielectric loss is particularly high at the relaxation or resonance frequencies of polarization mechanisms, as the polarization lags behind the applied electric field. This lag results in an interaction between the electric field and the dielectric polarization, which leads to heating. A low dielectric loss is desirable in applications where energy efficiency is important [16].

Typically, dielectric loss is characterized by the loss tangent ($tan\delta$), defined as the ratio of the imaginary part (ε_r'') to the real part (ε_r') of the complex permittivity when a dielectric material is subjected to an electric field [18].

$$tan\delta = \frac{\varepsilon_r''}{\varepsilon_r'} \tag{1.11}$$

The parameter δ denotes the phase shift angle between the voltage applied to the dielectric and the current flowing through it. This loss can also be expressed in terms of the quality factor Q, defined as follows:

$$tan\delta = \frac{1}{Q} \tag{1.12}$$

Dielectric loss arises from the work required to establish polarization. Therefore, an increase in dielectric loss leads to a rise in internal temperature. Figure 1.9 illustrates the dielectric constant and the dielectric loss as a function of frequency.

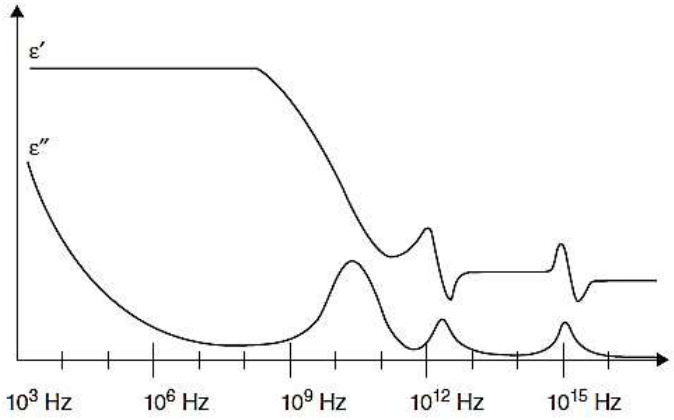

Figure 1.9: Dielectric constant and dielectric loss as a function of frequency.

Materials with a higher dielectric constant generally have higher dielectric loss. This is a disadvantage in practical applications.

1.5.4 Permeability

Permeability (μ) is a measure of the magnetic response of a material. It describes the interaction of a dielectric material with a magnetic field. Some materials, such as iron, cobalt, nickel, and their alloys, have significant magnetic properties, but many materials are non-magnetic.

Permeability is defined as the ratio of magnetic flux density (B) within a material to the magnetic field intensity (H), as expressed by the following formula [13]:

$$\mu = B/H \tag{1.13}$$

Therefore, the permeability of a non-magnetic dielectric material is very close to the permeability of free space. In this case, the relative permeability is given by the following relationship [4]:

$$\mu_r = \mu/\mu_0 = 1 \tag{1.14}$$

The permeability of free space is $\mu_0 = 4\pi \times 10^{-7}$ H/m.

1.5.5 Electrical conductivity

Electrical conductivity is the quantity that represents the ability of a material to conduct electric current and is commonly denoted by the Greek letter σ. The primary function of dielectric materials is to provide reliable insulation between regions with different electrical potentials. However, in practice, no insulating materials offer complete isolation.

Due to various additives and impurities, dielectric materials exhibit very low conductivity, which allows the free charges to move in a given direction when an electric field is applied. Electrical conductivity is the inverse of the electrical resistivity, and the static conductivity is derived from the imaginary part of the complex permittivity by the following relationship [13, 17].

$$\sigma_s = \varepsilon_0 \varepsilon'' \omega \tag{1.15}$$

A perfect dielectric is a material that does not conduct electricity **($\sigma = 0$).**

1.5.6 Dielectric strength

Dielectric strength is a property of dielectric materials that represents the maximum electric field that a material can withstand before dielectric breakdown occurs. It is a critical parameter in determining the maximum voltage that a capacitor or insulator can tolerate. Breakdown of an insulator refers to the loss of its insulating property and its transition into a conductor. Typical dielectric strength values range from 10^6 to 10^9 Vm^{-1}. The exact value of dielectric strength depends on several factors, most obviously the size of the energy gap, as well as the geometry, microstructure of the sample, and the external conditions to which it is subjected. This property is particularly important in applications requiring high voltage [16].

1.5.7 Relaxation phenomena in dielectric materials

Dielectric relaxation is the momentary delay (or lag) in the dielectric constant of a material. This phenomenon is usually caused by the delay response of molecular polarization to a changing electric field in a dielectric medium. The dielectric relaxation time (τ) represents the time required for the dipoles to align with an external electric field or to return to their initial equilibrium state once the electric field is removed. At low frequencies, the dipoles have sufficient time to align with the electric field, whereas at high frequencies, they cannot respond quickly enough to follow the polarizing field. As a result, dielectric losses reach a maximum at the characteristic frequency ($w_{max} = 1/\tau$), where w is the angular frequency [5].

The phase shift between the polarization and the applied field leads to energy absorption in the dielectric [19]. The phenomenon of relaxation time becomes crucial when examining the response of the material to an alternating electric field. Dielectric relaxation in solids is one of the most extensively studied topics, and several models have been developed to explain these dielectric relaxation phenomena, such as:

- **Debye relaxation:** This simple model describes the relaxation behavior of a dielectric material characterized by a single relaxation time, representing the non-interactive relaxation of dipoles in response to an external alternating electric field. It is often used to model polar materials. The complex permittivity is expressed by the following Debye equation [20-22]:

$$\varepsilon^*(w) = \varepsilon_\infty + \frac{\Delta\varepsilon}{1 + iw\tau} \tag{1.16}$$

with $\Delta\varepsilon = \varepsilon_s - \varepsilon_\infty$

where ε_s is the static permittivity at low frequency, and ε_∞ is the permittivity at high frequency. The real and imaginary parts of the complex permittivity are given by:

$$\varepsilon'(w) = \varepsilon_\infty + \frac{\Delta\varepsilon}{1 + w^2\tau^2} \tag{1.17}$$

$$\varepsilon''(w) = \varepsilon_\infty + \frac{\Delta\varepsilon \times w\tau}{1 + w^2\tau^2} \tag{1.18}$$

For most dielectrics, deviation from the Debye model is observed. Therefore, several empirical modifications have been proposed to achieve better agreement with experimental results, such as the Cole-Cole and Cole-Davidson models.

- **Cole-Cole relaxation:** This model takes into account the distribution of relaxation times and more accurately describes the dielectric behavior of real materials, particularly polymers. Cole & Cole demonstrated that, for a material exhibiting Debye relaxation, each point in a plot of ε'' versus ε' corresponds to a particular frequency, which gives a semicircle. Cole & Cole modified the Debye equation to account for deviations from the ideal Debye model. They adjusted the Debye equation by introducing the parameter α into the complex permittivity, as shown below [5, 23, 24]:

$$\varepsilon^*(w) = \varepsilon_\infty + \frac{\Delta\varepsilon}{1 + (iw\tau)^{1-\alpha}} \tag{1.19}$$

The exponent parameter α takes a value between 0 and 1 and can be used to describe different spectral shapes. When $\alpha = 0$, the Cole-Cole model reduces to the Debye model. When $\alpha > 0$, the relaxation is stretched; in other words, it extends over a wider range than the Debye relaxation.

- **Davidson-Cole Relaxation:** This model is similar to the Cole-Cole model but allows for a wider distribution of relaxation times. Davidson and Cole introduced the parameter β, which accounts for deviations from ideal behavior in the high-frequency region of the Debye relaxation. This modification is expressed by the following equation for the complex permittivity [24-26]:

$$\varepsilon^*(w) = \varepsilon_\infty + \frac{\Delta\varepsilon}{1 + (iw\tau)^\beta} \tag{1.20}$$

When the parameter β is equal to 1, the Davidson-Cole model becomes a Debye model.

The figure below shows graphical representations of the Debye, Cole-Cole, and Davidson-Cole models in two plots: (a) the variation of the real and imaginary parts as a function of frequency, and (b) the imaginary part (ε'') versus the real part (ε') of the complex permittivity.

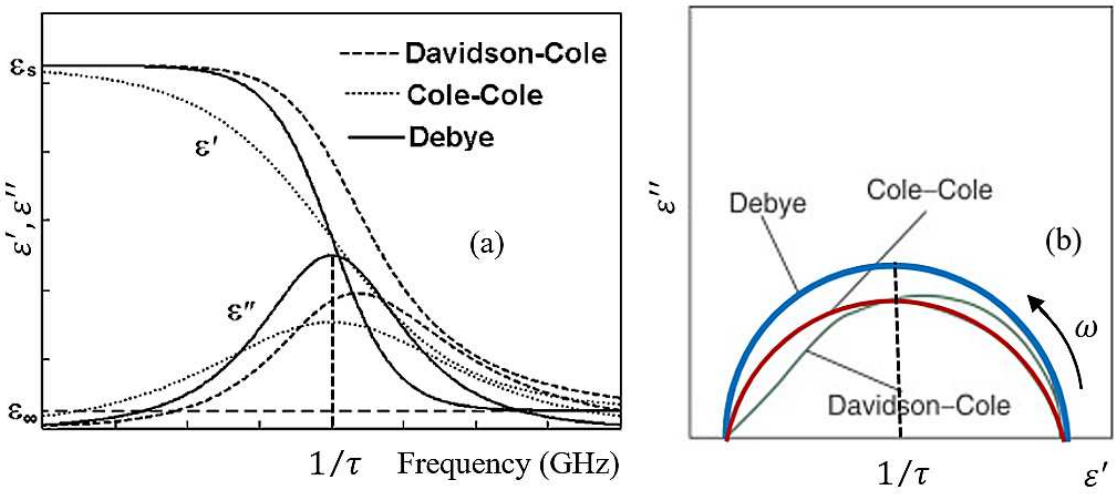

Figure 1.10: Schematic representation: (a) the variation of the real and imaginary parts as a function of frequency, (b) the imaginary part versus the real part.

The dielectric relaxation phenomena occur in all polarization mechanisms but are particularly important for orientation polarization, which exhibits the longest relaxation time.

1.5.8 Resonance phenomena in dielectric materials

Resonance phenomena in dielectric materials occur when the frequency of the applied alternating electric field coincides with the natural resonance frequency of a specific polarization mechanism, such as ionic or electronic polarization. In this condition, the oscillations of the bound charges

reach their maximum amplitude, resulting in a pronounced increase in polarization. This enhanced polarization leads to a temporary rise in the dielectric constant. However, excessive energy absorption at the resonance frequency can also increase dielectric losses due to the conversion of electrical energy into heat, as shown in Figure 1.11. Therefore, understanding resonance behavior is essential for optimizing the dielectric performance of materials, particularly in high-frequency and microwave applications.

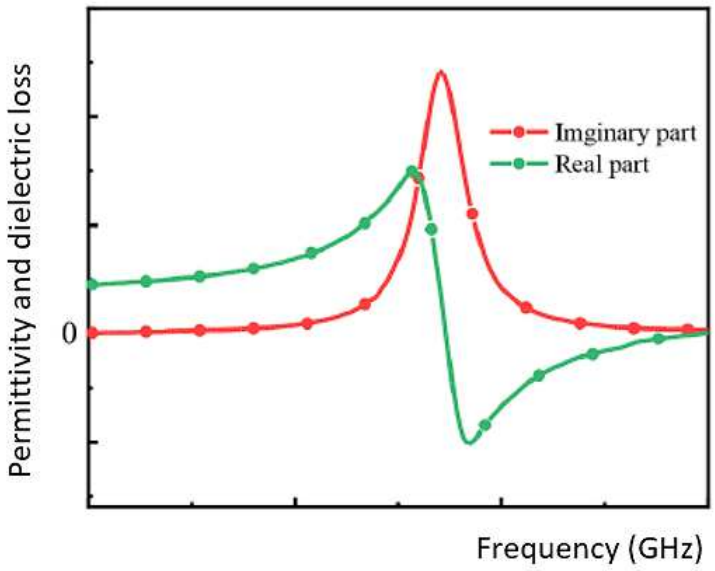

Figure 1.11. Resonance phenomena are represented by the variation of ε' and ε'' as a function of frequency.

1.6 Local field in dielectric materials

In dielectric materials, the electric field experienced by an individual molecule or atom is not necessarily identical to the macroscopic field applied to the material. This discrepancy arises from the polarization of the dielectric, which generates a local electric field that may either enhance or oppose the externally applied field.

When an external electric field is applied to a point M within a dielectric material surrounded by three dipoles, as illustrated in Figure 1.12, the point experiences the influence of two sources of electric field: one arising from the dipole moments of the surrounding molecules or atoms, and the other from the externally applied field. The resultant electric field acting at point M, produced by the combined effect of these two sources, is referred to as the local electric field [2, 13].

$$\vec{E}_{loc} = \overrightarrow{E_{ext}} + \vec{E}_{dipoles} \quad (1.21)$$

In a dense medium, such as a liquid or solid, the particles are closely spaced. The electric field generated by the surrounding dipoles at a given point within the material is therefore significant and cannot be neglected. For a linear, isotropic, and uniform dielectric, the local field within the material can be expressed as:

$$\vec{E}_{loc} = \overrightarrow{E_{ext}} + \vec{P}/3\varepsilon_0 \quad (1.22)$$

The term $\vec{P}/3\varepsilon_0$ represents the field created by the dipoles and is called the Lorentz field.

Polarization is the process by which molecules or atoms within a material acquire electric dipole moments in response to an applied electric field. These induced dipoles, in turn, generate their own electric field. Consequently, the net electric field at a point within the material is the sum of the externally applied field and the local fields produced by the polarization of neighboring molecules, as illustrated in Figure I.12 below.

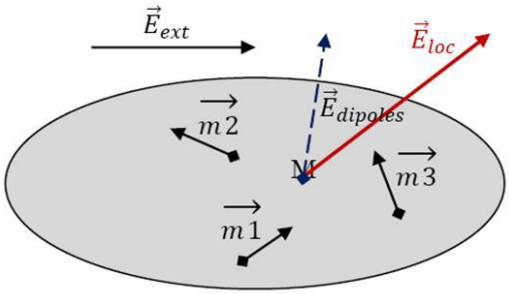

Figure 1.12: External electric field applied to a point M within material surrounded by three dipoles.

1.7 Maxwell's equations

In the 1860s, James Clerk Maxwell published his famous unified theory of electricity, magnetism, and electromagnetic radiation. He also formulated the so-called Maxwell relations for non-polar materials [27].

The propagation of an electromagnetic field within a medium is governed by Maxwell's equations, which describe how electric and magnetic fields are generated and interact with charges and currents, as well as how time-varying electric field can induce a magnetic field and vice versa.

In the late 19th century, Maxwell's theoretical framework was unified and reformulated into a set of equations that describe electromagnetic phenomena across all frequency ranges and spatial scales larger than the atomic level.

Today, Maxwell's equations remain fundamental tools for electrical engineers in the design of all types of electrical and electronic equipment related to electromagnetic field. They are critical to understanding antennas and electromagnetics. The four unified Maxwell equations describe the propagation of electric and magnetic fields and their interaction with materials [28, 29].

1.7.1 Gauss's law

Gauss's law is a mathematical statement that the total electric flux through any closed surface is equal to the net electric charges enclosed within that surface. This law describes how an electric field is generated by electric charges. Gauss's law for electric fields states that the divergence of the electric flux density D is equal to the free electric charge density within the material.

$$\nabla \cdot D = \rho \tag{1.23}$$

1.7.1 Gauss's law for magnetic field

This equation describes the magnetic flux through any closed surface, which is equal to zero. There are no magnetic monopoles (north or south pole). In other words, the poles of a magnet cannot be separated. There is no such thing as "magnetic charge" analogous to an electric charge. Gauss's law for magnetism states that the divergence of the magnetic field B is zero.

$$\nabla \cdot B = 0 \tag{1.24}$$

1.7.2 Faraday's law

Faraday discovered how a changing magnetic field can induce an electric current in a circuit. This phenomenon is known as electromagnetic induction. This equation describes how a varying magnetic field with time can generate an electric field. For example, a rotating magnet produces a varying magnetic field, which in turn induces an electric field.

$$\nabla \times E = -\frac{\partial B}{\partial t} \tag{1.25}$$

1.7.1 Ampere's law

Ampere's law states that magnetic fields are related to electric currents. When an electric current I flows through a straight conducting wire, a magnetic field H is generated around the wire. Ampère's Law states that magnetic fields H are generated by both current density J and a varying electric displacement field with time D and is expressed as follows:

$$\nabla \times H = J + \frac{\partial D}{\partial t} \tag{1.26}$$

The Maxwell's equations involve the following units, which are appropriate for the corresponding physical quantities:

ρ: Electric charge density (C/m^3)

J: Electric current density (A/m^2)

D: Electric flux density or electric displacement field (C/m^2)

E: Electric field intensity (V/m)

H: Magnetic field intensity (A/m)

B: Magnetic flux density ($Tesla = Wb/m^2$)

In addition to the Maxwell's equations, the following equations are necessary to describe the electromagnetic behavior of a material [4].

- **Lorentz force law**

Lorentz force, the force exerted on a charged particle q moving with velocity v through an electric field E and magnetic field B.

$$\vec{F} = q\left(\vec{E} + v \times \vec{B}\right) \tag{1.27}$$

Where F is the force (N/m) and v is the velocity (m/s)

- **Ohm's law**

For a conductive medium, the current density J is proportional to the electric field:

$$J = \sigma \cdot E \tag{1.28}$$

where σ is electric conductivity of medium (S/m).

❖ Convection current law

The physical motion of charged particles through the material causes a convection current. This type of current occurs in liquids, gases, and vacuum. The electric current density J is expressed as follows:

$$J = \rho v \tag{1.29}$$

❖ Constitutive equations for dielectric materials

For a dielectric medium:

$$D = \varepsilon \cdot E \tag{1.30}$$

where ε is the absolute permittivity (F/m) and D is the electric flux density (C/m^2)

$$D = \varepsilon_0 E + P \tag{1.31}$$

The polarization vector P represents the electric dipole moment per unit volume, arising from pairs of positive and negative charges. For isotropic and linear materials, the electric polarization is proportional to the applied electric field.

$$P = \varepsilon_0 \chi_e E \tag{1.32}$$

where χ_e is the electric susceptibility.

The electric flux density can be rewritten as:

$$D = \varepsilon_0 \varepsilon_r E \tag{1.33}$$

where the relative dielectric constant ε_r is defined as:

$$\varepsilon_r = 1 + \chi_e \tag{1.34}$$

The term $\varepsilon_0$is the dielectric constant of free space and it is given by:

$\varepsilon_0 = \frac{1}{36\times\pi} 10^{-9} = 8.854 \times 10^{-12}\ F/m.$

1.8 Factors affecting the dielectric properties of materials

The dielectric properties of a material, such as its dielectric constant and dielectric loss, are influenced by several factors, including:

1.8.1 Effect of the frequency of the applied field on the dielectric constant

The dielectric properties of most materials vary considerably with the frequency of the applied electric field. Dielectric constant of a dielectric material is not a constant value but can vary depending on the frequency of the applied electric field. This phenomenon is called frequency dispersion. The frequency dependence of the dielectric constant is due to the different polarization mechanisms that occur in each frequency range. At low frequencies, the dipoles have sufficient time to align with the external electric field. However, at high frequencies the ability of the dipoles to respond to the external electric field decreases, and they are unable to change their orientation. In other words, the orientation of the dipoles cannot keep up with the oscillating electric field, meaning they can no longer contribute to the overall polarization, often leading to a reduction in the dielectric constant [5].

Furthermore, when an external electric field is applied to a dielectric material, the potential energy required to align a dipole in the direction of the field is lower than that required to orient it in the opposite direction. Consequently, an increase in energy absorption results in a corresponding increase in the dielectric constant.

When the frequency of the applied field coincides with the natural resonance frequency associated with the ionic or electronic polarization mechanism, resonance occurs. Under this condition, the bound charges oscillate with maximum amplitude, resulting in an enhanced polarization response and, consequently, an increase in the dielectric constant.

1.8.2 Effect of humidity on the dielectric constant

Water possesses a significantly higher dielectric constant than most dry materials. When a material absorbs moisture, polar water molecules are introduced that can easily align with an applied electric field. This enhanced alignment of polar molecules greatly increases the material's ability to store electrical energy, thereby raising its dielectric constant. Furthermore, moisture often creates conductive pathways within the material, resulting in greater energy dissipation as heat. Many dielectric materials, including wood, certain carbon-based materials, and paper, can easily

absorb water. This absorption can significantly increase their dielectric constant due to the inherently high dielectric constant of water [13].

1.8.3 Effect of structure on the dielectric constant

Structural properties of a material, such as crystal symmetry, bonding nature, and atomic arrangement, strongly influence its dielectric constant. Materials with asymmetric or distorted crystal structures often exhibit higher dielectric constants because such asymmetry facilitates the formation and alignment of electric dipoles under the influence of an external electric field. Conversely, materials with highly symmetrical crystal structures tend to have lower dielectric constants, as their atomic configurations restrict dipole formation and reduce polarizability. Additionally, the type and strength of interatomic bonds play a critical role: ionic and covalent bonds contribute differently to polarization mechanisms. For instance, in ferroelectric materials such as barium titanate ($BaTiO_3$), structural distortions within the perovskite lattice lead to spontaneous polarization, resulting in exceptionally high dielectric constants. Therefore, the degree of structural asymmetry and bonding characteristics directly govern the dielectric response of a material.

The difference in the crystallographic structure and chemical nature of the fillers determine the variations in the dielectric constant and dielectric loss of composites based on the same matrix [30]. The thickness of a sample also has a significant influence on its dielectric properties, particularly in the low-frequency region, where the dielectric constant increases with increasing sample thickness [11].

Furthermore, the dielectric behavior of composites is affected by many factors such as filler size and shape, interfacial characteristics, and porosity. As the content of fillers increases, there is typically a significant rise in the dielectric constant [31]. Impurities that enhance the electrical conductivity of a material can reduce its dielectric constant while increasing dielectric loss. In addition, pressure can affect the dielectric properties of materials, especially in gases and liquids.

1.8.4 Effect of temperature on the dielectric constant

For materials that possess permanent dipoles, the dielectric constant varies significantly with temperature. This behavior arises from the influence of heat on orientational polarization. In general, as the temperature increases, molecular motion becomes more vigorous, disrupting the alignment of the dipoles, which in turn reduces polarization and lowers the dielectric constant [16].

Electronic polarization is slightly influenced by temperature, while ionic polarization is affected because the strength of ionic bonds varies with temperature.

This does not imply that the dielectric constant increases continuously as the temperature decreases. Several discontinuities in the dielectric constant can occur as the temperature changes. In particular, the dielectric constant may exhibit abrupt variations at phase boundaries due to phase transitions. Since the crystal structure changes during such transitions, and the permittivity is strongly dependent on structural characteristics, the dielectric constant can either increase or decrease depending on the specific phases involved.

1.9 Variation of the dielectric constant in alternating fields

A dielectric material becomes polarized in response to an applied electric field, with the polarization aligning in the direction of the field. When the direction of the field changes, the polarization also reorients to align with the new field direction. This process requires time, as it involves the movement of charges or the rotation of dipoles.

When the field is switched, the orientational polarization (or average dipole orientation) requires a characteristic time to adjust, known as the relaxation time. At high frequencies, such as in the microwave range (around 10^{11} Hz), the dipolar polarization cannot follow the rapid oscillations of the alternating field. Consequently, the polarization can no longer remain aligned with the field, and this mechanism ceases to contribute to the polarization of the dielectric material.

In an alternating electric field, both ionic and electronic polarization mechanisms can be modeled as damped harmonic oscillators, with their frequency dependence governed by resonance phenomena. This behavior results in distinct peaks in the plot of dielectric constant versus frequency, corresponding to the resonant frequencies of the ionic and electronic polarization modes. Immediately above each resonance peak, a dip appears, a general characteristic of all damped resonant systems indicating that the system's response is out of phase with the driving field. In these regions, the polarization lags behind the applied electric field. At still higher frequencies, the motion of the charges can no longer follow the rapid alternations of the field, and the corresponding polarization mechanism ceases to contribute to the overall polarization of the dielectric material [16].

1.10 Conclusion

In this chapter, we introduced the basic concepts from a materials science perspective that help explain the behavior of dielectric materials resulting from the interaction between an electric field and the dielectric medium, based on Maxwell's equations.

We began with a brief definition of dielectric materials and electric dipoles. Then we described the different mechanisms involved in dielectric polarization and the properties of dielectric materials. Furthermore, we discussed the theoretical approaches used to calculate the local electric field within the framework of the Lorentz electric field hypothesis. We also provided a brief review of Maxwell's equations and the key relationships necessary to describe the electromagnetic behavior of dielectric material. Finally, we examined the factors influencing the dielectric properties of materials and the variation of permittivity with an alternating electric field. The experimental procedures and techniques used to determine the dielectric properties are presented in detail in the following chapter.

References

[1] C.J.F. Böttcher. *"Theory of Electric Polarization*, *Volume 1, Dielectrics in Static Fields", Elsevier, Amsterdam,* 1973.

[2] Ashim Kumar Bain, Prem Chand, *"Ferroelectrics: Principles and Applications",* Wiley-VCH, 2017.

[3] Rachita Lahri. *"Effects and benefits of nanoparticle assisted microwave imaging for the detection of breast cancer",* doctor of philosofy thesis, King's College London, 2019.

[4] Arlon T. Adams, Jay K. Lee, *"Principles of Electromagnetics 2-Dielectric and Conductive Materials",* Cognella Academic Publishing, 2015.

[4] Perambur S. Neelakanta, *"Handbook of Electromagnetic Materials: Monolithic and Composite Versions and their Applications",* CRC-Press, 1995.

[5] Georgios Giannoukos, Mart Min and Toomas Rang, "Relative complex permittivity and its dependence on frequency", *World Journal of Engineering,* vol. 14, no. 6, pp. 532-537, 2017.

[6] Ben Makhlouf Aymen, *"Elaboration and characterization of PZT-type ceramics",* Doctoral thesis, University Mohamed Khider of Biskra, 2023.

[7] A. Brahimi, N. Bourouba, J. P. Martinez Jimenez, and N. Bouzit. "A high frequency dielectric behavior modeling of a ReXTMnO2 ternary composite as an equivalent binary mixture", *Journal Composite and Advanced Materials*, vol. 31, no. 4, pp. 181-191, 2021.

[8] R. Delfouf, N. Bouzit, N. Bourouba, J. P. Martinez Jiménez, A. Brahimi, H. Khouni, and T. Arab, "Dielectric characterization and modeling of composite materials based on epoxy resin/black iron oxide/titanates in several frequency ranges", *ECS Journal of Solid State Science and Technology*, vol. 11, no. 7, 073006, 2022.

[9] H.-L. Wang, "Structure and Dielectric Properties of Perovskite Barium Titanate (BaTiO3) ", *Partial Fulfillment of Course Requirement for MatE 115, San Jose State University, San Jose,* 2002.

[10] Juan Martinez-Vega, *"Dielectric Materials for Electrical Engineering"*, Wiley, 2010.

[11] M. K. Maurya, Pramila Yadav, Sangeeta Pandey, "Study of dielectric properties of typical electrical insulating materials by terahertz wave spectroscopy", *International Journal for Research in Applied Science and Engineering Technology,* Vol. 12, no. 8, pp. 632-640, 2024.

[12] X. Hu, A.M. Sansi Seukep, V. Senthooran, L. Wu, L. Wang, C. Zhang, and J. Wang, "Progress of Polymer-Based Dielectric Composites Prepared Using Fused Deposition Modeling 3D Printing", *Nanomaterials*, vol. 13, no. 19 , pp. 2711-2734, 2023.

[13] Abdelhalim Brahimi, *"Élaboration et validation expérimentale de modèles prédictifs du comportement diélectrique des composites à base de titanate multi-phases en hyperfréquence"*, Thèse de doctorat, Université Ferhat Abbas-Sétif 1, 2022.

[14] H. Wu, F. Zhuo, H. Qiao, L. Kodumudi Venkataraman, M. Zheng, S. Wang, H. Huang, B. Li, X. Mao, and Q. Zhang, "Polymer-/Ceramic-based Dielectric Composites for Energy Storage and Conversion", *Energy and Environmental Materials,* vol. 5, no. 2, pp. 486-514, 2022.

[15] A H. Li, Y. Zhou, Y. Liu, L. Li, Y. Liu, and Q. Wang, "Dielectric polymers for high-temperature capacitive energy storage", *Chemical Society Reviews*, vol. 50, no. 11, pp. 6369-6400, 2021.

[16] Teaching and Learning Package (Online), " *Dissemination of IT for the Promotion of Materials Science (DoITPoMS) "*, University of Cambridge, 2021.

Link: https://www.doitpoms.ac.uk/tlplib/dielectrics/index.php.

[17] E. Tuncer, *Y.* V. Serdyuk, and S. M. Gubanski, "Dielectric Mixtures: Electrical Properties and Modeling", *IEEE Transactions on Dielectrics and Electrical Insulation*, vol. 9, no. 5, pp. 809-828, 2002.

[18] R. Chelghoum, Z. Messai A. Brahimi, N. Bourouba, J.P. Martinez Jiménez and F. Bouttout, "Dielectric Behavior Characterization of RE/BaTiO3 Using Time Domain Spectroscopy: Application on high performance dielectric resonator antennas", *ECS Journal of Solid State Science and Technology,* vol.13, no. 4, 043018, 2024.

[19] Rabah Delfouf, *"Modélisation et Caractérisation des Matériaux Composites à Base de (Polymère / Titanates / Magnétite) en Hyperfréquences"*, Thèse de doctorat, Université Ferhat Abbas-Sétif 1, 2023.

[20] P. Debye, "Polar Molecules", Dover, New York, 1929.

[21] Yositaka Onodera, "Breakdown of Debye's model for dielectric relaxation in high frequencies", *Journal of the physical society of Japan*, vol.62, no.11, pp.4104-4107, 1993.

[22] P. Q. Mantas, "Dielectric response of materials: Extension to the Debye model", *Journal of the European Ceramic Society*, vol.19, no. 12 , pp. 2079-2086, 1999.

[23] K. S. Cole and R. H. Cole, "Dispersion and Absorption in Dielectrics - I Alternating Current Characteristics", *The Journal of Chemical Physics,* vol. 9, pp. 341-352, 1941.

[24] R A Gerhardt, "Impedance Spectroscopy and Mobility Spectra", Elsevier, 2005.

[25] D.W. Davidson and R.H. Cole, "Dielectric Relaxation in Glycerol, Propylene Glycol, and n-Propanol", *The Journal of Chemical Physics*, vol. 19, no. pp. 1484-1490, 1951.

[26] R. R. Nigmatullin, and Ya. E. Ryabov, "Cole–Davidson dielectric relaxation as a self-similar relaxation process", *Physics of the Solid State,* vol. 39**,** no. 1, pp. 87-90, 1997.

[27] D.W. van Krevelen, K. Te Nijenhuis, *"properties of polymers"*, Fourth edition, Elsevier, 2009.

[28] M. L. Levin, and M. A. Miller, "Maxwell's 'Treatise on Electricity and Magnetism'", *Soviet Physics Uspekhi*, vol. 24, no, 11, pp. 904-913, 1981.

[29] Minoru Taya, "*Electronic Composites Modeling, Characterization, Processing, and MEMS Applications*", Cambridge University Press, 2005.

[30] A. A. Al-Ghamdi, O. A. Al-Hartomy, F. R. Al-Solamy, N. Dishovsky, D. Zaimova, R. Shtarkova, And V. Iliev, "Some Factors Influencing the Dielectric Properties of Natural Rubber Composites Containing Different Carbon Nanostructures", *Materials Sciences and Applications*, vol. 7, no. 2, pp. 108-118, 2016.

[31] B. Ghule, M. Laad, "Polymer Composites with Improved Dielectric Properties", Ukrainian Journal of Physics, vol. 66, no. 2, pp. 166, 2021.

Chapter 2

Manufacturing Method and Experimental Characterization Results

Chapter 2: Manufacturing method and experimental characterization results

2.1 Introduction

Materials science has played a crucial role in the advancement of technology and the evolution of modern civilization. Research in this field continuously seeks new dielectric materials with improved and tailored properties. Consequently, the use of composite materials has significantly increased across various industrial applications.

The study of dielectric materials has been extensive since the time of James Maxwell in the nineteenth century. Characterizing these materials to predict their behavior requires both an appropriate experimental method and a mathematical model to extract their dielectric properties. Numerous measurement techniques exist, each differing in specific parameters. In our case, we use the time domain spectroscopy (TDS) technique.

This chapter provides an overview of the composite materials, the different materials used, and the techniques and procedures for preparing binary mixtures of epoxy resin and barium titanate (RE-$BaTiO_3$). It includes the selection of the volume fractions, the mixing method, mold loading, and the final phase of sample preparation. It also presents the equipment used, the experimental measurement procedure, and the methodology to extract the dielectric properties, such as dielectric constant, loss, and conductivity.

2.2 Composite materials

A composite material is generally a heterogeneous system consisting of a mixture or combination of two or more constituent materials to achieve a specific set of enhanced or desired properties that cannot be obtained from any of the original components acting alone. In such systems, a material is typically used as the matrix, while another material serves as the filler to combine the unique properties of both components.

Composite materials offer numerous advantages. Owing to their superior properties compared to conventional materials, they have become essential in a wide range of engineering applications. Their simplicity of fabrication, low cost, and high productivity make them particularly attractive for industrial use.

The dielectric properties of composites depend on several factors, including connectivity, polymer matrix type, the geometry of micro- or nanoparticles, the shape and distribution of inclusions within the matrix (with or without the use of coupling agents), as well as their volume fraction

(concentration), and the composite manufacturing process. A compromise between these different parameters is essential for developing composite materials suitable for dielectric applications [1]. Figure 2.1 illustrates the applications of dielectric composites in various fields.

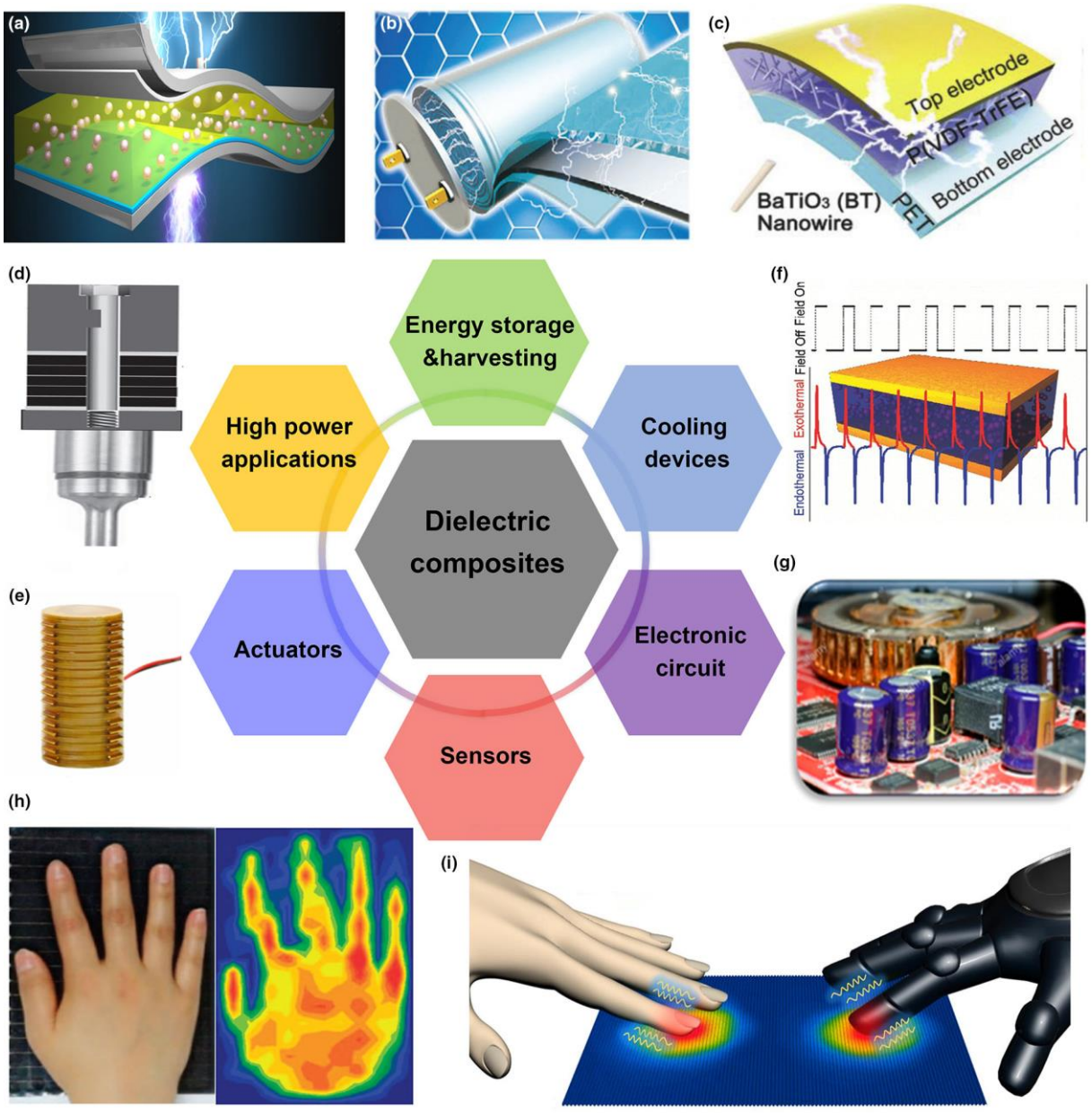

Figure 2.1: Applications of dielectric composites in various fields: (a), (b), and (c) energy storage and energy harvester; (d) high-power application; (e) actuators; (f) electrocaloric solid-state cooling devices; (g) electronic circuit; (h) and (i) pressure and temperature sensors [2].

2.3 Types of mixtures

The mixture consists of two or more substances combined into a single entity. In other words, it represents the distribution of particles within a given medium. The simple preparation process used in this study allowed for the production of dielectric composites with good particle dispersion, benefiting from the viscosity of the epoxy resin as the main mixing parameter. There are two basic types of mixtures: homogeneous and heterogeneous.

2.3.1 Homogeneous mixture

A homogeneous mixture is a system in which the components are uniformly distributed throughout the medium and exhibit the same properties across its entire volume. In other words, it does not contain clusters of different substances, and only a single phase of the material is visible.

2.3.2 Heterogeneous mixture

A heterogeneous mixture is a system in which the constituent materials are not completely mixed, and the individual particles can be observed under a microscope. The different components can be easily distinguished, and more than one phase is visible to the naked eye.

2.4 Materials used

In this work, we investigate the dielectric behavior of a binary mixture based on epoxy resin (RE) used as the polymer matrix and barium titanate ($BaTiO_3$) used as the ceramic filler.

Polymer-ceramic composites can exhibit superior dielectric properties compared to their individual constituent.

2.4.1 Epoxy resin (RE)

Epoxy resins are a typical class of thermosetting polymers made from monomers containing at least two epoxy groups. They have a wide range of industrial applications in various fields, as shown in Figure 2.2, including coatings, adhesives, and polymer matrices for advanced composites. They are also widely used in the fabrication of printed circuit boards (PCBs). This material is employed to encapsulate and package electronic components, particularly the chips and memory arrays found in a computer, because of its key performance attributes, which include excellent high-temperature stability, high mechanical strength, outstanding chemical and water resistance, good adhesion to various surfaces, and durability.

The many processing options available for epoxy resins allow them to be used in a wide range of applications [3].

The term "epoxy" has been widely adopted for various applications beyond its original use in fiber-reinforced polymer composites. However, the resin is less rigid than epoxy. The viscosity of the epoxy resin is an important parameter in the manufacture of composite materials. It ensures good dispersion of the particles.

Figure 2.2: Application of epoxy resin in various fields [3, 4].

The global demand for epoxy resins has been steadily increasing, as illustrated in Figure 2.3, which presents their distribution across various application sectors.

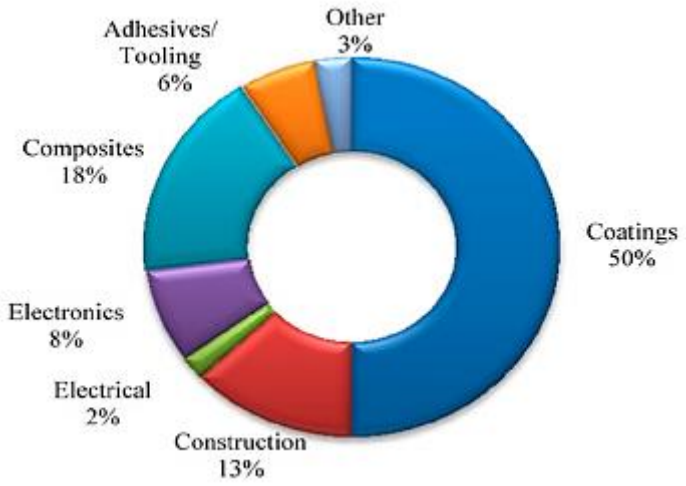

Figure 2.3: Global epoxy resin demand by sector [3].

2.4.2 Barium titanate

Barium titanate ($BaTiO_3$ *or* BT) was discovered during World War II, between 1941 and 1944, in the United States, the USSR (Russia), and Japan. In the U.S.A., research was accelerated due to wartime demands. The material was sought as a potential replacement for mica in capacitors. This interest arose from the specific properties of barium titanate, which is characterized by high dielectric permittivity [5].

Barium titanate is an inorganic compound with the chemical formula $BaTiO_3$. It is a white ceramic material in powder form and becomes transparent when prepared as large crystals. Its Curie temperature is in the range of 120 to 130 °C. Barium titanate has excellent properties, such as a high dielectric constant, low loss, high chemical stability, and a wide operating temperature range. These characteristics make it an ideal material for various applications in the fabrication of electronic components, such as capacitors, multilayer capacitors (MLCs), electromechanical transducers, and nonlinear optics, and it has found extensive use in semiconductor technology. Moreover, barium titanate is an insulating material with a large energy gap of 3.05 eV at room temperature [6].

Barium titanate is one of the most important ferroelectric, pyroelectric, and piezoelectric ceramic materials that exhibits the photorefractive effect. It is a member of a large group of compounds, which is called the perovskite family (ABO_3). The perovskite form of barium titanate exhibits one of four crystallographic structures as a function of temperature, as shown in Figure 2.4.

In the crystal structure, the barium atoms are located at the top corner of the cell, oxygen atoms occupy the centers of the faces of the cubic plane, and titanium atoms are found at the center of the octahedron formed by oxygen atoms. With decreasing temperature, barium titanate undergoes a phase transition from cubic to tetragonal (at 120 °C), then to orthorhombic (at 0 °C), and finally to rhombohedral (at -90 °C) [7]. When the temperature is higher than 120 °C, the cubic phase of barium titanate is stable and has a paraelectric property [8]. When the temperature is lower than 120 °C, the other three crystalline phases exhibit ferroelectric properties, which are attributed to the self-polarization of $BaTiO_3$ [9].

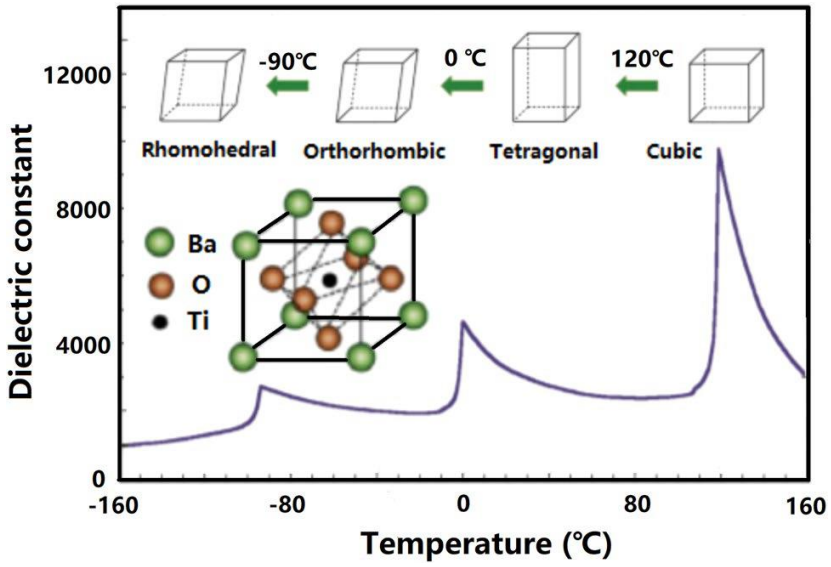

Figure 2.4: Crystallographic structures and dielectric constant of barium titanate versus temperature [10].

2.5 Experimentation Protocol

This section presents step by step, the experimental procedure for preparing samples of binary mixtures (RE-$BaTiO_3$) under laboratory conditions. It also outlines the methodology used to extract the dielectric properties in order to obtain the corresponding numerical results.

2.5.1 Samples preparation protocol

The fabricated samples are binary composites made of epoxy resin and barium titanate with their characteristics shown in Table 2.1.

Table 2.1: The used materials properties.

Material	**Molecular formula**	**Manufacture company**	**Form**	**Color**	**Volumic mass [g/cm^3]**	**Purity**	**Grain size**
Barium titanate	$BaTiO_3$	SIGMA-ALDRICH	Powder	White	6.08	99%	100 ηm
Epoxy resin (Scapa 41002)	RE	SCAPA POLYMERICS	Viscous liquid (Resin + Hardener)	Red-Yellow	1.07	/	/

The samples of binary composite are produced according to a production protocol [11–13], permitting us to obtain composite materials with reproducible dielectric properties. The manufactured polymer (epoxy resin) is utilized as a matrix that acts as a binder for barium titanate grains. Each sample includes X% epoxy resin, while the barium titanate load ratios represent Y% (Y = 100-X) of the composite, and their components change complementarily in increments of 5% up to X = 50%, as depicted in the Table below.

Table 2.2: Constituents volume fractions variation.

Volume fractions (%) / Samples	Epoxy resin (RE)	Barium titanate ($BaTiO_3$)
01	100	00
02	95	05
03	90	10
04	85	15
05	80	20
06	75	25
07	70	30
08	65	35
09	60	40
10	55	45
11	50	50

The mixtures depend on volume fractions, where the titanates are in powder form, their volume cannot be directly measured. Therefore, it is necessary to determine the corresponding masses for the desired volume fractions by following the steps below.

- Define the total volume V_{tot} of a the sample based on the dimensions of the mold.
- Determine the volume fraction of the matrix (epoxy resin) F_{matrix}, and calculate its volume: $V_{matrix} = V_{tot} * F_{matrix}$
- Determine the volume fraction of the filler ($BaTiO_3$) F_{charge}, and calculate the corresponding volume: $V_{charge} = V_{tot} * F_{charge}$
- Finally, calculate the mass of the filler m_{charge} using its density:

$$m_{charge} = D_{charge} * V_{charge}$$

The different powders were weighed using a high-precision electronic balance.

The resin is prepared by pouring equal volumes of pure epoxy resin and hardener into a container. The two components are mixed until a uniform viscous liquid is obtained.

During mixing, air bubbles may appear, but they are gradually released from the resin.

Next, the desired fillers are added, and the entire mixture is stirred thoroughly until no isolated powder grains remain. The powder grains become bound together after the epoxy resin polymerizes, which should coat all of the grains.

Mixing continues in order to obtain the most homogeneous mixture possible, ensuring that the resin uniformly coats the powder. It should be noted that the mixing stage plays a crucial role in determining the homogeneity and overall quality of the final product.

After that, the mixture is gently poured into the chosen mold.

These combos are prepared at ambient temperature and beneath atmospheric pressure. Once the specimens have been hardened, the resulting specimens are machined in a way to adapt the specimens to the size of the coaxial line measuring cell used in the TDR measuring device. These specimens have a toroidal form compatible with the used APC-7 mm coaxial guide, as illustrated in Figure 2.5.

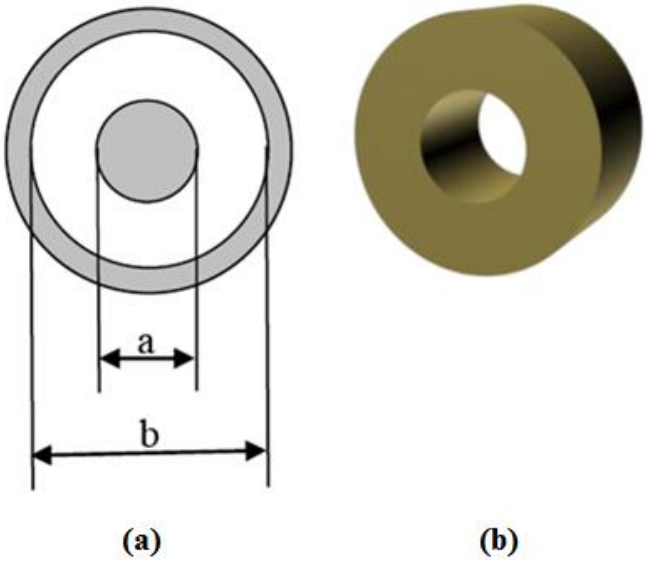

Figure 2.5: The shape of: (a) the guide and (b) the sample.

2.5.2 Measurement experimental procedure

The dielectric properties were determined using time domain spectroscopy (TDS) [14, 15]. This measurement method is based on a system constructed of a step generator (HP 54121 model) offering a 200 mV amplitude level and has a 35 ps rise time with an embedded sampling head, combined with a digital oscilloscope mainframe (HP 54120B model). The signal coming from the

step generator propagates alongside an APC-7mm precision standard coaxial guide providing characteristic impedance equal to 50 Ω. This line is attached to an APC-7 mm/ 50 Ω probe, in which our toroidal form specimen is placed at its input, and a matched load (50 Ω) is placed at the other end (termination) to remove undesired reflections following the "matched line" measurement technique used in this work. This apparatus requires, in addition to a digital acquisition system connected to a computer, an appropriate set of software to process and store experimental data in the time and frequency domain [16–18]. Figure 2.6 depicts an illustration of such a system.

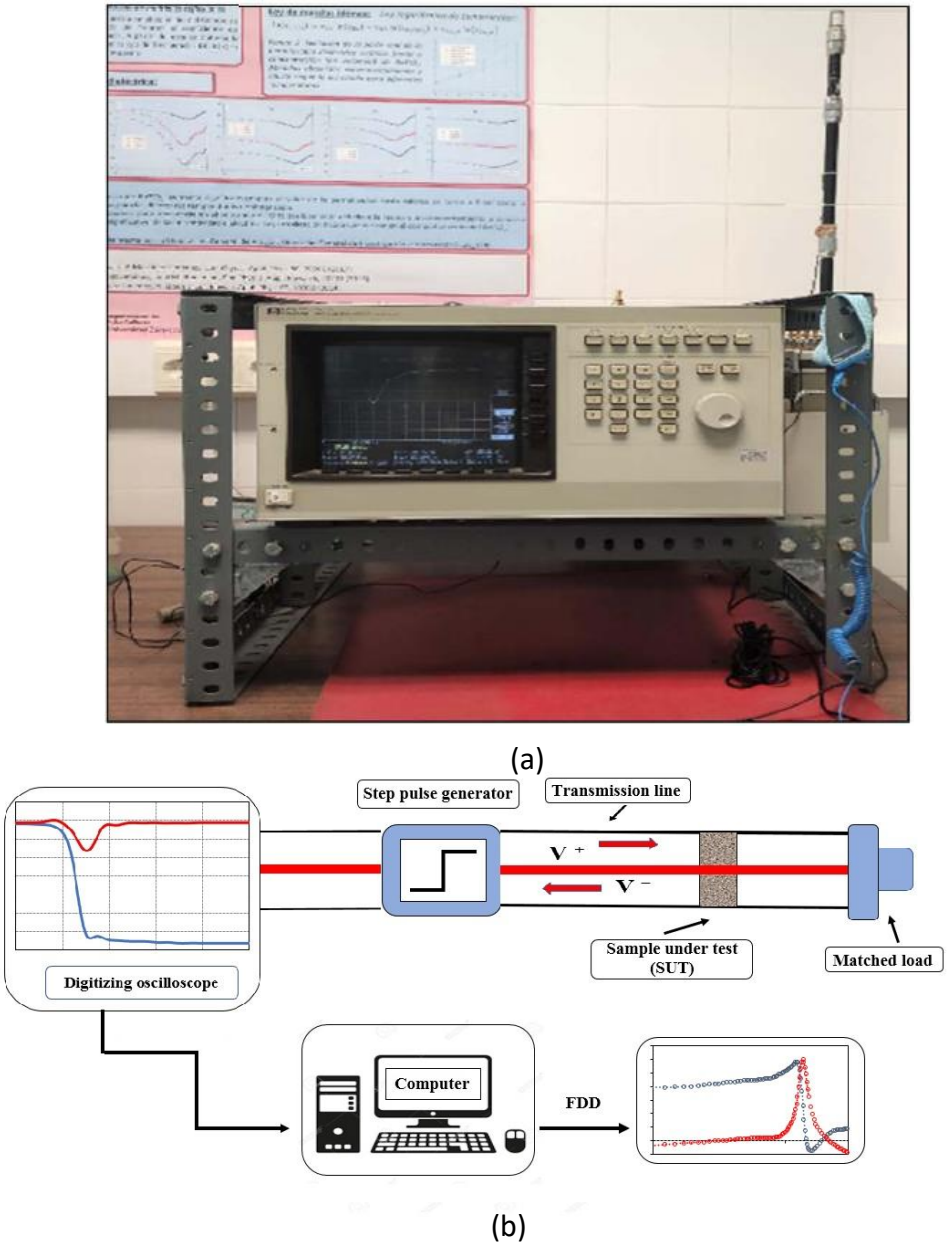

Figure 2.6: (a) TDS experimental setup. (b) TDS circuit diagram.

2.5.3 Data processing and parameters extraction

Multiple reflections have been chosen as the experimental strategy. To cast off unwanted reflections, the line is load matched on the end. The set-up is depicted in Figure 2.6. This technique uses time signal processing that is obtained accurately from a digital sampling oscilloscope. This signal indicates the sample under test's (SUT), TDR system response. The reflection coefficient $\Gamma(\omega)$ is the first variable on which all calculations are made. This is constructed from the experimental data after applying the Fourier transform [19].

This parameter is defined in the frequency domain as the ratio of the reflected signal $V^-(t)$ to the incident signal $V^+(t)$

$$\Gamma(\omega) = \frac{V^-(\omega)}{V^+(\omega)} \tag{2.1}$$

where $V^-(\omega)$ and $V^+(\omega)$ are derived from the measured time response of the sample $V_s(t)$ which is written as:

$$V_s(t) = V^-(t) + V^+(t) \tag{2.2}$$

The complex dielectric permittivity, which gives facts about the dielectric behavior and the Ohmic aspect of the processed material produced by this element, is another essential parameter in our study. It may be determined from the admittance ratio that is expressed by:

$$\frac{Y_{in}(\omega)}{Y_0} = \frac{\sqrt{\varepsilon^*}.\tanh\left(j.\frac{\omega d}{c}.\sqrt{\varepsilon^*}\right) + 1}{1 + \frac{\tanh(j.\frac{\omega d}{c}.\sqrt{\varepsilon^*})}{\sqrt{\varepsilon^*}}} \tag{2.3}$$

where:

$$Y_{in}(\omega) = \frac{1 - \Gamma(\omega)}{1 + \Gamma(\omega)} \tag{2.4}$$

and ω is the angular frequency, d the sample thickness, and c the vacuum light speed. The $tanh$ function, which may be deduced by many numerical techniques [20], helps efficaciously to solve the transcendental equation on a complex plane by showing different solutions.

The Debye model is needed for the study in a wide frequency band to generate a complex dielectric permittivity withinside the shape of ε_s and ε_∞, representing the static and high frequency permittivities, respectively.

$$\varepsilon^* = \varepsilon' - j\varepsilon'' = \varepsilon_\infty + \frac{\varepsilon_s - \varepsilon_\infty}{1 + j\omega\tau} - j\frac{\sigma_s}{\omega\varepsilon_0} \quad (2.5)$$

In the third term of this equation, we can see the presence of the parameter σ_s, representing the material's static conductivity. This parameter, which is predominant in low frequency domain, is included in the complex permittivity imaginary component as follows:

$$\varepsilon'' = \frac{\sigma_s}{\omega \,.\, \varepsilon_0} \quad (2.6)$$

The losses in dielectrics are usually described using a parameter called the dielectric loss tangent, which is defined as the ratio between the imaginary component and the real portion of the complex permittivity (ε^*):

$$tan\delta = \frac{\varepsilon''}{\varepsilon'} \quad (2.7)$$

where δ represents the phase shift angle between the voltage applied to the dielectric and the current flowing through it. These losses are also expressed through the quality factor (Q) as follows:

$$tan\delta = \frac{1}{Q} \quad (2.8)$$

2.5.4 Dielectric behavior results and discussion

The focus is on presenting the different dielectric properties experimental results for the binary composite ($RE\text{-}BaTiO_3$), which is obtained using the time domain spectroscopy method. This research objective is to examine the effect of barium titanate on the dielectric behavior with several volume fractions of resin epoxy (from 50% to 100% in steps of 5%).

Figure 2.7 illustrates the evolution of the real part of the complex permittivity as a function of volume fraction of the barium titanate, for the binary composite based on epoxy resin, and barium titanate. Examining the graphs, it can be observed that the real permittivity (ε') of the composite increases appreciably while the concentration of barium titanate rises. The peak value estimated at 11.88 is reached with a 50% volume fraction of barium titanate. On the other hand, the lower value obtained for this composite is 2.4058, and it is reached for a 100% volume fraction of epoxy resin (without barium titanate). With this volume fraction, we speak of pure epoxy resin.

This obtained dielectric parameter is probably due to the real permittivity value of epoxy resin, which is lower than that of barium titanate.

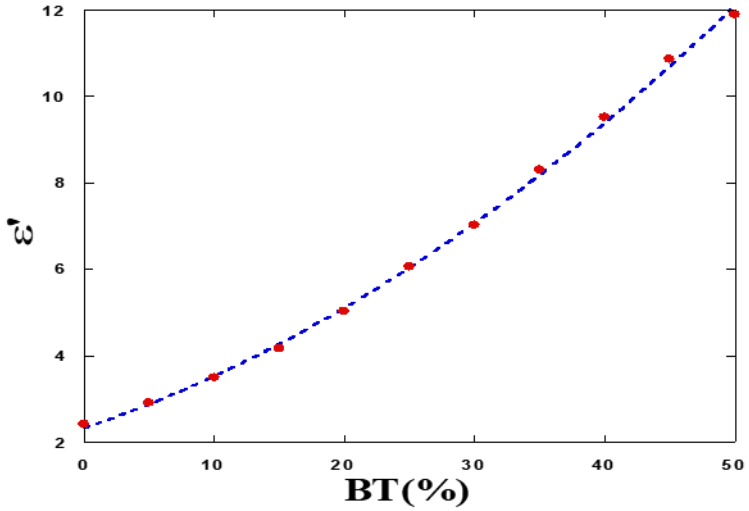

Figure 2.7: Real permittivity (ε') evolution as a function of the volume fraction of barium titanate.

The same behavior was noticed in composites based on epoxy resin and titanate with Fe_3O_4, CuO, MgO, ZnO, or CaO, but the opposite phenomenon was observed for the composite made of epoxy resin and titanate with MnO_2, this is due to the effect of titanate on epoxy resin and the different oxides [12, 13, 21, 22].

Figure 2.8 shows the imaginary part of the complex permittivity, the variation of the binary composite ($RE\text{-}BaTiO_3$) as a function of the barium titanate concentration.

Upon analyzing the graphical outcomes, it appears clear that the imaginary permittivity (ε'') is near zero at all volume fractions of barium titanate. This is consistent with the very low conductivity values that characterize the two components: barium titanate and epoxy resin.

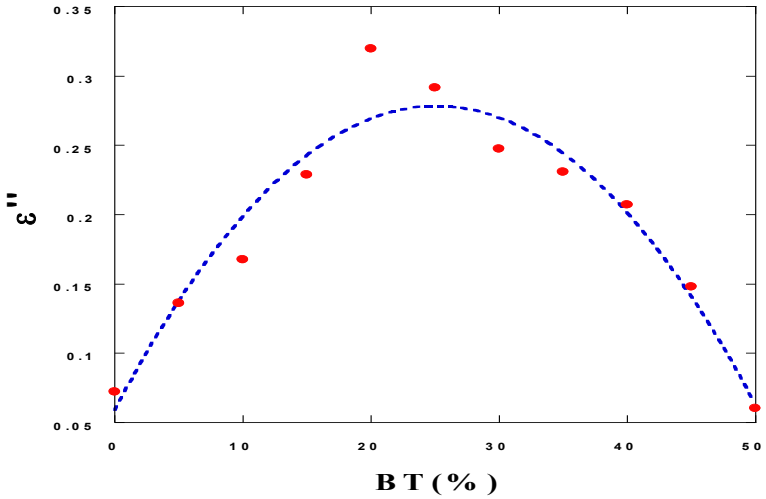

Figure 2.8: Imaginary permittivity (ε'') evolution as a function of the volume fraction of barium titanate.

Figure 2.9 represents dielectric loss tangent ($\tan\delta$) evolution for the binary composite (RE-$BaTiO_3$) as a function of the barium titanate concentration. By analyzing the graph, we can see that the loss tangent values show a strong change in the behavior for a 20% concentration of barium titanate. Below this volume fraction, the dielectric loss tangent varies between 0.0299 and 0.0636 which in fact explains the drop in the quality factor (Q) from 33.41 to 15.72. However, above this concentration, a decrease in this parameter to reach a minimum value of 0.005 can be observed, which actually explains the increase in the quality factor from 15.72 to 196.68. The resulting values are considered to be relatively high, enabling us to store the maximum amount of energy with the least amount of dissipation. We noticed the opposite behavior with composites based on epoxy resin and titanate with Fe_3O_4, this is probably due to the oxide effect [21].

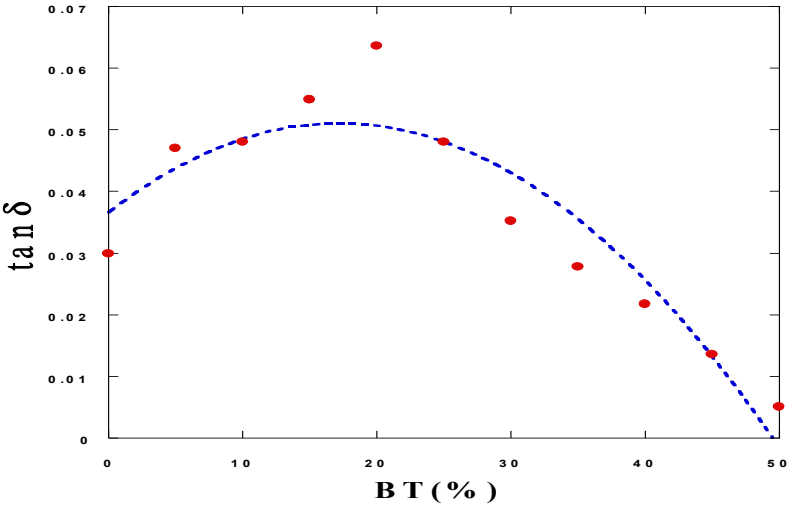

Figure 2.9: Dielectric loss tangent ($\tan\delta$) variation.

Regarding the conductivity (σ), Figure 2.10 illustrates the variation of this parameter as a function of the barium titanate concentration. Through this representation, we can see that for a concentration of the order of 20% barium titanate appears to cause a strong change in the mixture behavior. Below this volume fraction, it is essential to note an increment in a quasi-polynomial manner of the conductivity with the barium titanate proportions to reach a maximum value of 10.6543×10^{-3} $(\Omega.m)^{-1}$. Above this concentration, one can observe a drop in this parameter reaching a minimum value of 2.0169×10^{-3} $(\Omega.m)^{-1}$. The opposite behavior was observed in Ref. [23] which is a binary composite made of epoxy resin and calcium titanate.

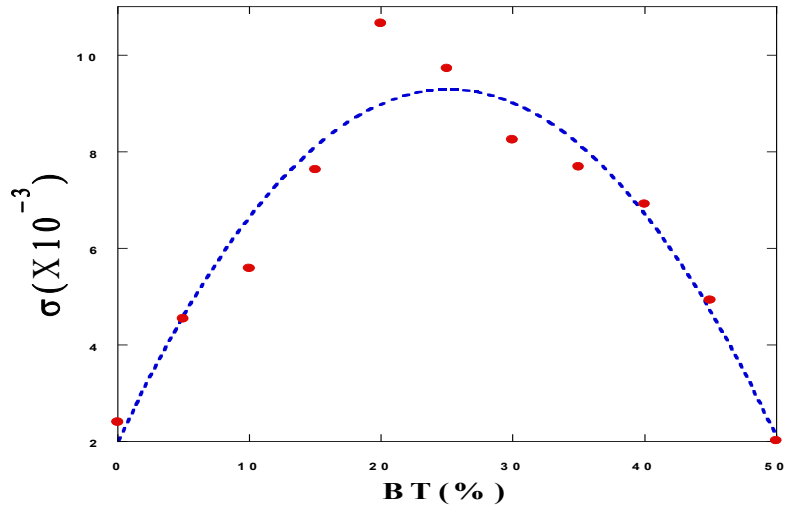

Figure 2.10: Conductivity (σ) profile.

Figure 2.11 represents the evolution of resonance frequency (f_r) for the binary composite based on epoxy resin and barium titanate. It is shown graphically that increasing the quantity of barium titanate caused an almost polynomial drop of the resonance frequency from a maximum value equal to 27.669 GHz for a barium titanate concentration of 5% to reach a minimum value equal to 9.969 GHz for a barium titanate concentration of 50%. The same behavior was found in Ref. [21]. Increasing in the inclusion quantity of barium titanate has led to a drop in the resonance frequency and thus, reaching a minimum value.

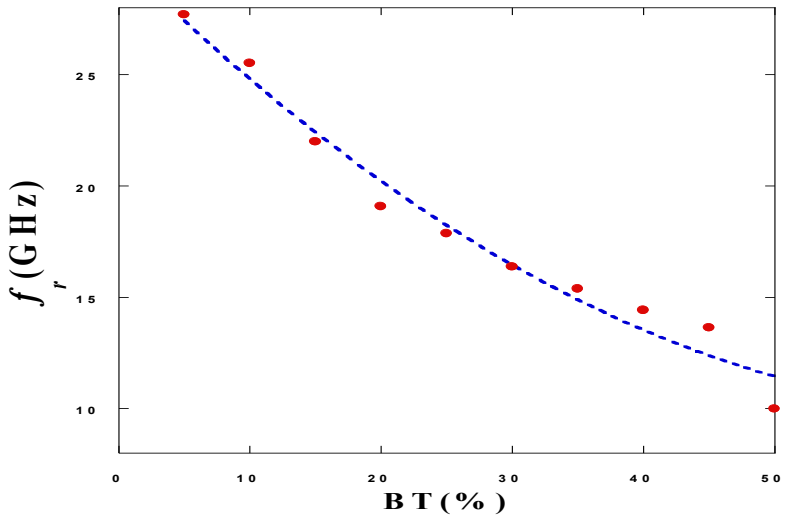

Figure 2.11: Variation of the resonance frequency(f_r).

2.6 Conclusion

In this chapter, we presented the different steps of the experimental method used to predict the behavior of dielectric materials. We also provided an overview of the composite materials and the various materials employed. Additionally, we described the techniques and procedures used to prepare samples of a binary mixture based on epoxy resin and barium titanate ($RE\text{-}BaTiO_3$). The experimental measurement procedures, including the equipment used and the methodology applied to extract the dielectric properties, were also discussed. Findings presented in terms of the properties of the binary composites demonstrate that the materials exhibit low permittivity values and low dielectric losses.

The results obtained are expected to contribute to the development of new materials suitable for potential applications in the telecommunications domain, specifically focusing on microelectronic components utilized in telecommunication systems, such as resonators, substrates, cavities, PTC

devices, filters, antennas, wave absorbers, pulse-generating devices, multilayer ceramic capacitors, ultrasonic transducers, and sensors.

References

[1] Adel Zyane. "*Utilisation de voie écologique et économique pour l'élaboration de nouveaux matériaux composites diélectriques verts*", Thèse de doctorat en cotutelle de l'Université Cadi Ayyad de Marrakech et de l'Université du Québec à Trois-Riviéres, 2016. ""

[2] H. Wu, F. Zhuo, H. Qiao, L. Kodumudi Venkataraman, M. Zheng, S. Wang, H. Huang, B. Li, X. Mao, and Q. Zhang, "Polymer-/Ceramic-based Dielectric Composites for Energy Storage and Conversion", *Energy and Environmental Materials,* vol. 5, no. 2, pp. 486-514, 2022.

[3] H. Memon, Y. Wei, and C. Zhu, "Recyclable and reformable epoxy resins based on dynamic covalent bonds–Present, past, and future", *Polymer Testing,* vol. 105, no. 10, pp. 1-19, 2022.

[4] M.A. Rashid, W. Liu, Y. Wei, and Q. Jiang. "Review on intrinsically recyclable flame retardant thermosets enabled through covalent bonds", *Journal of Applied Polymer Science,* vol. 139, no. 27, pp. 1-22, 2022.

[5] C.A. Randall, R.E. Newnham, and L.E. Cross. "History of the First Ferroelectric Oxide, BaTiO3", *Materials Research Institute. The Pennsylvania State University*. University Park, PA 16802 USA, 2004.

[6] Katsuyoshi Kondoh, *Powder Metallurgy*, InTech, 2012.

[7] M.J. Pan, and C.A. Randall, "A brief introduction to ceramic capacitors", *IEEE Electrical Insulation Magazine.* vol. 26, no. 3, pp. 44-50, 2010.

[8] J. Döring, D. Lang, L. Wehmeier, F. Kuschewski, T. Nörenberg, S.C. Kehr, and L.M. Eng, "Low-temperature nanospectroscopy of the structural ferroelectric phases in single-crystalline barium titanate", *Nanoscale,* vol. 10, no. 37, pp. 18074– 18079, 2018.

[9] Dang-Hyok Yoon, "Tetragonality of barium titanate powder for a ceramic capacitor application", *Journal of Ceramic Processing Research,* vol. 7, no. 4, pp. 343-354, 2006.

[10] Jun Su, and Jun Zhang. "Recent development on modification of synthesized barium titanate ($BaTiO_3$) and polymer/$BaTiO_3$ dielectric composites", *Journal of Materials Science: Materials in Electronics.* vol. 30, no. 3, pp. 1957–1975, 2019.

[11] N. Bouzit, J.M. Fornies-Marquina, A. Benhamouda, and N. Bourouba. "Modeling and dielectric behavior of ternary composites of epoxy (BaTiO3/CaTiO3)", *The European Physical Journal Applied Physics,* vol. 38, no. 2, pp. 147-152, 2007063, 2007.

[12] A. Benhamouda, J. M. Fornies-Marquina, N. Bouzit, and N. Bourouba. "Dielectric behavior of ternary composites of epoxy/BaTiO3/(CuO or MgO)", *The European Physical Journal Applied Physics,* vol. 46, no. 2, pp. 1-6, 20404, 2009.

[13] N. Bourouba, K. Lalla, J. P. Martinez Jimenez, and N. Bouzit. "Dielectric behavior of ternary mixtures: epoxy resin plus titanates (MgTiO3, CaTiO3 or BaTiO3) associated to oxides (CaO, MnO2 or ZnO)", *The European Physical Journal Applied Physics,* vol. 65, no. 1, pp. 1-8, 10202, 2014.

[14] A. M. Bottreau, N. Bouzit, and A. Merzouki. "dielectric behavior study of some composites polyester/MTiO3 by time domain spectroscopy", *The European Physical Journal Applied Physics,* vol. 18, no. 1, pp. 17-24, 2002022, 2002.

[15] M. Bouchaour, J. P. Martinez Jimenez, N. Bouzit, and N. Bourouba. "Dielectric behavior of a quaternary composite (RE, BT, MnO2, CaO) in the band (DC–2GHz)", *The European Physical Journal Applied Physics,* vol. 84, no. 1, pp. 1-10, 10201, 2018.

[16] D. Djouada, N. Bouzit, R. Delfouf, L. Chioukh, and J. P. Martinez Jiménez. "Dielectric characterization of heterogeneous composites using time domain spectroscopy and microwave test benches in microwave frequency", *ECS Journal of Solid State Science and Technology,* vol. 12, no. 6, 063003, 2023.

[17] H. Bakhti, N. Bouzit, N. Bourouba, and J. P. Martinez Jimenez. "Dielectric behavior of a sintered heterogeneous ternary composite resin/BT/Cu_2O", *The European Physical Journal Applied Physics,* vol. 80, no. 2, pp. 1-9, 20202, 2017.

[18] T. Arab, R. Delfouf, H. Khouni, N. Bouzit, D. Djouada, J. P. Martinez Jiménez, and N. Bourouba. "Investigation on dielectric, electric and magnetic properties of (epoxy resin-titanate-oxide-ferrite) ternary composites at microwave frequency", *ECS Journal of Solid State Science and Technology,* vol. 12, no. 4, 043005, 2023.

[19] T. Arab, H. Khouni, N. Bouzit, and J. P. Martínez Jiménez. "Study of dielectric behavior of ternary composites of epoxy-barium titanate with iron oxide and ferrite in the band (DC-12.5 GHz)", *Inorganic and Nano-Metal Chemistry*, vol. 54, no. 2, pp. 191-199, 2024.

[20] H. Khouni, N. Bouzit, J. P. M. Jiménez, and M. Bouamar. "Study of dielectric behavior of ternary mixtures of epoxy/titanates (MgTiO3, CaTiO3, SrTiO3 and BaTiO3) with carbon black", *The European Physical Journal Applied Physics,* vol. 76, no. 2, pp. 1-9, 10201, 2016.

[21] R. Delfouf, N. Bouzit, N. Bourouba, J. P. Martinez Jiménez, A. Brahimi, H. Khouni, and T. Arab. "Dielectric characterization and modeling of composite materials based on epoxy resin/black iron oxide/titanates in several frequency ranges", *ECS Journal of Solid State Science and Technology*, vol. 11, no. 7, 073006, 2022.

[22] A. Brahimi, N. Bourouba, J. P. Martinez Jimenez, and N. Bouzit. "A high frequency dielectric behavior modeling of a ReXTMnO2 ternary composite as an equivalent binary mixture", *Journal of Composite and Advanced Materials*, vol. 31, no. 4, pp. 181-191, 2021.

[23] V. Pascariu, G. N. Pascariu, and P. Gasner. "Characterization of dielectric mixtures TCA/RE and TBA/RE by the time domain reflectometry (T.D.R)", *Journal of Optoelectronics and Advanced Materials*, vol. 10, no. 7, pp. 1857-1860, 2008.

Chapter 3

Basic Principles of Dielectric Resonator Antennas

Chapter 3: Basic principles of dielectric resonator antennas

3.1 Introduction

Since the beginning of humanity, means of communication have taken various forms, such as words, gestures, signals, etc. Humans have made both intellectual and physical efforts to develop reliable means of communication. Among these, the antenna has proven to be one of the most effective tools for transmitting and sharing information anywhere in the world, at any time. The current boom in communications requires major innovations in antenna design to achieve high-speed and high-data-rate transmission. Meeting this challenge requires combining advanced materials and optimized geometries designed for specific functions. Today, antennas are applied in numerous technological fields, including mobile communications, radar, satellites, broadcasting, identification systems, automobiles, airplanes, health, the Internet of Things, etc. Antenna technology represents a revolutionary field that continues to be the focus of extensive research and development.

This chapter presents the most important theoretical concepts of dielectric resonator antennas (DRAs), highlighting their basic parameters, attractive features, commonly used shapes, and typical feeding mechanisms. The discussion then focuses on rectangular and cylindrical dielectric resonator antennas on which this thesis is based, including their main resonant modes, field distribution, and resonance frequencies. Next, we talk about the different ways to improve bandwidth and gain, as well as methods employed for multiband operation. Understanding these concepts is crucial for optimizing the design and performance of dielectric resonator antennas. Moreover, having a general understanding of how these principles work is essential when selecting an antenna and serves as the basis for the following chapter.

3.2 Definition of an antenna

The concept of the first antenna was introduced by the German physicist Heinrich Hertz, who experimentally demonstrated the existence of electromagnetic waves transmitted through the air in 1887, thereby confirming Maxwell's hypothesis [1]. In 1901, Guglielmo Marconi achieved the first long-distance wireless communication link across the Atlantic Ocean [2].

In wireless communication systems, an antenna is an essential component for radiating or receiving electromagnetic waves. The function of a transmitting antenna is to convert electrical energy into electromagnetic waves, enabling transmission between a transmitting antenna and a

receiving antenna in free space. Conversely, a receiving antenna captures electromagnetic waves propagating through free space and converts them into an electric current.

The purpose of transmitting and receiving radio waves is to communicate or broadcast information at the speed of light. The term "radiation" refers to the propagation of the waves emitted by a source in free space. In other words, a radiation source can be defined as a localized distribution of time-varying current density.

Antennas can take many forms to meet specific requirements. Consequently, there are numerous types of antennas, including wire, horn, microstrip, dielectric resonator, and array, among others.

3.3 Dielectric resonator antenna (DRA)

Richtemeyer first introduced dielectric resonators in 1939, being the first to demonstrate that a dielectric object can resonate in different modes [3]. Initially, these resonators were primarily used in applications such as filters, oscillators, and microwave components during the 1960s [4-6]. Until 1983. Long et al. [7] were the first to suggest that dielectric resonators possess properties suitable for use as radiating devices. They reported an experiment called dielectric resonator antennas (DRAs). Since then, extensive research has been devoted to the analysis of various geometric shapes using different feeding techniques to improve antenna parameters. DRAs offer excellent performance and provide an alternative solution to microstrip technology in terms of bandwidth, compactness, and radiation efficiency, owing to the absence of metallic losses. Furthermore, the presence of multiple resonant modes in a single radiating element means that multiple frequency bands or a wide bandwidth can be achieved. A dielectric resonator antenna can be fabricated from dielectric materials with various relative permittivity (dielectric constant) values and low loss. Its resonant frequency depends on its shape, size, and material permittivity. The DRA is becoming an important device for microwave and millimeter-wave radiation applications. The frequency spectrum used for different communication is given in Figure 3.1.

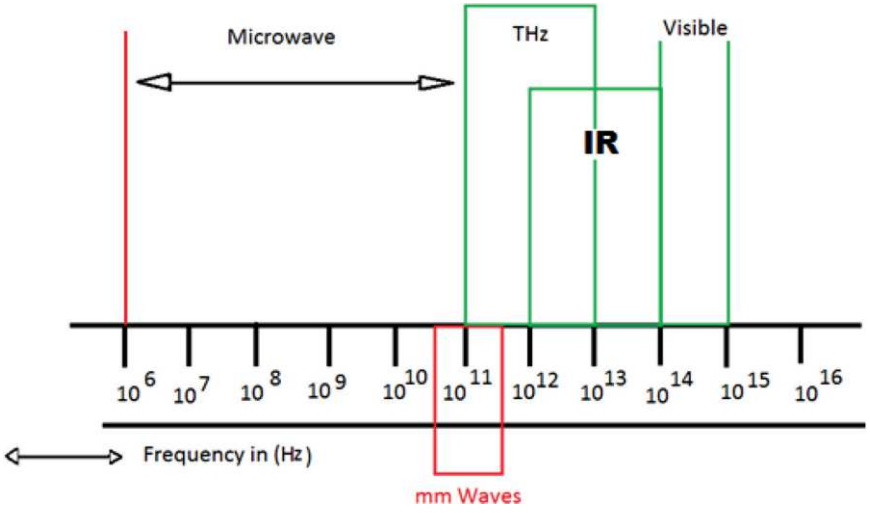

Figure 3.1: Frequency spectrum used for communication [8].

3.4 Antenna parameters

To describe an antenna and evaluate its performance, it is necessary to define its parameters. The main antenna parameters can be classified into two groups. The first group characterizes the antenna as an electrical circuit element (Z_{in} and S_{11}), while the second group describes its radiation properties, including radiation pattern, directivity, and gain [8-11].

3.4.1 Reflection coefficient

The reflection coefficient of a transmission line is defined as the ratio of the complex amplitude of the reflected wave to the complex amplitude of the incident wave.

$$\Gamma = \frac{E_r}{E_i} \tag{3.1}$$

The reflection coefficient (Γ or S_{11}) is used to characterize the antenna. It is related to the input impedance of the antenna through a classical relationship when its equivalent circuit as a transmitting element represents the antenna.

$$\Gamma = \frac{Z_{in} - Z_0}{Z_{in} + Z_0} \tag{3.2}$$

Where $Z_{in} = R_{in} + jX_{in}$ is the input impedance, and Z_0 is the normalized impedance, usually equal to 50 ohms in microwave technology. The input impedance Z_{in} is an important parameter that determines the incident and reflected waves.

Normally, Z_{in} is kept as close as possible to Z_0 to achieve an impedance matching condition between the feed and the antenna. Under perfect matching conditions, the reflection coefficient (Γ) is zero, the voltage standing wave ratio ($VSWR$) is 1, and the return loss (RL) is infinite, which is the ideal case with no reflected wave.

where the voltage standing wave ratio ($VSWR$) is defined by the following expression:

$$VSWR = \frac{1 + |\Gamma|}{1 - |\Gamma|} \tag{3.3}$$

and the reflection coefficient (S_{11}), can also be expressed in decibels as follows:

$$S_{11}(dB) = 20 \times log(|\Gamma|) \tag{3.4}$$

For the value of the reflection coefficient ($S_{11} \leq -10\ dB$), the reflected power is 10% of the incident power. In other words, 90% of the power is radiated into free space. The value of the reflected power can be calculated as follows:

$$-10 = 10 \times log\left(\frac{P_r}{P_i}\right) \tag{3.5}$$

$$P_r = 0.1 \times P_i \tag{3.6}$$

3.4.2 Bandwidth

The bandwidth is another fundamental antenna parameter that defines the frequency range over which the antenna operate properly while maintaining the desired radiation characteristics. Bandwidth is one of the most important requirements in wireless communication systems, as it directly influences data transmission rates. Typically, the impedance bandwidth (BW) is obtained from the reflection coefficient curve and is defined as the frequency range between the upper (f_h) and lower (f_l) cut-off frequencies in the plot of the reflection coefficient ($S_{11} \leq -10dB$), as illustrated in Figure 3.2. The Fractional bandwidth (FBW) is defined by the following relationship:

$$FBW = 2 \times \frac{f_h - f_l}{f_h + f_l} \times 100\% \tag{3.7}$$

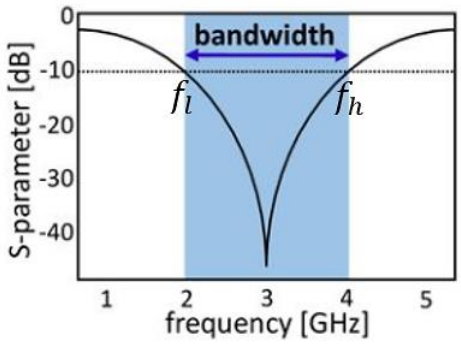

Figure 3.2: The impedance bandwidth of an antenna.

3.4.3 Radiation pattern

The radiation pattern of an antenna is a mathematical function or graphical representation that illustrates the power radiated by an antenna in different spatial directions, this radiation pattern characterizes the electromagnetic field at a given frequency. In most cases, the radiation pattern in the far field (at a sufficient distance from the antenna) is considered a function of the direction of radiation. The radiation characteristics include power flux intensity, directivity, and gain.

The radiation pattern of the antenna can be represented in three dimensions ($3D$). By taking cross-sections of the 3D pattern in the xz and yz planes, two-dimensional (2D) radiation patterns can be obtained, as illustrated in Figure 3.3. The spherical coordinate system showing the beam area is conveniently used to describe the radiation of an antenna, as shown in Figure 3.4. The radiation pattern is typically plotted on a logarithmic scale, most often in decibels (dB).

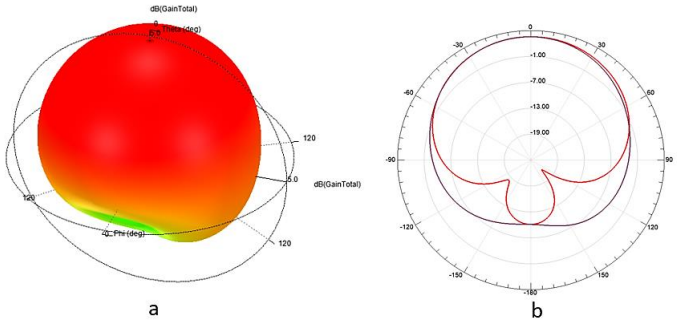

Figure 3.3: Radiation pattern, (a) $3D$ and (b) $2D$.

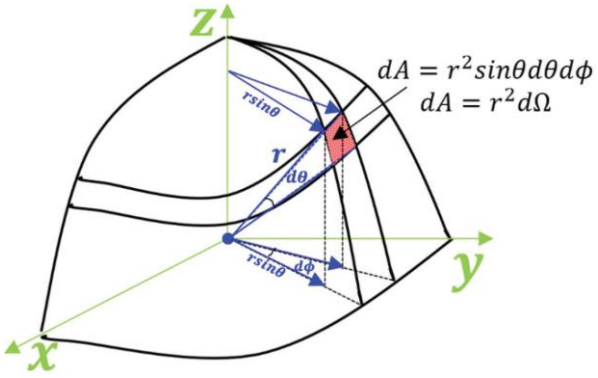

Figure 3.4: Spherical coordinate system showing the beam area [8].

Where Ω represents the solid angle subtended by the area dA. The solid angle subtended by a sphere is 4π. Hence, the area of a sphere is $4\pi r^2$. The unit of the solid angle is the steradian (sr) or square degree.

3.4.4 Directivity

Directivity is a measure of the concentration of the radiation from an antenna in a particular direction. It is defined as the ratio of the radiation intensity in the main beam to the average radiation intensity in all directions (power radiated by an isotropic antenna). Directivity is a unitless quantity.

An antenna that radiates equally in all directions is called isotropic. An antenna that radiates equally in all horizontal directions but not in the vertical direction is called omnidirectional. And an antenna that concentrates its radiation in a specific direction is known as directional. For an isotropic antenna, $D = 1$ or $0\ dBi$. Directivity is expressed as a function of the directional angles.

$$D(\theta, \varphi) = \frac{U(\theta, \emptyset)}{U_{iso}} = \frac{4\pi \cdot U(\theta, \emptyset)}{P_{rad}} \tag{3.8}$$

Where θ and $\emptyset$ represent the elevation and azimuth angles, respectively, in the standard spherical coordinate system, $U(\theta, \emptyset)$ is the radiation intensity, and P_{rad} is the total power radiated by the antenna.

3.4.5 Antenna gain

Antenna gain is an important parameter that determines how effectively an antenna transmits or receives signals. In simple terms, gain indicates how well an antenna concentrates its radiated power in a particular direction compared to an ideal isotropic antenna, which radiates equally in

all directions. In practice, real antennas do not radiate uniformly. They focus energy more strongly in certain directions, resulting in improved range in those directions but reduced coverage elsewhere. This balance is important when selecting an appropriate antenna. The gain is given by the following relation:

$$G(\theta,\varphi) = \frac{4\pi \cdot U(\theta,\emptyset)}{P_{in}} \tag{3.9}$$

Where $U(\theta,\emptyset)$ is the radiation intensity and P_{in} is the power available at the antenna input.

3.4.6 Radiation efficiency

The difference between the power available at the antenna input P_{in} and the radiated power P_{rad} corresponds to the various losses within the antenna, these losses are characterized by the radiation efficiency η_{rad} of an antenna.

$$\eta_{rad} = \frac{P_{rad}}{P_{in}} \tag{3.10}$$

Therefore, the gain is related to the directivity by the following equation.

$$G(\theta,\emptyset) = \eta_{rad} \times D(\theta,\emptyset) \tag{3.11}$$

3.4.7 Polarization in dielectric resonator antenna

The polarization of an antenna is defined as the polarization of the transmitted (radiated) waves. In other words, polarization is determined by the electric field vector of an antenna oriented in space as a function of time. There are three types of antenna polarization: linear, circular, and elliptical, as illustrated in Figure 3.5. In wireless communication systems, antenna polarization plays a critical role in determining the propagation characteristics of transmitted signals and can significantly affect signal quality and reliability. If the electric field vector traces a straight line over time, the wave is said to be linearly polarized. If it traces a circle, the wave is circularly polarized (with either a left-hand or right-hand sense). Most antennas are linearly polarized because circular or elliptical polarization requires a specialized design that combines both vertical and horizontal linear polarization components. The components of the electric field can be expressed as follows:

$$E_x = E_{x0}\cos(wt + kz + \emptyset_x) \tag{3.12}$$

$$E_y = E_{y0}\cos(wt + kz + \emptyset_y) \tag{3.13}$$

where E_{x0} and E_{y0} are the amplitudes of the electric field components in the x and y directions, respectively.

❖ Linear polarization (LP)

In this case, the electric field oscillates in a single plane.

We have $\Delta\emptyset = \emptyset_y - \emptyset_x = n\pi$ where $n = 0,1,2,3$ ...

1. When $E_{x0} = E_{y0}$ and $\Delta\emptyset = 0$, the polarization is called slant polarization, where the electric field oscillates at an angle of 45^0.
2. When $E_{x0} = 0$ and $\Delta\emptyset \neq 0$, the polarization is called vertical polarization.
3. When $E_{y0} = 0$ and $\Delta\emptyset \neq 0$, the polarization is called horizontal polarization.

❖ Circular polarization (CP)

Circular polarization occurs when the amplitude of two field components are equal and the phase difference between them is an odd multiple of $\pi/2$, that is:

$E_{x0} = E_{y0}$ and $\Delta\emptyset = \emptyset_y - \emptyset_x = \pm(\frac{\pi}{2} + n\pi)$ where $n = 0,1,2,3$ ...

Circular polarization can be classified into two categories, such as right-hand circular polarization (RHCP) and left-hand circular polarization (LHCP).

❖ Elliptical polarization (EP)

Elliptical polarization refers to an electrical field that propagates in an elliptical helix. It occurs when the amplitudes of the two components are unequal and the phase difference between them is an odd multiple of $\pi/2$, or when the phase difference between them is not a multiple of $\pi/2$, regardless of their amplitudes. This means that:

$E_{x0} \neq E_{y0}$ and $\Delta\emptyset = \emptyset_y - \emptyset_x = \pm(\frac{\pi}{2} + n\pi)$ where $n = 0,1,2,3$ ...,

Or $\Delta\emptyset = \emptyset_y - \emptyset_x = \pm n\frac{\pi}{2}$ where $n = 0,1,2,3$ ...,

Elliptical polarization can also be classified into two categories: either right-hand (RHEP) or left-hand (LHEP).

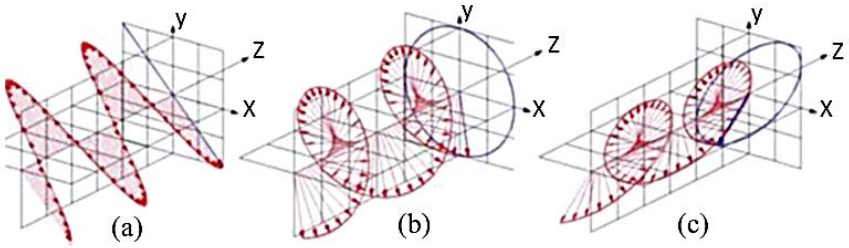

Figure 3.5: Polarized waves by an antenna: (a) linear, (b) circular, and (c) elliptical.

3.4.8 Aaxial ratio

The axial ratio (AR) is defined as the ratio of the major axis to the minor axis of an ellipse, as illustrated in Figure 3.6. It is expressed by the equation $AR = OA/OB$. When $AR = 1$, this is the circular polarization, and when $AR = \infty$, it is linear polarization.

In general, it is difficult to obtain $AR = 1$. Therefore, in the case $OB = OA/\sqrt{2}$, which means $AR = 3\ dB$, we consider the criteria for obtaining the circular polarization waves from an antenna.

The AR bandwidth refers to the frequency range where AR remains less than or equal to $3\ dB$. Any antenna is considered circularly polarized if both the impedance passband $S_{11} \leq -10\ dB$ and the axial ratio condition $AR \leq 3\ dB$ are satisfied.

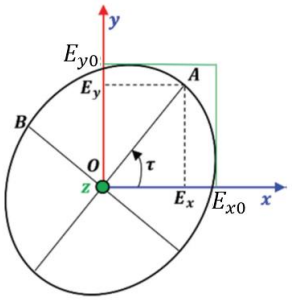

Figure 3.6: Graphical representation of elliptical polarization.

3.5 The main characteristics of the dielectric resonator antenna (DRA)

The dielectric resonator antenna is very promising for use in wireless communications applications and offers numerous attractive features, such as compact size, a design process that is simple to manufacture, low manufacturing cost, low loss, light weight, multiple feeding mechanisms, high radiation efficiency, and enhanced bandwidth compared to other antenna types. These characteristics make the DRA an excellent choice for antenna applications in the microwave and mm-wave range systems [12-16]. The main characteristics of the DRAs are outlined below:

Basic principles of dielectric resonator antennas

a) The size of a dielectric resonator antenna is proportional to $\lambda_0/\sqrt{\mu_r \cdot \varepsilon_r}$, where λ_0 is the free space wavelength, μ_r is the relative permeability, and ε_r is the permittivity of the dielectric material forming the radiating structure, where $\mu_r = 1$ for purely dielectric materials. The expression simplifies to $\lambda_0/\sqrt{\varepsilon_r}$. DRAs are characterized by a smaller shape when a dielectric material with a high dielectric constant (ε_r) is used.

b) DRAs can be easily fabricated in various geometric forms, such as cylindrical, rectangular, hemispherical forms, etc. Moreover, they offer greater flexibility in antenna design, enabling the achievement of desired resonant frequencies.

c) DRA is characterized by high radiation efficiency in the microwave frequency range due to the absence of intrinsic losses in the dielectric material, the lack of a conductor, and the elimination of surface waves. This feature makes them well suited for very high-frequency applications.

d) DRAs can achieve a wide impedance bandwidth if the dimensions of the dielectric resonator are properly chosen and the dielectric material has a low dielectric constant. As the Q-factor of the dielectric resonator decreases, the antenna bandwidth increases.

e) DRAs can be excited using a variety of feeding techniques, such as coaxial probe, aperture coupling, microstrip line, and coplanar waveguide, making them suitable for a wide range of applications.

f) The resonant modes in the DRA depend on the dimensions and permittivity of the dielectric resonator, as well as the feeding mechanism [17].

g) The resonant frequency, gain, bandwidth, and polarization characteristics of a DRA can be effectively controlled through various design techniques.

h) DRAs exhibit excellent thermal stability, making them suitable for a wide range of environmental conditions, as their resonant frequency remains largely unaffected by temperature variations.

i) DRAs are non-metallic and exhibit no inherent conduction losses. Consequently, they possess a high quality factor (Q) and are well suited for the design of antennas operating at millimeter-wave frequencies.

j) Dielectric resonators offer a wide range of dielectric constant (permittivity) values, which can be exploited to control both the antenna parameters and its physical size.

3.6 Geometric shapes of dielectric resonators

There are many geometric shapes of dielectric resonators, and the most commonly used are cylindrical, rectangular, hemispherical, triangular, ring, conical, hexagonal, etc. As illustrated in Figure 3.7. The geometric shape of a dielectric resonator can be tailored to meet specific design requirements and easily adjusted to achieve the desired resonant frequency.

Dielectric resonators can generally be classified into three basic shapes. The rectangular shape offers an advantage over other geometries, as it provides two degrees of freedom, allowing independent adjustment of the length-to-width and length-to-height ratios [18]. The cylindrical shape has one degree of freedom with two dimensions, the radius and the height [7]. The hemispherical shape has only a single dimension, the radius, for selecting design parameters [19]. Our work focuses on cylindrical and rectangular geometric shapes.

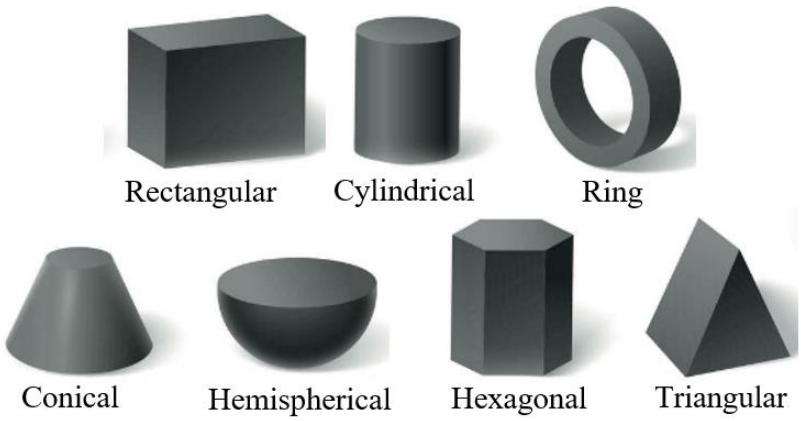

Figure 3.7: The most popular geometric shapes of dielectric resonators (DRs).

3.7 Feeding mechanisms of the dielectric resonator antenna

The feed mechanism is a crucial factor influencing the performance of dielectric resonator antennas, as it significantly affects both the resonant frequency and Q-factor. Power is coupled into or near the dielectric resonator through one or more feed ports. The type and placement of the feed port relative to the DRA determine the excitation mode and the amount of power transferred between the feed port and the antenna. Common feeding techniques used to excite DRAs include aperture coupling, coaxial probe coupling, microstrip line coupling, and coplanar waveguide coupling [8, 20].

3.7.1 Aperture coupling method

Aperture-coupling method is a common technique for feeding a dielectric resonator antenna. In this method, power is delivered from a microstrip feedline through an aperture that is etched into the ground plane. The dielectric resonator is then positioned above this aperture, as illustrated in Figure 3.8. The aperture can be realized in various shapes, such as a rectangular slot [21], a loop, a cross [22], a C-shaped slot, etc. It is cut into the ground plane. The main advantage of this technique is that the feed line is positioned beneath the substrate, which effectively isolates the radiating aperture from unwanted coupling or spurious radiation originating from the feed [14].

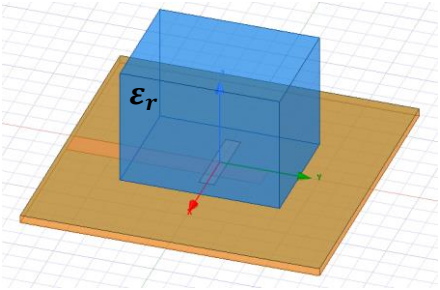

Figure 3.8: Aperture-coupling method for a dielectric resonator antenna.

3.7.2 Coaxial probe coupling method

In this coupling method, the probe can be placed inside or next to the dielectric resonator, as shown in Figure 3.9. Placing the probe inside the dielectric resonator offers the advantage of achieving strong coupling, resulting in high radiation efficiency. The disadvantage of this structure is that a hole must be drilled inside the dielectric resonator, and the dimensions of the hole must precisely match the length and diameter of the probe. Otherwise, the dielectric constant of the dielectric resonator will be affected, resulting in a shift in the resonant frequency. A probe adjacent to the dielectric resonator will result in weaker coupling. The accuracy of the probe position and height is critical to matching the input impedance and resonant frequency of the DRA [23].

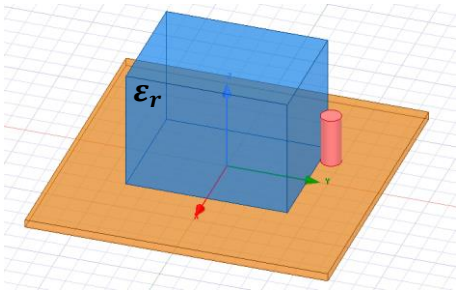

Figure 3.9: Coaxial probe coupling method for a dielectric resonator antenna.

3.7.3 Microstrip feedline coupling method

Microstrip feedline coupling offers the significant advantage of easy implementation. In this method, a microstrip printed on the substrate feeds the dielectric resonator. The dielectric resonator is typically positioned directly above the microstrip line, as shown in Figure 3.10. The length and width of the microstrip line, as well as the position of the dielectric resonator, determine the coupling strength and excitation mode. Strong coupling can be achieved by choosing a strip length slightly shorter than one-quarter wavelength of the resonance frequency. The effect of coupling between the dielectric resonator and the microstrip line can be controlled by adjusting the lateral position of the dielectric resonator or by shifting the microstrip line from the center position [24].

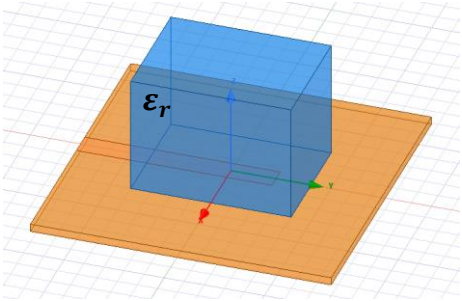

Figure 3.10: Microstrip feedline coupling method for a dielectric resonator antenna.

3.7.4 Coplanar waveguide coupling method

The coplanar waveguide coupling seems to be very promising because it allows easy feeding. The excitation of the desired mode can be achieved by progressively sliding the dielectric resonator element on the coplanar structure. Impedance tuning can be achieved by adding stubs, slots, or loops at the end of the coplanar line, as illustrated in Figure 3.11. This technique is best suited for antennas operating at millimeter wave frequencies [25].

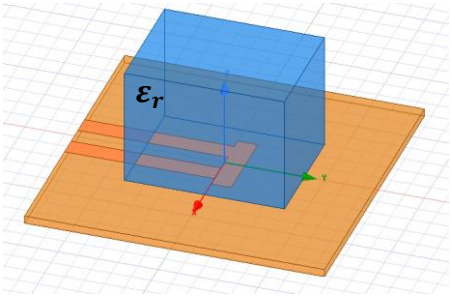

Figure 3.11: Coplanar waveguide coupling method for a dielectric resonator antenna.

3.8 Bandwidth enhancement techniques

Since the introduction of dielectric resonator antenna technology, various techniques have been developed to extend the impedance bandwidth by optimizing the antenna's geometry, feeding mechanism, and material properties. These improvements enable enhanced performance over a wider frequency range, which is essential for modern wireless communication systems.

Dielectric resonator antennas with a low dielectric constant are characterized by wide bandwidths, while those with a high dielectric constant exhibit narrow bandwidths. In other words, the bandwidth of a dielectric resonator antenna is inversely related to its dielectric constant [26]. To extend the impedance bandwidth of a dielectric resonator antenna, the most effective methods proposed in the literature are summarized below:

- The most commonly used methods involve combining several structures with single or multiple dielectric constants. Examples: a small dielectric disk embedded within a larger disk [27]. A turtle-shaped (stair pyramid) structure [28]. A stair-shaped half-cylindrical [29]. Two-layer hemispherical structure [30]. Linear array in which each element consists of several layers [31]. Hybrid shape [21].
- A wider bandwidth can also be achieved by increasing the loss tangent and using a dielectric material with a low dielectric constant [21].
- Numerous techniques have been proposed to increase the bandwidth by modifying the feed geometry or introducing a defected ground structure, such as 0M-shaped [32]. Two adjacent cylindrical structures coupled with an offset aperture [33]. Two dielectric disks excited by a coaxial probe [34].
- Various geometric structures of the dielectric resonator antennas provide wider bandwidths, including Z-shaped [35]. Ring-shaped [36]. Tetrahedral [37]. T-shaped [38], H-shaped [39], etc.
- Using the mode merging technique, Young and Long have improved the bandwidth of the DRA by varying the geometric parameters to excite two modes [40].

3.9 Multiband dielectric resonator antenna

Multiband antennas are essential to meet the growing demands of modern wireless communication systems. For instance, mobile devices must operate simultaneously across multiple frequency bands, such as Wi-Fi, GPS, and Bluetooth. To achieve this capability, multiband antennas are

required. The most common techniques employed to realize multiband operations are as follows:

- The use of multiple dielectric resonators [41].
- Hybrid dielectric resonator (combination of several dielectric resonating structures) [42].
- Generation of multiple radiating modes in a dielectric resonator [43, 44].

3.10 Improved gain of dielectric resonator antenna

The higher the gain, the more directional the antenna becomes. For example, a 3 dB increase in gain doubles the signal power, while a 6 dB increase doubles the range. It is important to note that increasing the gain does not amplify the signal itself. Rather, it focuses the existing energy into a narrower beam.

Typically, the gain of the dielectric resonator antenna is limited. The most important techniques have been developed in the last three decades to improve the gain of DRAs, such as stacking multiple dielectric resonators with different permittivities, as mentioned in [45]. In [46], a layered Arlon 25N substrate was used to excite a combination of higher-order hybrid electromagnetic modes. A hybrid-shaped dielectric resonator antenna is surrounded by a metallic dented cavity [47]. A resonant cavity antenna (RCA) consists of two layers of orthogonal dipole arrays, each located at a certain height above the ground plane of a microstrip patch antenna [48]. Resonant cavity antennas (RCA) with partially reflecting surfaces (PRS) are typically made of a single dielectric material [49]. A conical plastic-based dielectric horn with an annular notch combined with side lobe levels (SLLs) [50].

3.11 The electric and magnetic wall interface in a dielectric resonator

The electric and magnetic wall boundary conditions are usually employed to analyze and isolate the dielectric resonator, which can be utilized to explain the operating principle of the DRA [51].

Dielectric resonator antennas can be analyzed using the general mode classification proposed by Van Bladel for arbitrary dielectric resonator shapes with very high permittivity [52, 53]. In practice, the excitation source may resonate multiple modes simultaneously. The field strength for a typical mode depends on the accuracy of the feed position and its operating frequency.
The resonant modes satisfy two important conditions. The boundary conditions at the dielectric-air interface play a crucial role in determining the resonant modes.

An electric wall is a surface in which the tangential component of the electric field must be zero, and the normal component of the magnetic field must also be zero, as illustrated in the following equations. At microwave frequencies, good conductors such as copper provide a surface with a very small skin depth (the depth to which most of the microwave power penetrates). The boundary of these good conductors can be approximately regarded as an electric wall [8, 54].

$$\hat{n} \times \vec{E} = 0 \tag{3.14}$$

$$\hat{n} \cdot \vec{H} = 0 \tag{3.15}$$

A magnetic wall is a surface where the normal component of the electric field must be zero, and the tangential component of the magnetic field is absorbed by the magnetic surface, as illustrated in the following equations [8, 54].

$$\hat{n} \cdot \vec{E} = 0 \tag{3.16}$$

$$\hat{n} \times \vec{H} = 0 \tag{3.17}$$

where $\hat{n}$ is the unit vector normal to the surface of the dielectric resonator (DR), $\vec{H}$ is the magnetic field intensity, and $\vec{E}$ is the electric field intensity.

The modes that satisfy both conditions (3.16) and (3.17) are called confined modes, while those that satisfy only condition (3.16) are referred to as non-confined modes [8, 55].

Van Bladel in [52] demonstrated that confined modes can exist only in the geometries that support the bodies of revolution, such as cylindrical and hemispherical shapes, whereas the non-confined modes occur only in rectangular geometries [55].

3.12 Cylindrical dielectric resonator antenna (CDRA)

The cylindrical dielectric resonator provides flexibility in choosing the radius, height, and dielectric constant ε_r, which enables control over its operating frequency band. Cylindrical dielectric resonator antennas (CDRAs) are the most commonly used type of antenna in practice because their geometry is easier to fabricate and therefore less expensive compared to other shapes, as illustrated in Figure 3.12. This section presents the main aspects of CDRA operation, including the fundamental resonant modes and their corresponding resonant frequencies, as well as schematic representations of the electromagnetic field distributions [20].

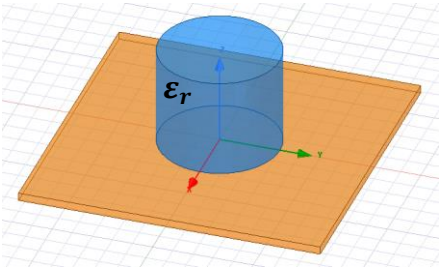

Figure 3.12: Cylindrical dielectric resonator antenna.

3.12.1 Resonant modes of a cylindrical dielectric resonator antenna

A cylindrical dielectric resonator antenna can resonate with an infinite number of modes, which can be classified into three types, such as transverse electric ($TE_{mnp+\delta}$), transverse magnetic ($TM_{mnp+\delta}$), and hybrid electromagnetic ($HEM_{mnp+\delta}$) [54].

The three integers m, n, and p represent the number of field variations in the azimuthal, radial, and longitudinal directions, respectively, and describe the spatial configuration of the electromagnetic field in the cylindrical coordinate system, as illustrated in Figure 3.13.

$m(m = 0, 1, 2 \ldots)$ represents the number of azimuthal variations of the field (along $\emptyset$).

$n(n = 0, 1, 2 \ldots)$ represents the number of radial variations of the field (along r).

$p(p = 0, 1, 2 \ldots)$ represents the number of longitudinal variations of the field (along z).

The third index is expressed by $p + \delta$, where δ is a real number such that $(0 < \delta < 1)$.

In the transverse electric (TE) mode, the Ez component is equal to zero. This means that the azimuthal component is zero ($m = 0$).

In the transverse magnetic (TM) mode, the Hz component is equal to zero. This means that the azimuthal component is zero ($m = 0$).

In the hybrid mode (HEM), all six components of the electromagnetic field are not equal to zero.

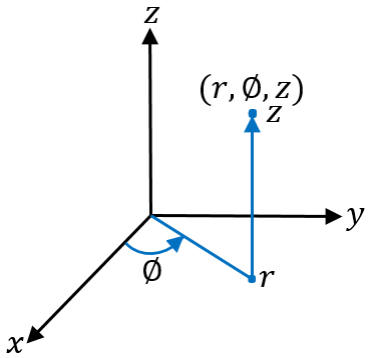

Figure 3.13: Cylidrical coordinate system

3.12.2 Fundamental modes of CDRA

There are three fundamental modes commonly used for radiation applications that can resonate in a cylindrical dielectric resonator: $HEM_{11\delta}$, $TE_{01\delta}$, and $TM_{01\delta}$. Each of these modes resonates at a specific frequency. The field distributions of the modes in the cylindrical dielectric resonator have been sketched, and the analytical expressions for the resonance frequencies of the three fundamental resonant modes are given below [57-60].

- **Hybrid electromagnetic mode ($HEM_{11\delta}$)**

The resonance frequency of the $HEM_{11\delta}$ mode is given by the following equation:

$$fr/_{HEM_{11\delta}} = \frac{c * 2.735}{2\pi * a * {\varepsilon_r}^{0.436}} * \left(0.543 + 0.589 * \frac{a}{2h} - 0.05 * \left(\frac{a}{2h}\right)^2\right) \quad (3.18)$$

Figure 3.14 illustrates the electric field and magnetic field distribution of the hybrid electromagnetic mode ($HEM_{11\delta}$).

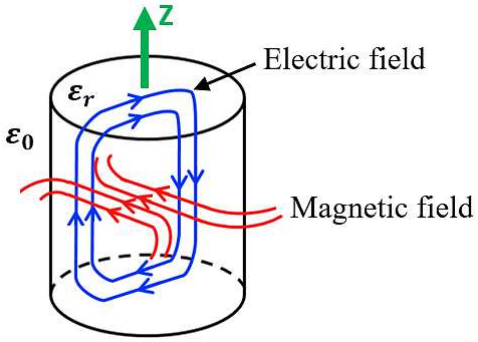

Figure 3.14: Sketch of the field distribution of the $HEM_{11\delta}$ mode.

- **Transverse electric mode ($TE_{01\delta}$)**

The resonance frequency of the $TE_{01\delta}$ mode is given by the following equation:

$$fr/_{TE_{01\delta}} = \frac{c * 2.921}{2\pi * a * {\varepsilon_r}^{0.456}} * \left(0.691 + 0.319 * \frac{a}{2h} - 0.035\left(\frac{a}{2h}\right)^2\right) \quad (3.19)$$

Figure 3.15 illustrates the electric field and magnetic field distribution of the transverse electric mode ($TE_{01\delta}$).

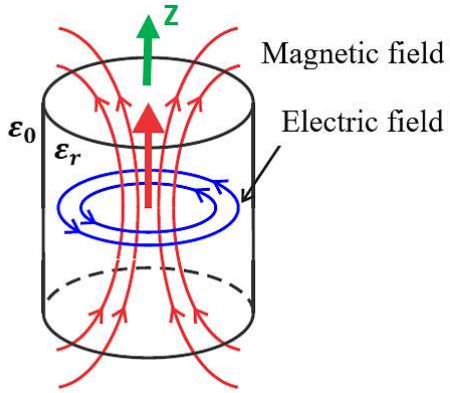

Figure 3.15: Sketch of the field distribution of the $TE_{01\delta}$ mode.

❖ Transverse magnetic mode ($TM_{01\delta}$)

The resonance frequency of the $TM_{01\delta}$ mode is given by the following equation:

$$fr/_{TM_{01\delta}} = \frac{c \ * 2.933}{2\pi * a * {\varepsilon_r}^{0.468}} * \left(1 - \left(0.075 - 0.05 * \frac{a}{2h}\right) * \left(\frac{\varepsilon_r - 10}{28}\right)\right) * \left(1.048 + 0.377 * \frac{a}{2h} - 0.071 * \left(\frac{a}{2h}\right)^2\right) \quad (3.20)$$

Figure 3.16 illustrates the electric field and magnetic field distribution of the transverse magnetic mode ($TM_{01\delta}$).

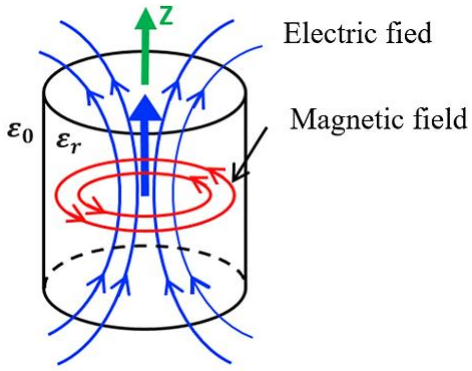

Figure 3.16: Sketch of the field distribution of the $TM_{01\delta}$ mode.

3.13 Rectangular dielectric resonator antenna (RDRA)

The rectangular dielectric resonator antenna offers an advantage over the other shapes, providing greater flexibility in optimizing the desired frequency band, with two degrees of freedom: the length-to-width and length-to-height ratios, as well as the dielectric constant ε_r, as shown in Figure 3.17. An appropriate choice of the dimensions of the dielectric resonator helps avoid mode degeneration and facilitates avoiding the excitation of higher-order modes. In addition, RDRAs

are relatively easy to fabricate. However, the analysis of RDRA is very complex and cannot be solved analytically, but only by approximation. Numerical techniques have been developed to solve this problem [55, 61].

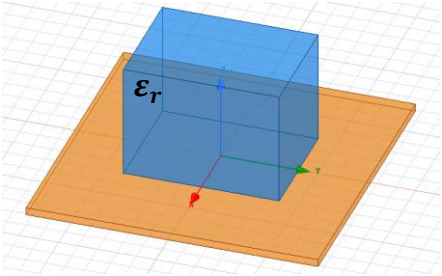

Figure 3.17: Rectangular dielectric resonator antenna.

3.13.1 The resonant frequency of the rectangular dielectric resonator antenna

Marcatili proposed the dielectric waveguide model in 1969, which is used to determine the wavelength in dielectric waveguides with rectangular cross-sections [62].

The resonance frequency (f_r) of the rectangular shape is calculated as follows [20, 63]:

$$f_r = \frac{c}{2\pi\sqrt{\varepsilon_r}}\sqrt{k_x^2 + k_y^2 + k_z^2} \tag{3.21}$$

$$k_x \tan\left(\frac{k_x w}{2}\right) = \sqrt{(\varepsilon_r - 1)k_0^2 - k_x^2} \tag{3.22}$$

$$k_x^2 + k_y^2 + k_z^2 = \varepsilon_r k_0^2 \tag{3.23}$$

In addition, $k_y = \frac{m\pi}{l}$ and $k_z = \frac{n\pi}{2h}$, where m and n are positive integers, in the lowest order mode ($m = n = 1$), and k_0 denotes the free space wave number corresponding to the resonant frequency.

The value of δ can be defined as the fraction of a half-cycle of the field variation in the z-direction and is given by $\delta = \frac{k_x}{\pi/w}$, where δ is a real number such that $(0 < \delta < 1)$.

Where ε_r is the dielectric constant of the RDRA, l, w, and h are the length, width, and height of the rectangular dielectric resonator, respectively, c is the speed of light in free space, and the symbols k_x, k_y, and k_z represent the wave numbers in the x, y, and z directions, respectively. These equations can also be used to determine the parameters and dimensions of the dielectric resonator for a desired operating frequency.

3.13.2 Resonant modes of a rectangular dielectric resonator antenna

A rectangular dielectric resonator supports only non-confined modes because it is not a body of revolution. The resonant modes in a rectangular dielectric resonator shape are typically called transverse electric (TE_{mnp}) or transverse magnetic (TM_{mnp}), with a single fundamental mode (TE_{111}).

Where m, n, and p are integers representing the number of the field variations along the x, y, and z directions, respectively. The electric field distribution of the fundamental mode (TE_{111}), as illustrates in Figure 3.18.

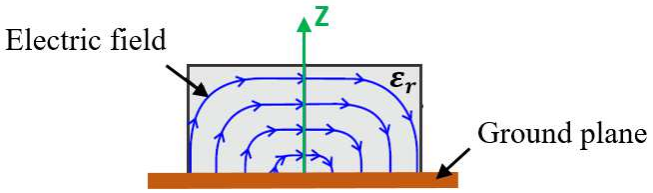

Figure 3.18: Electric field distribution of the fundamental mode (TE_{111})

3.14 Channel capacity

Channel capacity, also known as Shannon channel capacity, provides an excellent illustration of the motivations and advantages of ultra-wideband (UWB) systems. These systems can achieve very high data rates, reaching up to 10 Gbps in 5G networks.

$$C = B * log_2\left(1 + \frac{S}{N}\right) \tag{3.24}$$

where C is the channel capacity (in bits/s), B is the bandwidth of the channel (in Hz), S is the signal power (in watts), and N is the noise power (in watts). S/N is the signal-to-noise ratio (SNR) [64].

In 2002, the Federal Communications Commission (FCC) classified an antenna as ultra-wideband if it operates over a bandwidth of 7.5 GHz, ranging from 3.1 to 10.6 GHz [65].

3.15 Simulation and measurement software

There are several electromagnetic simulation software available for the design, analysis, and optimization of electromagnetic (EM) components and systems based on numerical methods. Some of the most commonly used simulation software are listed below.

- **High-Frequency Structure Simulator (HFSS):** based on the finite element method (FEM).
- **Microwave Studio (CST):** based on the finite integration technique (FIT).
- **Advanced Design System (ADS):** based on the finite element method (FEM) and finite difference time domain (FDTD).
- **COMSOL Multiphysics:** based on the finite element method (FEM).

The ease of simulation offered by these software tools allows designers to explore various antenna structures and identify components that meet specific design requirements.

3.15.1 Principle of operation Ansys, HFSS

Ansys HFSS is the most common software used in antenna design. It is a 3D electromagnetic (EM) simulation tool for the design and analysis of high-frequency electronic components such as antennas, antenna arrays, RF and microwave components, high-speed interconnects, filters, connectors, IC packages, and printed circuit boards. Engineers worldwide use Ansys HFSS software to design high-frequency, high-speed electronics found in communications systems, advanced driver assistance systems (ADAS), satellites, and internet-of-things (IoT) products [66].

3.15.2 Finite Element Method (FEM)

The numerical technique used in HFSS is the Finite Element Method. In this method, a structure is divided into many small sections called finite elements. In HFSS these finite elements are in the tetrahedral forms. The entire collection of tetrahedra constitutes the finite element mesh. A solution is found for the fields within these tetrahedra. These fields are interrelated so that the equations of Maxwell are satisfied across inter-element boundaries yielding a field solution for the entire original structure. Once the field solution is found, the generalized S-matrix solution is determined.

HFSS uses the automatic adaptive mesh refinement process to solve an EM problem. Automatic adaptive mesh refinement is a critical part of the overall solution process and the key to producing accurate results. This meshing technique helps you focus on setting up your design efficiently rather than spending time in determining and creating the best mesh.

To set up the design, you need only to create the geometry and specify material properties, boundary conditions, excitations, and the solution frequency.

In the adaptive mesh refinement process, the mesh is refined iteratively and is localized to regions where the electric field solution error is high.

This iterative refinement technique increases the solution's accuracy with each adaptive solution. The refinement process continues until HFSS converges to an accurate solution. Convergence is determined by monitoring a parameter from one adaptive pass to the next. The most common convergence criterion is to ensure that the difference in the S-parameter value between two consecutive solves is less than the specified magnitude.

3.16 Conclusion

In this chapter, we presented a general overview of dielectric resonator antennas (DRAs), including a brief discussion of their main parameters, the different types of polarization involved in electromagnetic wave propagation, their basic characteristics, the most common DRA geometries, and the various feeding mechanisms used to excite them. We also briefly reviewed several techniques for enhancing the bandwidth and gain of DRAs, along with methods commonly employed to achieve multiband operation. In addition, the electric and magnetic wall boundary conditions typically used to analyze and isolate the dielectric resonator were presented. A detailed study was conducted on two fundamental shapes: cylindrical and rectangular, which serve as the building blocks for all other geometric designs. The fundamental modes and field distributions of cylindrical and rectangular dielectric resonator antennas were outlined, and their corresponding resonant frequencies were provided. Finally, we introduced the electromagnetic simulation software most commonly used for antenna design. Therefore, a general theoretical understanding of antenna operation is essential, as it provides the foundation for achieving optimal design and performance.

References

[1] T. Simpson, "Revisiting Heinrich Hertz's 1888 Laboratory [Historical Corner] ", *IEEE Antennas and Propagation Magazine,* vol. 60, no. 4, pp. 132–140, 2018.

[2] P. K. Bondyopadhyay, "Guglielmo Marconi - The father of long distance radio communication - An engineer's tribute", *25th European Microwave Conference*, 1995.

[3] R. D. Richtmyer, "Dielectric resonators", *Journal of Applied Physics*, vol. 10, no. 6, pp. 391–398, 1939.

[4] A. Okaya, and L.F. Barash, "The dielectric microwave resonator", *Proceeding of the IRE*, Vol.50, no. 10, pp. 2081-2092, 1962.

[5] H. Y. Yee, "Natural Resonant Frequencies of Microwave Dielectric Resonators", IEEE Transactions on Microwave Theory and Techniques, vol. MTT-13, no. 2, pp. 256-256, 1965.

[6] S.B. Cohn, "Microwave Bandpass Filters Containing High-Q Dielectric Resonators", *IEEE Transactions on Microwave Theory and Techniques,* vol. MTT-16, no. 4, pp. 218-227, 1968.

[7] S. Long, M. McAllister, and L. Shen, "The resonant cylindrical dielectric cavity antenna", *IEEE Transactions on Antennas and Propagation,* vol. 31, no. 3, pp. 406-412, 1983.

[8] R. S. Yaduvanshi and G. Varshney, "*Nano Dielectric Resonator Antennas for 5G Applications*", CRC Press, Taylor & Francis, Boca Raton, 2020.

[9] David M. Pozar, "*Microwave engineering*", Fourth Edition, Wiley, 2012.

[10] Constantine A. Balanis, "*Antenna Theory Analysis and Design*", Fourth Edition, Wiley, 2016.

[11] Arpan Pal, "*Low Profile Pattern Reconfigurable Sauare Loop Antenna*", Doctoral thesis, Swansea University, U.K., 2013.

[12] R.K. Mongia, and P. Bhartia, "Dielectric resonator antennas – a review and general design relation for resonant frequency and bandwidth", *International journal of Microwave and Millimeter wave Computer-aided Engineering,* vol. 4, pp. 230-247, 1994.

[13] Massinissa Belazzoug, "*Contribution à l'étude et à la conception des antennes planaires pour des applications Multi-Input Multi-output (MIMO) ",* Thèse de doctorat, Université Mohamed El-Bachir EL-Ibrahimi de Bordj Bou Arréridj, 2021.

[14] Fauzi O. M. Elmegri, "*Model and design of small compact dielectric resonator and printed antennas for wireless communications applications",* Doctoral thesis, University of Bradford, 2015.

[15] A. Petosa, A. Ittipiboon, Y. M. M Antar, D. Roscoe, and M. Cuhaci, "Recent Advances in Dielectric-Resonator Antenna Technology", *IEEE Antennas Propag. Mag.*, vol. 40, no. 3, pp.35-48, Jun. 1998.

[16] Samira Mekki, "*Modeling of planar microwave sensor and optimized dielectric resonator antenna",* University Setif 1-Ferhat Abbas, 2024.

[17] A. H. Majeed, A. S. Abdullah, F. Elmegri, K. H. Sayidmarie, R. A. Abd-Alhameed, and J. M. Noras, "Aperture-coupled asymmetric dielectric resonators antenna for wideband applications", *IEEE Antennas and Wireless Propagation Letters*, vol. 13, pp. 927-930, 2014.

[18] Long, S. A., M. W. McAllister, and L. C. Shen, "Rectangular Dielectric Resonator Antenna", *IEEE Electronics Letters*, vol. 19, pp. 218-219, March, 1983.

[19] M. W. McAllister and S. A. Long, "Resonant hemispherical dielectric antenna", *Electronics Letters,* vol. 20, no. 16, pp. 657-659, Aug. 1984.

[20] A. Petosa, "*Dielectric Resonator Antenna Handbook*", Norwood, MA, USA: Artech House, 2007.

[21] R. Chelghoum, Z. Messai A. Brahimi, N. Bourouba, J.P. Martinez Jiménez and F. Bouttout, "Dielectric Behavior Characterization of RE/$BaTiO_3$ Using Time Domain Spec-troscopy: Application on high performance dielectric resonator antennas", *ECS Journal Solid State Science and Technology,* vol. 13, 043018, 2024.

[22] A. Abdulmajid, Y. Khalil and S. Khamas, "Higher order mode circularly polarized two-layer rectangular dielectric resonator antenna", *IEEE Antennas and Wireless Propagation Letters*, vol. 17, no. 6, pp. 1114-1117, 2018.

[23] Gregory P. Junker, Ahmed A. Kishk, and Allen W. Glisson, "Input Impedance of Dielectric Resonator Antennas Excited by a Coaxial Probe", *IEEE Transactions on antennas and propagation*, vol. 42, no. 7, pp. 960-966, 1994.

[24] A. Sharma and R. K. Gangwar, "Compact dual-band ring dielectric resonator antenna with moon-shaped defected ground structure for WiMAX/WLAN applications". International Journal of RF and Microwave Computer-Aided Engineering, vol. 26, no. 6, pp. 503–511, 2016.

[25] S. Keyrouz, and D. Caratelli, "Dielectric Resonator Antennas: Basic Concepts, Design Guidelines, and Recent Developments at Millimeter-Wave Frequencies", *International Journal of Antennas and Propagation,* ID: 6075680, pp. 1–20, 2016.

[26] A. Petosa and A. Ittipiboon, "Dielectric Resonator Antennas: A Historical Review and the Current State of the Art", *IEEE Antennas and Propagation Magazine,* vol. 52, no. 5, 2010.

[27] Ahmed A. Kishk, "Experimental study of broadband embedded dielectric resonator antennas excited by a narrow slot", *IEEE Antennas and wireless propagation letters,* vol. 4, 2005.

[28] P. Sharma, A. Vaish, and R.S. Yaduvanshi, "The design of a turtle-shaped dielectric resonator antenna for ultrawide-band applications", *Journal of Computational Electronics*, vol. 18, pp. 1333-1341, 2019.

[29] M. F. M. Omar, I. A. Zubir, S. Kamal, and M. F. Ain, "A tri-hybrid of Al2O3-SiO2-MgZrO3 stair shaped half-cylindrical dielectric resonator antenna (SHCDRA) for wideband wireless communication systems", *Engineering Science and Technology an International journal*, vol. 35, 101187, 2022.

[30] Xiao Sheng Fang and Kwok Wa Leung, "Design of wideband omnidirectional two-layer transparent hemispherical dielectric resonator antenna", *IEEE Transactions on antennas and propagation*, vol. 62, no. 10, pp. 5353-5357, 2014.

[31] Fan Wang, Chuanfang Zhang, Houjun Sun and Yu Xiao, "Ultra-wideband dielectric resonator antenna design based on multilayer form", *International Journal of Antennas and Propagation*, ID : 4391474, 10 pages, 2019.

[32] S. Kumar Yadav, A. Kaur, and R. Khanna, "An ultra-wideband 'OM' shaped DRA with a defected ground structure and dual polarization properties for 4G/5G wireless communications", *International Journal of RF Microwave Computer Aided Engineering*, vol. 30, e22327, 2020.

[33] C. Zebiri, D. Sayad, I. T. E. Elfergani, J. S. Kosha, W. F. A. Mshwat, C. Hwang See, M. Lashab, J. Rodriguez, K. H Sayidmarie, H. A. Obeidat and R. A. Abd-Alhameed, "Antenna for ultra-wideband applications with non-uniform defected ground plane and offset aperture-coupled cylindrical dielectric resonators", *IEEE Access*, vol. 7 pp. 166776-166787, 2019.

[34] Ahmed A. Kishk, Xiao Zhang, Allen W. Glisson, Darko Kajfez, "Numerical analysis of stacked dielectric resonator antennas excited by a coaxial probe for wideband applications", *IEEE Transactions on antennas and propagation*, vol.51, no. 8, pp. 1996-2006, 2003.

[35] Tayeb A. Denidni, Zibin Weng, and Mahmoud Niroo-Jazi, "Z-shaped dielectric resonator antenna for ultra-wideband applications", *IEEE Transactions on antennas and propagation*, vol. 58, no. 12, 2010.

[36] G. Das, A. Sharma, and R. K. Gangwar, "Wideband self-complementary hybrid ring dielectric resonator antenna for MIMO applications", *IET Microwave, antenna & propagation*, vol. 12, no. 1, pp. 108-114, 2018.

[37] Ahmed A. Kishk, "Wide-band truncated tetrahedron dielectric resonator antenna excited by a coaxial probe", *IEEE Transactions on antennas and propagation*, vol. 51, no. 10, pp. 2913-2917, 2003.

[38] Monika Chauhan and Biswajeet Mukherjee, "Investigation of T-shaped compact dielectric resonator antenna for wideband application", *Radioelectronics and Communications Systems,* vol.62, no. 11, pp. 594-603, 2019.

[39] Xian-Ling Liang, & Tayeb A. Denidni, "H-Shaped Dielectric Resonator Antenna for Wideband Applications", *IEEE Antennas and Wireless Propagation Letters,* vol. 7, pp. 163-166, 2008.

[40] C. S. De Young, and S. A. Long, "Investigation of dual mode wideband rectangular and cylindrical dielectric resonator antennas". *IEEE Antennas and Propagation Society International Symposium*, 2005.

[41] Z. Fan and Y.M.M. Antar, "Slot-coupled DR antenna for dual-frequency operation", *IEEE Transactions on antennas and propagation*, vol. 45, no. 2, pp.306-308, 1997.

[42] Yi-Fang Lin, Hua-Ming Chen and Chia-Ho Lin, "Compact Dual-Band Hybrid Dielectric Resonator Antenna With Radiating Slot", IEEE Antennas and Wireless Propagation Letters, vol. 8, pp. 6-9, 2009.

[43] D. Guha, P. Gupta and C. Kumar, "Dualband Cylindrical Dielectric Resonator Antenna Employing $HEM_{11\delta}$ and $HEM_{12\delta}$ Modes Excited by New Composite Aperture", IEEE Transactions on antennas and propagation, vol. 63, no. 1, pp. 433-438, 2015.

[44] A. Sharma, P. Ranjan and R.K. Gangwar, "Multiband cylindrical dielectric resonator antenna for WLAN/WiMAX application", *Electronics letters,* vol. 53, no. 3, pp. 132–134, 2017.

[45] Y. M. Pan, S. Y. Zheng, "A low-profile stacked dielectric resonator antenna with high-gain and wide bandwidth", *IEEE Antennas and wireless propagation letters,* vol. 15, pp. 68-71, 2016.

[46] Michal Mrnka, Zbynek Raida, "Enhanced-gain dielectric resonator antenna based on the combination of higher-order modes", *IEEE Antennas and wireless propagation letters,* vol. 15, pp. 710-713, 2016.

[47] Elham Erfani, Tayeb Denidni, Serioja Tatu, Mahmoud Niroo-Jazi, "A broadband and high gain millimeter-wave hybrid dielectric resonator antenna", *17th International Symposium on Antenna Technology and Applied Electromagnetics*, Montreal, Canada, 2016.

[48] Hamid Moghadas, Mojgan Daneshmand and Pedram Mousavi, "A dual-band high-gain resonant cavity antenna with orthogonal polarizations", *IEEE Antennas and wireless propagation letters,* vol. 10, pp. 1220-1223, 2011.

[49] Affan A. Baba, Raheel M. Hashmi, Karu P. Esselle and Andrew R. Weily, "Compact high-gain antenna with simple all-dielectric partially reflecting surface", *IEEE Transactions on antennas and propagation,* vol. 66, no. 8, pp. 4343-4348, 2018.

[50] Edoardo Baldazzi, Ali Al-Rawi, Renato Cicchetti, Adrianus Bart Smolders, Orlandino Testa, Carlos de Jong van Coevorden Moreno, and Diego Caratelli, "A high-gain dielectric resonator antenna with plastic-based conical horn for millimeter-wave applications", *IEEE Antennas and wireless propagation letters,* vol. 19, no. 6, pp. 949-953, 2020.

[51] Robert E. Collin, *"Foundations for Microwave Engineering",* Second Edition, Wiley-IEEE Press, 2001.

[52] J. Van Bladel, "On the Resonances of a Dielectric Resonator of Very High Permittivity", *IEEE Transactions on Microwave Theory and Techniques*, vol. 23, no. 2, pp. 199-208, 1975.

[53] J. Van Bladel, "The Excitation of Dielectric Resonators of Very High Permittivity", IEEE Transactions on Microwave Theory and Techniques, vol. 23, no. 2, pp. 208-217, 1975.

[54] Longfang Zou, *"Dielectric Resonator Antenna: From Multifunction Microwave Devices to Optical Nano-antennas"*, Doctoral thesis, University of Adelaide, Australia, 2013.

[55] Rajesh Kumar Mongia, Apisak Ittipiboon, "Theoretical and Experimental Investigations on Rectangular Dielectric Resonator Antennas", *IEEE Transactions on Antennas and Propagation*, vol. 45, no. 9, pp. 1348-1356, 1997.

[56] Ahmed Benomar, *"Etude des antennes à résonateurs diélectriques. : application aux réseaux de télécommunications",* Thése de doctorat, Thèse en Cotutelle de l'université de Tlemcen et de l'université de Limoges, 2015.

[57] Darko Kajfez, Allen W. Glisson and Joseph James, "Computed modal field distributions for isolated dielectric resonators", *IEEE Transactions on microwave theory and techniques,* vol. 32, no. 12, 1609-1616, 1984.

[58] K. M. Luk and K. W. Leung, "*Dielectric Resonator Antennas*", Research Studies Press ltd, Baldock, Hertfordshire, England, 2003.

[59] Muhammad Faiz Alam, "*Dielectric Resonator Antennas (DRA) for satellite and body area network applications*", Doctoral thesis, université Paris-Est, 2013.

[60] M. Ene-Dobre, m. G. Banciu, L. Nedelcu, G. Stoica, C. Busuioc, H. V. Alexandru, "Microwave antennas based on $Ba_{1-x}pb_xNd_2Ti_5O_{14}$", *Journal of optoelectronics and advanced materials,* vol.13, no. 10, pp. 1298-1304, 2011.

[61] Mian Shahzad Iqbal, *"Analysis and Design of Wideband Dielectric Resonator Antennas in Frequency and Time Domains"*, Doctoral thesis, Macquarie University, Sydney, Australia, 2015.

[62] E. A. J. Marcatili, "Dielectric rectangular waveguide and directional coupler for integrated optics", *The Bell System Technical Journal*, vol. 48, no. 7, pp. 2071-2102, 1969.

[63] Poonam Kshirsagar, Shubha Gupta and Biswajeet Mukherjee, "A two-segment rectangular dielectric resonator antenna for ultra-wideband application", Electromagnetics, vol. 38, no. 1, pp. 20-33, 2018.

[64] C.E. Shannon, "A Mathematical Theory of Communication", *The Bell System Technical Journal*, vol. 27, 379–423, 623–656, July, October, 1948.

[65] *Revision of Part 15 of the Commission's Rules Regarding Ultra-Wideband Transmission Systems*, FCC 02-48, Federal Communications Commission, 2002. https://transition.fcc.gov/Bureaus/Engineering_Technology/Orders/2002/fcc02048.pdf.

[66] Ansys, HFSS a 3D electromagnetic (EM) simulation software, https://www.ansys.com/products/electronics/ansys-hfss.

Chapter 4

Study and design of dielectric resonator antennas

Chapter 4: Study and design of dielectric resonator antennas

4.1 Introduction

The number of connected electronic devices is growing exponentially every day. Thanks to the rapid development of antennas, these devices can communicate with each other anytime and anywhere. In recent decades, dielectric materials have become a preferred choice for antenna design due to their numerous advantages as a radiating element. Consequently, it has become essential to enhance the performance of dielectric resonator antennas to enable high-speed transmission of large data volumes and to support multiple frequency bands. This need has driven researchers to explore innovative designs and materials capable of meeting these requirements. Understanding how antennas work is crucial to enabling the optimization of their performance and design.

This chapter focuses on the design and analysis of four types of dielectric resonator antennas (DRAs). It examines the effects of dielectric resonator geometry and their material properties on key antenna parameters, such as reflection coefficient (S_{11}), bandwidth, and radiation pattern. The experimentally obtained dielectric properties of each composite material sample ($RE - BaTiO_3$) are applied in the electromagnetic simulation software Ansys HFSS to evaluate their suitability for fabricating high-performance dielectric resonator antennas. The four antenna types are classified as follows:

Type 1: Cylindrical dielectric resonator antennas. The dielectric properties of each ($RE - BaTiO_3$) sample are successively applied to a cylindrical dielectric resonator until the final sample.

Type 2: A composite structure consisting of four dielectric resonator shapes: three rectangular joined with one cylindrical, with the same heights, using a single composite material sample composed of 60% of RE and 40% of $BaTiO_3$.

Type 3: A dielectric resonator antenna structure comprising four identical adjacent rectangular elements, utilizing two samples of the binary composite mixture ($RE - BaTiO_3$) with different volume fractions: the first sample comprises 60% of RE and 40% of $BaTiO_3$, while the second sample contains 50% of RE and 50% of $BaTiO_3$.

Type 4: A hybrid structure consisting of two adjacent identical resonator elements, each formed by a cylindrical and a rectangular component joined together, both having the same height, using a single composite material sample composed of 60% of RE and 40% of $BaTiO_3$.

4.2 Cylindrical dielectric resonator antennas (CDRAs)

In this type, we carried out a study of eleven cylindrical dielectric resonator antennas using the dielectric properties of each composite material sample. The eleven antennas, corresponding to the eleven samples, are identified by the capital letters A to K.

4.2.1 Antenna structure and geometry

The structure of the antennas is cylindrical, as depicted in Figure 4.1. The dielectric materials used are binary composites based on epoxy resin and barium titanate of dielectric constant (permittivity) ranging from $2.4058 \leq \varepsilon' \leq 11.88$, with a loss tangent varying between 0.005 and 0.0636 is mounted on the FR-4 substrate with $\varepsilon'_{sub} = 4.4$, $tan\delta = 0.02$, with a thickness of $T = 0.8\ mm$ and a size of $L_S * W_S = 30 * 30\ mm^2$. Then, a micro strip feed line underneath the substrate, with a 50 Ω characteristic impedance, is used for antenna excitation, and the aperture coupling is cut in the center of the ground plane, which is located above the substrate.

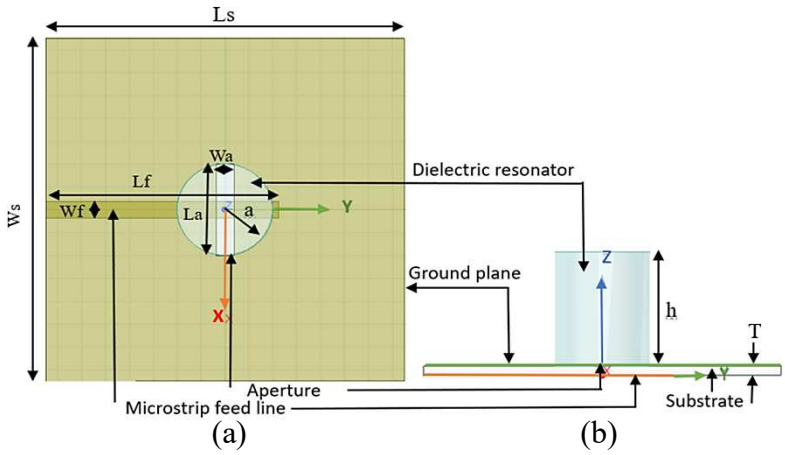

Figure 4.1: Cylindrical Dielectric Resonator Antenna, (a) Top view. (b) Side view.

The following geometric parameters are chosen for the better performances of the CDRAs, for each sample composite material ($RE - BaTiO_3$). The geometric parameters of the cylindrical dielectric resonator antennas are $a = 4\ mm$, $L_f = 19.5\ mm$, and $W_f = 1.5\ mm$.

The remaining geometric parameters are given in Table 4.1.

Table 4.1: Optimized geometric parameters of the antennas (CDRAs).

Volume fractions (RE-BT) (%)	Parameter h (mm)	Parameter La (mm)	Parameter Wa (mm)
(100-00)	6	6	1.2
(95-05)	6	6	1.2
(90-10)	6	6	1.2
(85-15)	6	6	1.2
(80-20)	6	7	1.4
(75-25)	6	7.5	1.5
(70-30)	6	7.5	1.5
(65-35)	9	7.5	1.5
(60-40)	10	8	1.5
(55-45)	10	8	1.5
(50-50)	10	8	1.5

4.2.2 Results analysis and discussion

We have carried out a study of cylindrical dielectric resonator antennas, which present the first structure used of all other geometric shapes [1]. Eleven cylindrical dielectric resonator antennas are considered and represented with capital letters A to K. These correspond to single, dual and three-frequency band operations.

Figures 4.2 and 4.3 illustrate simulated reflection coefficients of the five antennas A, B, C, D and E, according to dielectrics properties with fractions volume of the composite materials (100–00), (95–05), (90–10), (85–15) and (80–20) respectively. These antennas operate at frequencies between 20.7 and 29.95 GHz and give a single frequency band. It is seen, from these figures that the bandwidths of antennas increase from 17.42 to 33.06%, due to the increase in the loss tangent value of the composite materials.

Note that for antennas A and B, the simulated resonance frequency is in good agreement with the calculated values of the $TM_{01\delta}$ mode (27.49 and 25.18 GHz, respectively), using the following formula [2].

$$fr/_{TM01\delta} = \frac{c * 2.933}{2\pi * a * \varepsilon_r{}^{0.468}} * \left(1 - \left(0.075 - 0.05 * \frac{a}{2h}\right) * \left(\frac{\varepsilon_r - 10}{28}\right)\right) * \left(1.048 + 0.377 * \frac{a}{2h} - 0.071 * \left(\frac{a}{2h}\right)^2\right) \quad (4.1)$$

In this case, the effect of low dielectric permittivity on these antennas makes them operate in $TM_{01\delta}$ mode.

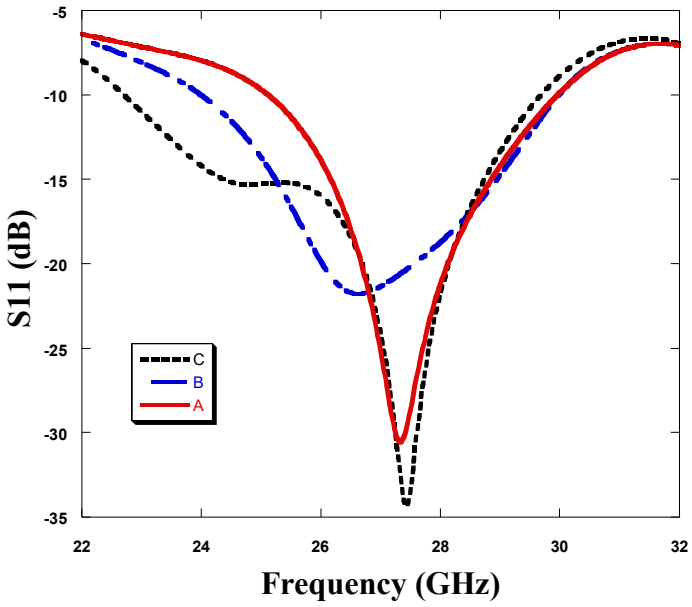

Figure 4.2: Simulated reflection coefficients (S_{11}) of the three antennas A, B and C, with volume fractions of materials (100-00), (95-05) and (90-10).

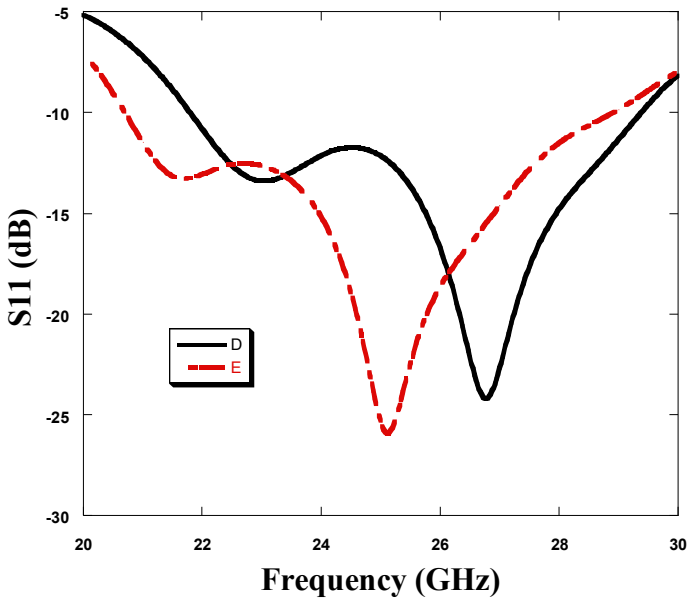

Figure 4.3: Simulated reflection coefficients (S_{11}) of the two antennas D and E, with volume fractions of materials (85-15) and (80-20).

Figure 4.4 shows simulated reflection coefficients of the three antennas F, G and H, with volume fractions of materials (75–25), (70–30) and (65–35) respectively. The antennas F and H give dual band and the antenna G gives three bands, these antennas operate in two frequency zones, the first covering the range from 8.54 to 14.08 GHz and the second varying between 21.2 and 28.3 GHz.

The lowest simulated resonant frequencies agree with the calculated values for the $HEM_{11\delta}$ mode (10.92, 10.25 and 8.71 GHz respectively), using the following formula [2].

$$fr/_{HEM11\delta} = \frac{c * 2.735}{2\pi * a * \varepsilon_r{}^{0.436}} * \left(0.543 + 0.589 * \frac{a}{2h} - 0.05 * \left(\frac{a}{2h}\right)^2\right) \quad (4.2)$$

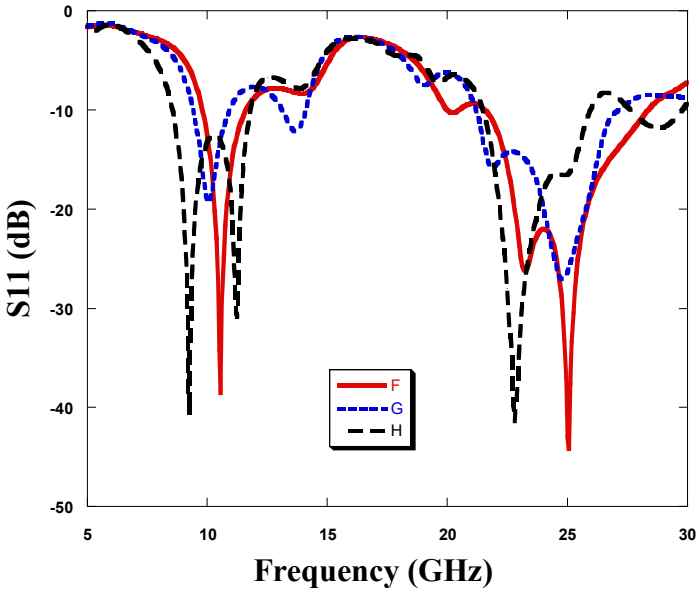

Figure 4.4: Simulated reflection coefficients (S_{11}) of the three antennas F, G and H with volume fractions of materials (75-25), (70-30) and (65-35).

The results obtained indicate that the antennas A, B, C, D, E, F, and G operate at frequencies between 20.7 and 29.95 GHz. According to the fifth-generation (5G) communication technology standards, this frequency range is particularly important in the n257 band (26.5 to 29.5 GHz), commonly called the 28 GHz band. The n258 band (24.25 to 27.5 GHz) is also known as the 26 GHz band. Additionally, the n261 band (27.5 to 28.35 GHz) is a subset of the n257 band [3-5].

Figure 4.5 shows the simulated reflection coefficients of the three antennas I, J and K, with volume fractions of materials (60–40), (55–45), and (50–50), respectively, which give a double band and its operate at frequencies ranging from 7.77 to 13.15 GHz. We see that resonance frequencies decrease as the real permittivity of materials increases and decreases in the bandwidth, due to the decrease of the loss tangent value of composite materials.

The lower and upper simulated resonance frequencies of these antennas are in agreement with the first $HEM_{11\delta}$ and the second $TE_{01\delta}$ modes calculated by the formulas (4.2) and (4.3) respectively [2], with some discrepancies between the values.

$$fr/_{TE01\delta} = \frac{c * 2.921}{2\pi * a * \varepsilon_r{}^{0.456}} * \left(0.691 + 0.319 * \frac{a}{2h} - 0.035\left(\frac{a}{2h}\right)^2\right) \quad (4.3)$$

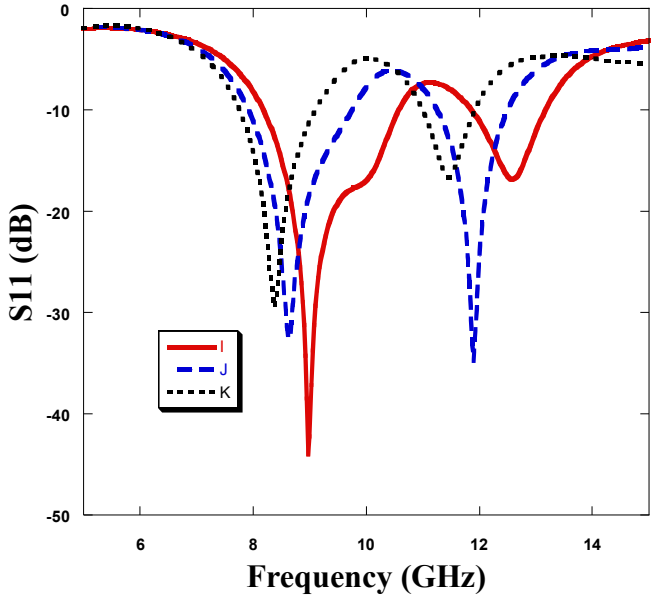

Figure 4.5: Simulated reflection coefficients (S_{11}) of the three antennas I, J and K with volume fractions of materials (60-40), (55-45) and (50-50).

Table 4.2: illustrates the simulated radiation patterns in XZ and YZ, with volume fractions of composite materials.

Volume fractions (%)	1st Resonant Frequency (GHz)	2nd Resonant Frequency (GHz)	3rd Resonant Frequency (GHz)	4rth Resonant Frequency (GHz)
(100-00)	Fr=27.32 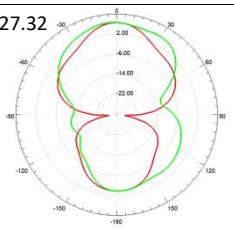	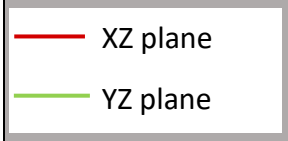		
(95-05)	Fr=26.63 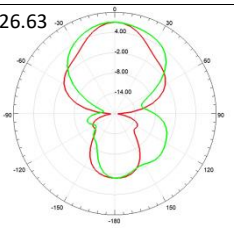			
(90-10)	Fr=27.43 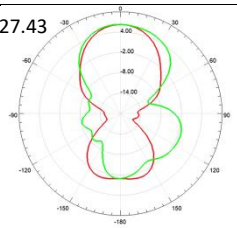			
(85-15)	Fr=23 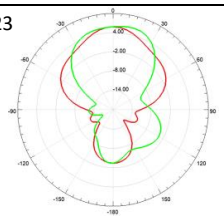	Fr=26.78 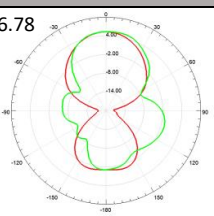		
(80-20)	Fr=21.7 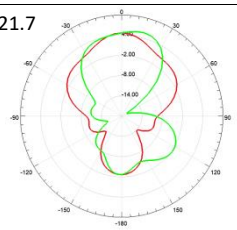	Fr=25.12 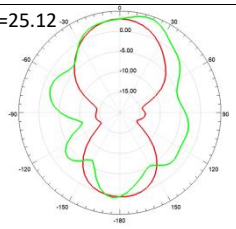		
(75-25)	Fr=10.56 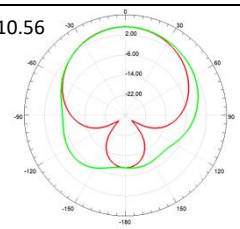	Fr=23.25 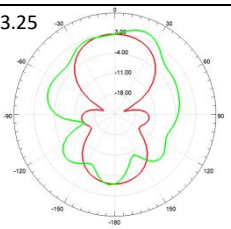	Fr=25.06 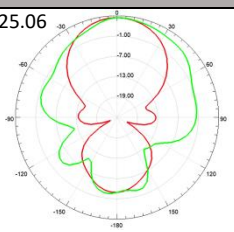	

Table 4.2 (continued)**.**

(70-30)	Fr=10.06 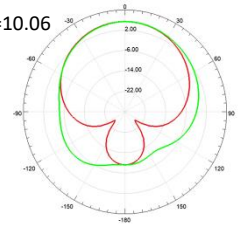	Fr=13.68 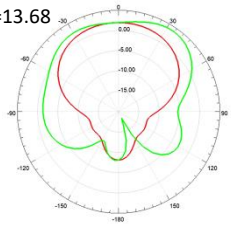	Fr=21.87 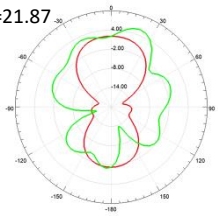	Fr=24.81 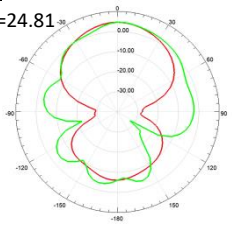
(65-35)	Fr=9.25 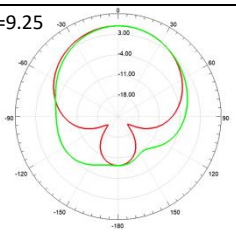	Fr=11.25 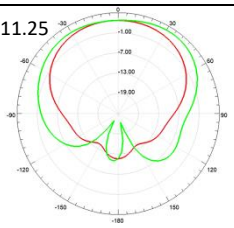	Fr=22.8 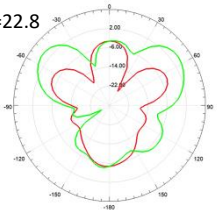	
(60-40)	Fr=8.98 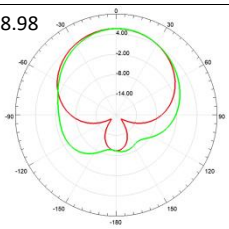	Fr=12.58 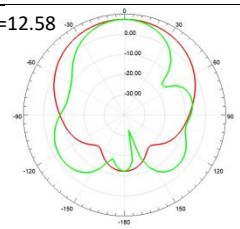		
(55-45)	Fr=8.63 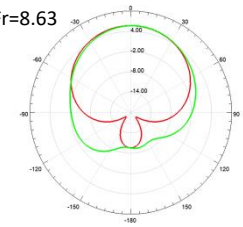	Fr=11.9 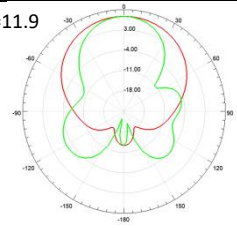		
(50-50)	Fr=8.37 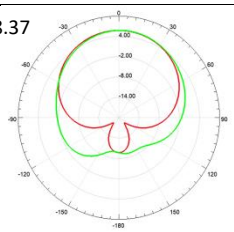	Fr=11.45 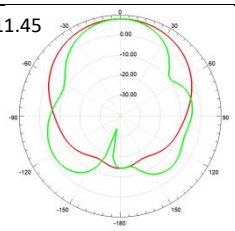		

Table 4.2 presents the simulated radiation patterns in the XZ and YZ planes of all composite material samples at different resonant frequencies. It is clearly observed from the figures in this table that the antennas exhibit broadside radiation due to the presence of the slot at the center of the substrate. The radiation pattern for most obtained antennas is omnidirectional, with maximum gains ranging from 3.68 to 8.15 dB.

The properties of all composite material samples, as well as the parameters of the antennas studied, are summarized in the following table.

Table 4.3: Parameters of antennas with different volume fractions of materials ($RE - BaTiO_3$).

Volume fractions	Permittivity ε' (Dielectric constant ε_r)	Dielectric losses $\frac{\varepsilon''}{\varepsilon'}$	Impedance bandwidth (GHz)	Bandwidth (%)	Resonant frequency (GHz)	Maximum gains (dB)
100-00	2.4058	0,0299	25.15-29.95	17.42	27.32	6.71
95-05	2.8951	0,0470	24-29.95	22.05	26.63	7.09
90-10	3.4828	0,0480	22.75-29.65	26.33	27.43	6.27
85-15	4.1605	0,0549	21.8-29.35	29.52	23 26.78	6.23 5.37
80-20	5.0179	0,0636	20.7-28.9	33.06	21.7 25.12	5.59 4.39
75-25	6.0547	0,0480	9.82-11.56 21.6-28.3	16.27 26.85	10.56 23.25 25.06	5.23 5.3 4.45
70-30	7.0087	0,0352	9.42-10.88 13.13-14.08 21.2-27.08	14.38 6.98 24.35	10.06 13.68 21.87 24.81	5.44 4.01 5.76 4.65
65-35	8.2838	0,0278	8.54-11.78 21.5-25.94	31.88 18.71	9.25 11.25 22.8	5.84 3.68 5.06
60-40	9.5179	0,0217	8.2-10.57 11.88-13.15	25.25 10.14	8.98 12.58	5.66 7.39
55-45	10.859	0,0136	7.92-9.73 11.27-12.48	20.5 10.18	8.63 11.9	5.69 7.72
50-50	11.88	0,0050	7.77-9.1 11-11.9	15.76 7.86	8.37 11.45	5.78 8.15

4.3 Dual-band dielectric resonator antennas (DBDRAs)

In this type, we carried out a study of eight dielectric resonator antennas, with a combination of several shapes, using a single dielectric material sample.

4.3.1 Geometry and antenna design

After optimizing the geometric parameters, the detailed design and dimensions of the proposed antenna are presented in Table 4.4 and Figure 4.6, respectively.

The antenna consists of a combination of four dielectric resonator shapes: three rectangular joined with one cylindrical, with the same height. Using a dielectric material sample made from 60% of RE and 40% of $BaTiO_3$, with a relative permittivity of $\varepsilon' = 9.5179$ and a loss tangent of 0.0217. The resonator is mounted on the FR-4 substrate with $\varepsilon_{sub} = 4.4$, $tan\delta = 0.02$, a thickness of 0.8 mm, and a size of $Ls * Ws = 30 * 25mm^2$. Moreover, a microstrip feed line underneath the substrate, with a characteristic impedance of 50 Ω, is used for antenna excitation. Additionally, the aperture coupling is cut into the ground plane. The ground plane is partially incomplete relative to the substrate dimensions and is positioned above the substrate.

Table 4.4: Optimized geometric parameters of the proposed antenna.

Parameter	Value (mm)	Parameter	Value (mm)
Ls	30	Ld	3
Ws	25	Lf	19.5
T	0.8	Wf	1.5
a	4.5	La	8
D	6	Wa	1.5
h	10	Lg	19.5

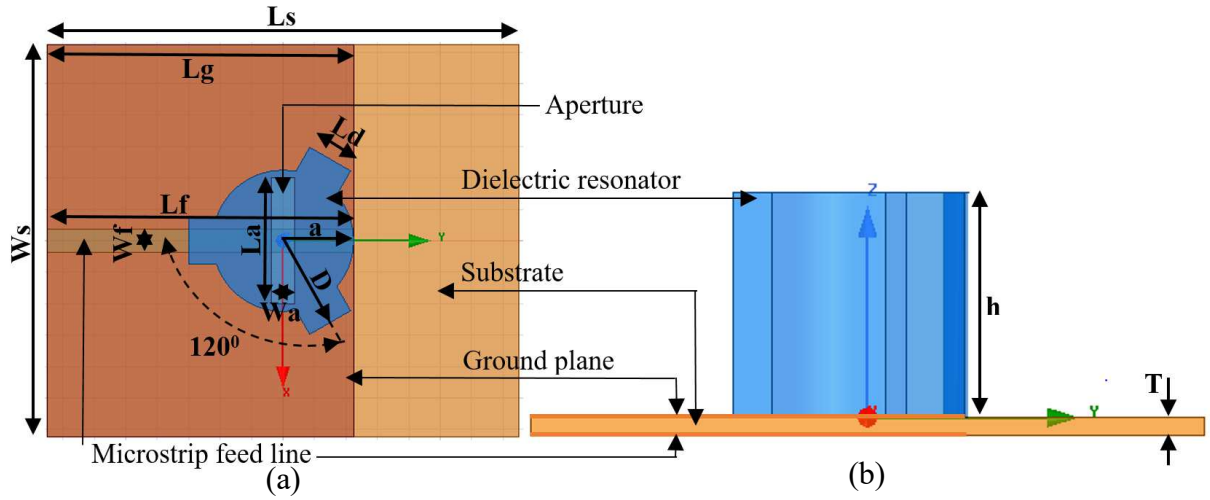

Figure 4.6: Proposed dielectric resonator antenna, (a) Top view. (b) Side view, with parameters shown.

4.3.2 Results and discussion

The resonant frequency of the cylindrical dielectric resonator antenna excited in the $HEM_{11\delta}$ mode can be derived from the following formula [6, 7].

$$fr = \frac{c}{2\pi a\sqrt{\varepsilon_r}}\left(1.71 + \frac{a}{h} + 0.1578\left(\frac{a}{2h}\right)^2\right) \qquad (4.4)$$

Where a and h represent the radius and height of the cylindrical dielectric resonator, c is the velocity of light in free space, and ε_r is the relative permittivity of the dielectric resonator. The calculated resonant frequency for these dimensions and material properties is 7.45 GHz.

Figure 4.7 shows the simulated reflection coefficient (S_{11}) of the dielectric resonator antenna with only the cylindrical element (without the rectangular). The antenna exhibits three frequency bands: the lower band from 7.4 to 9.04 GHz, the middle band from 9.6 to 10.46 GHz, and the upper band from 11.75 to 13.24 GHz.

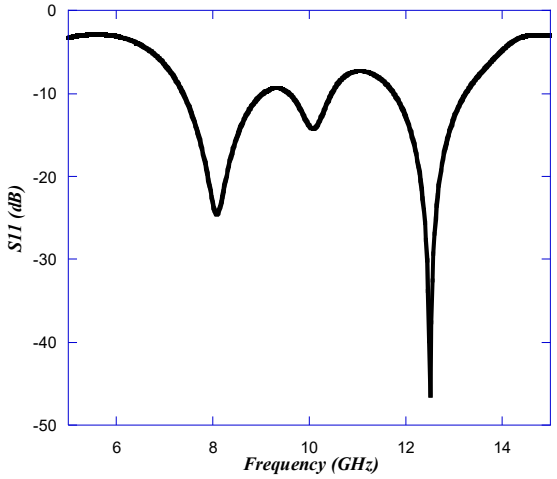

Figure 4.7: Simulated reflection coefficient (S_{11}) of dielectric resonator antenna, with a cylindrical only (without rectangular).

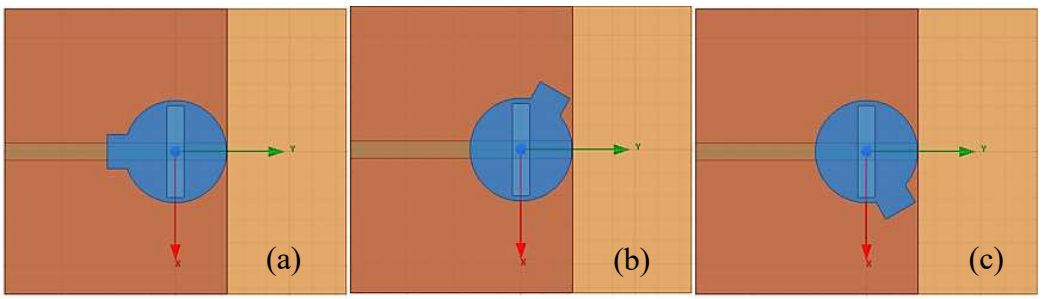

Figure 4.8: Top view of dielectric resonator antennas, the rotation effect of one rectangular joined with a cylindrical. (a) At 0^0. (b) At 120^0. (c) At 240^0.

Figure 4.9 illustrates the simulated reflection coefficient (S_{11}) of the three dielectric resonator antennas shown in figure 4.8. These antennas consist of a combination of a rectangular and a cylindrical shape, with the effect of their rotation (rotation angle 120^0). Antennas A, B, and C provide three frequency bands.

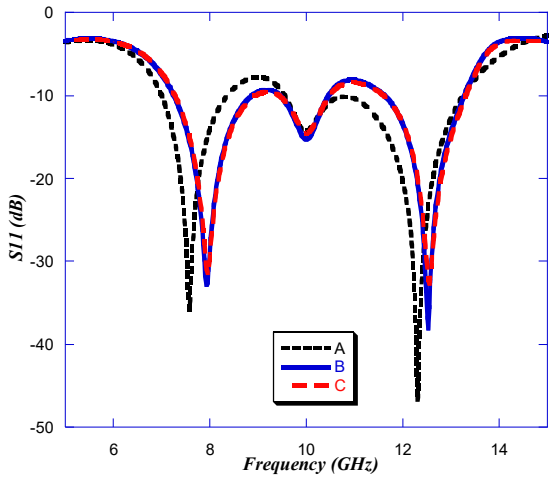

Figure 4.9: Simulated reflection coefficients (S_{11}) of the three antennas shown in Figure 4.8.

We observe that curves B and C are identical due to the symmetry of the dielectric structures when the rectangular resonator is positioned at either 120 or 240 degrees.

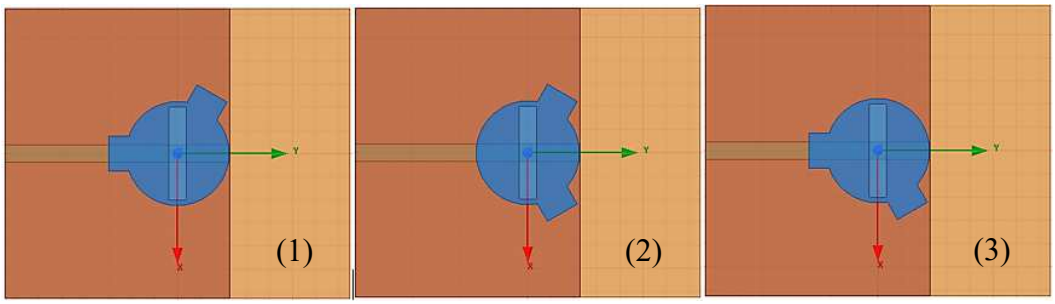

Figure 4.10: Top view of dielectric resonator antennas, the rotation effect of two rectangular joined with a cylindrical. (1) At 0^0 and 120^0. (2) At 120^0 and 240^0. (3) At 240^0 and 0^0.

Figure 4.9 illustrates the simulated reflection coefficient (S_{11}) of the three dielectric resonator antennas shown in figure 4.8. These antennas consist of a combination of a rectangular and a cylindrical shape, with the effect of their rotation (rotation angle 120^0). Antennas A, B, and C provide three frequency bands.

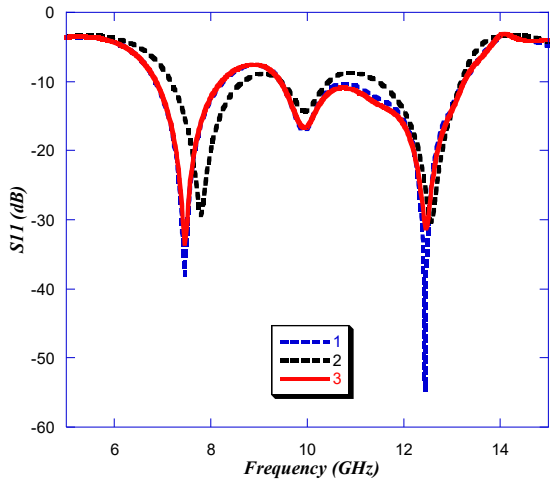

Figure 4.11: Simulated reflection coefficients (S_{11}) of the three antennas shown in Figure 4.10.

We see that curves 1 and 3 are identical due to the symmetry of the dielectric structures when the two rectangular resonators are positioned either at 0 and 120 degrees or at 240 and 0 degrees.

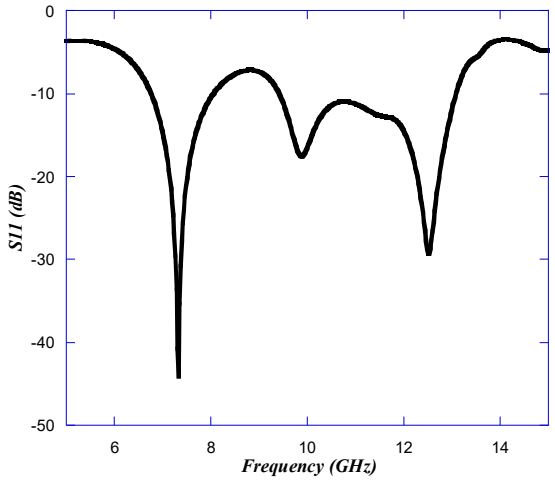

Figure 4.12: Simulated reflection coefficient (S_{11}) of the proposed dielectric resonator antenna.

Combining two or more dielectric material structures to create new resonant modes is an important technique for extending the bandwidth of dielectric resonator antennas.

The proposed antenna shown in Figure 4.12 exhibits dual-band and wideband characteristics. The lower band operates at 7.3 GHz, with a maximum gain of 4.6 dB, while the upper band has two

resonant frequencies at 9.88 and 12.5 GHz, with maximum gains of 4.7 and 4.8 dB, respectively. The 2D radiation pattern of the proposed antenna is presented in the Figure 4.13.

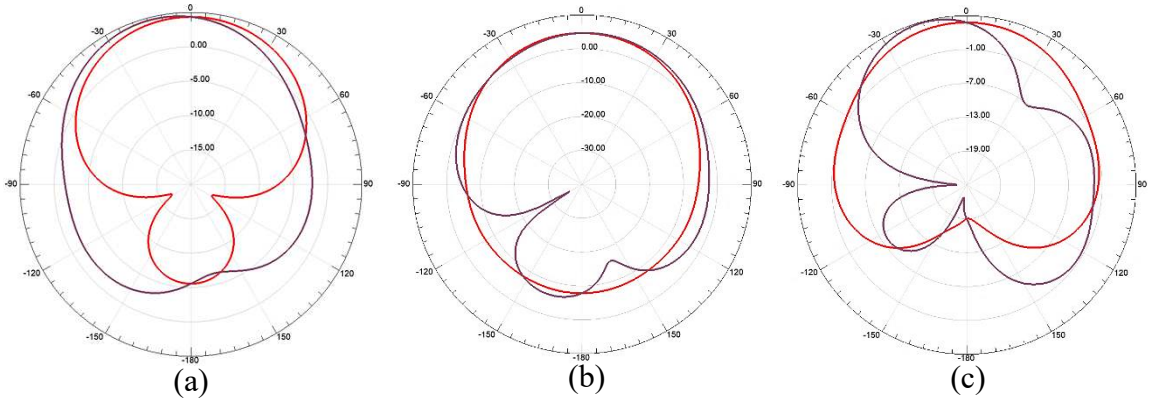

Figure 4.13: Simulated radiation patterns in XZ and YZ planes, (a) at 7.3 GHz. (b) at 9.88 GHz. (c) at 12.5 GHz.

4.4 Tri-band dielectric resonator antennas (TBDRAs)

In this type, we present a study of six dielectric resonator antennas, each consisting of four identical, adjacent rectangular resonators. Initially, a single sample of composite materials is applied to all of the rectangular resonators, followed by another sample applied to all of them. Next, two different composite material samples are used, with each sample applied to opposite rectangular resonators, which are then rotated by 45 degrees.

4.4.1 Antenna structure and geomerty

The dielectric structure consists of four identical adjacent rectangular resonators placed at the center of the aperture, as shown in Figure 4.14. Two dielectric materials based on binary composites ($RE - BaTiO_3$) are used, with dielectric constants of 9.5179 (brown) and 11.88 (blue) and loss tangent values of 0.0217 and 0.005, respectively. These resonators are mounted on FR-4 substrate with $\varepsilon_{sub} = 4.4$, $\tan\delta = 0.02$, and dimensions $Ls * Ws * T = 30 * 25 * 0.8\, mm^3$.
The antenna is excited by a 50 Ω microstrip feed line beneath the substrate, while an aperture coupling slot is etched at the center of the ground plane, which is positioned above the substrate.

Table 4.5: The optimal dimensions of the proposed antenna.

Parameter	Value (mm)	parameter	Value (mm)
La	7.5	Lf	19
Wa	1.5	Wf	1.5
Ld	8	h	10
Wd	4		

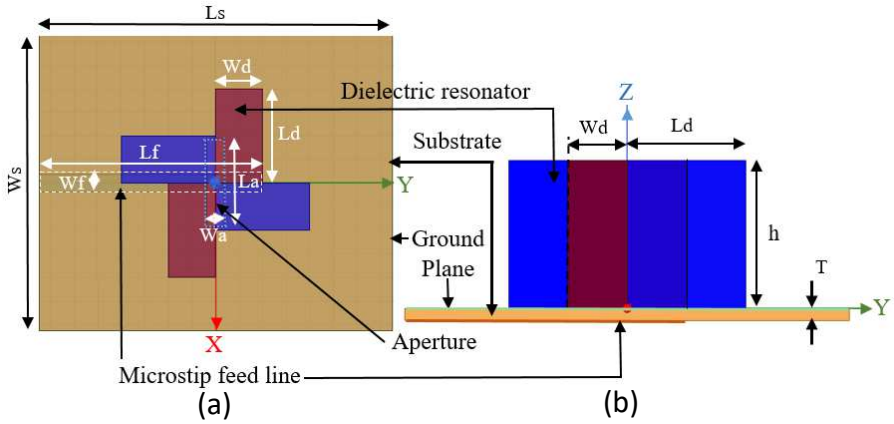

Figure 4.14: The proposed dielectric resonator antenna (a) Top view (b) Side view, with dimensions shown.

4.4.2 Results analysis and discussion

We study different dielectric resonator antennas using two samples of the binary composite mixture ($RE - BaTiO_3$) with the following volume fractions: the first sample, consisting of 60% of RE and 40% of $BaTiO_3$, is represented by the brown color, and the second sample, containing 50% of RE and 50% of $BaTiO_3$, is represented by the blue color in Figure 4.14. The aim is to observe their effect on the reflection coefficient (S_{11}), bandwidth ($S_{11} \leq -10dB$), and radiation pattern.

A- Effect of a single sample of composite materials

We applied a single sample of composite materials to all rectangular.

Figure 4.16 illustrates the simulated reflection coefficients (S_{11}) for antennas A and B. The results demonstrate that each antenna achieves three-band operation.

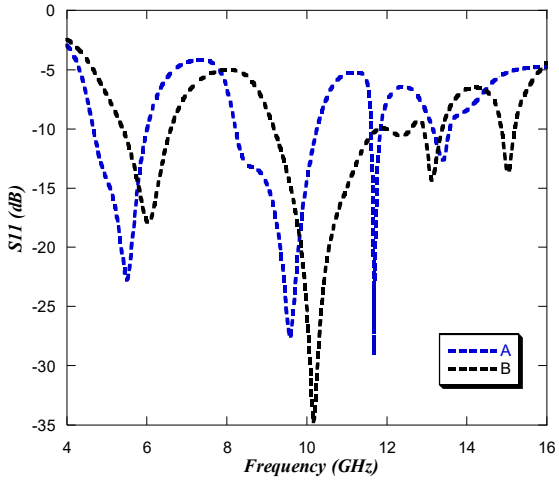

Figure 4.15: Simulated reflection coefficients (S_{11}) of the two antennas with volume fractions of (A) (50%-50%) and (B) (60%-40%) of ($RE - BaTiO_3$) composite.

B- Effect of two samples of composite materials

In this case, we applied two samples, each sample of composite materials to both opposite rectangular.

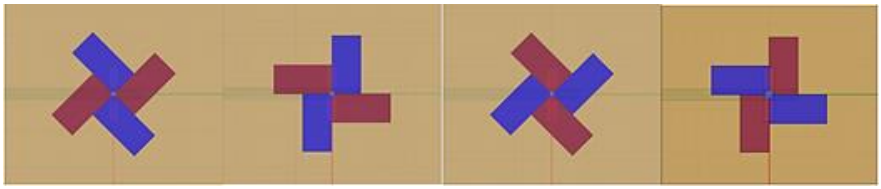

Figure 4.16: Top view of the dielectric resonator antennas, with rotation effect for all rectangular (1) at 45^0, (2) at 90^0, (3) at 135^0 and (4) at 180^0.

We observed that antenna number 4, shown in Figure 4.17, exhibits better performance than the other antennas. It can efficiently transmit and receive signals across three resonant frequency bands. This improvement can be attributed to the multi-structure configuration, the use of two dielectric materials, and their specific positioning.

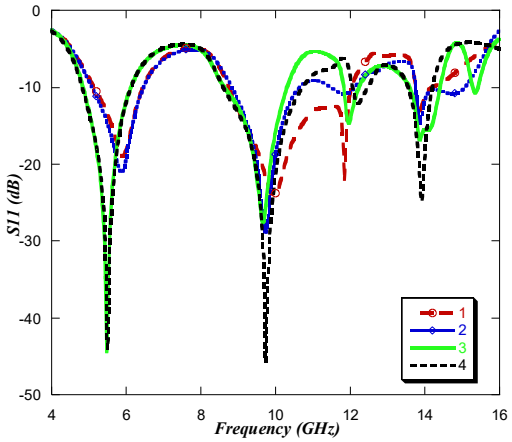

Figure 4.17: Simulated reflection coefficients (S_{11}) of the four antennas shown in Figure 4.16.

The obtained results are presented in terms of reflection coefficients (S_{11}), electric field distributions, and radiation patterns.

The proposed antenna, identified as antenna number 4 and shown in Figure 4.17, exhibits three operating bands. The resonant frequencies of these bands are as follows: the lower band operates at 5.47 GHz with a maximum gain of 3.6 dB, the middle band operates at 9.72 GHz with a maximum gain of 6.8 dB, and the upper band operates at 13.89 GHz with a maximum gain of 6.6 dB.

Figure 4.18 presents the simulated radiation patterns at resonant frequencies, showing that the antenna exhibits a wide radiation field covering approximately half of the area and is mainly linearly polarized.

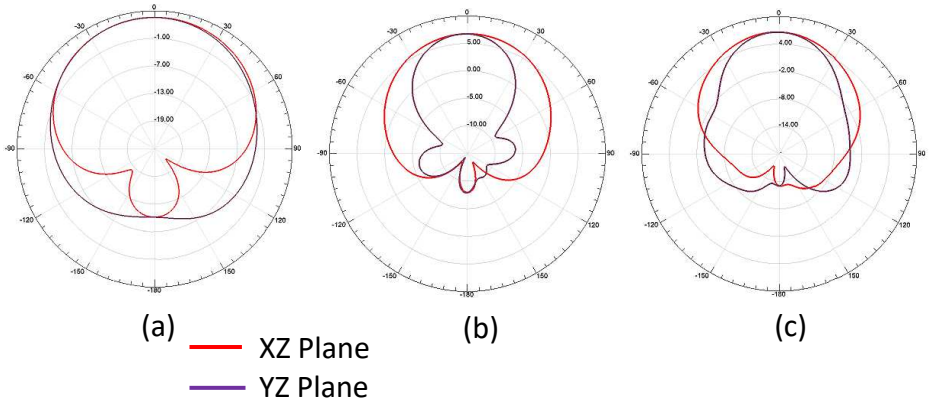

Figure 4.18: Simulated radiation patterns in XZ and YZ planes, (a) at 5.47 GHz, (b) at 9.72 GHz, and (c) at 13.89 GHz.

According to the sketches of the electric field distributions of the different modes of a single rectangular resonator given in [8,9]. The electric field distributions within the rectangular resonators depicted in Table IV.6, in the XY, XZ, and YZ planes, clearly indicate the appearance of $TE_{\delta 11}$, $TE_{\delta 21}$, and $TE_{\delta 13}$ modes, which correspond to the resonant frequencies 5.47, 9.72, and 13.89 GHz, respectively.

Table 4.6: The electric field distributions in the XY, XZ, and YZ planes at the resonant frequencies 5.47, 9.72 and 13.89 GHz.

Frequency (GHz)	XY plane	XZ plane	YZ plane
5.47	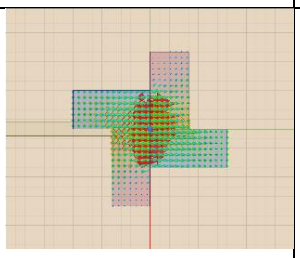	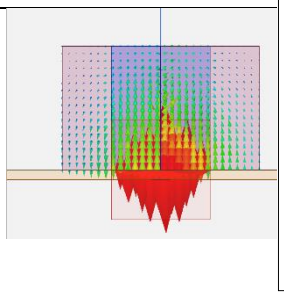	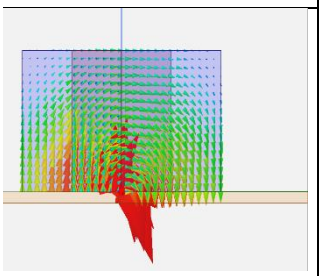
9.72	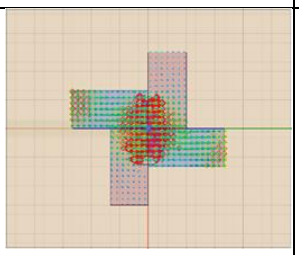	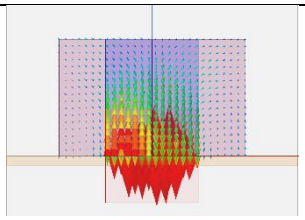	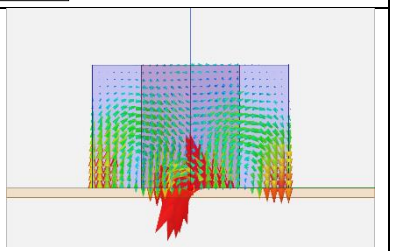
13.89	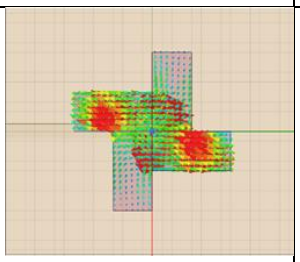	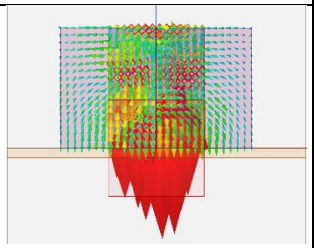	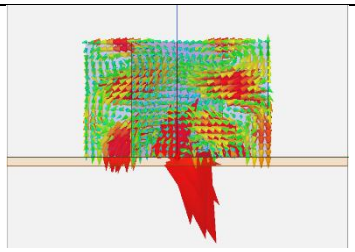

4.5 Hybrid shaped dielectric resonator antennas (HSDRAs)

In this type, we have done a study of hybrid dielectric resonator antennas, using a single dielectric material sample, which is a binary composite of (60% of RE and 40% of $BaTiO_3$). Nine structures of hybrid-shaped dielectric resonator antennas are studied.

4.5.1 Proposed antenna geometry and structure

The dielectric structure is two adjacent identical shapes. Each shape consists of a cylindrical and a rectangular, which are combined together with the same height, and are placed near the center of the aperture, are shown, in Figure 4.19, with a relative permittivity $\varepsilon' = 9.5179$ and a loss tangent of 0.0217. The dielectric structure is mounted on the FR-4 substrate with $\varepsilon'_s = 4.4$ and $tan\delta = 0.02$, with a thickness of $T = 0.8\,mm$, and a size of $L_S * W_S = 30 * 25\,mm^2$. The proposed antenna is fed by a 50 Ω micro strip feed line placed under the substrate, and two rectangular apertures of the same dimensions are placed asymmetrically above the substrate.

The optimum dimensions for the proposed antenna shown in Figure 4.18 are (all units in mm) $R = 4.9$, $h = 9$, $d = 0.2$, $L_a = 6.6$, $W_a = 3.5$, $L_f = 21$, $W_f = 1.5$, $W_r = 2.5$, $L_{stub1} = 7.9$, $L_{stub2} = 4.8$.

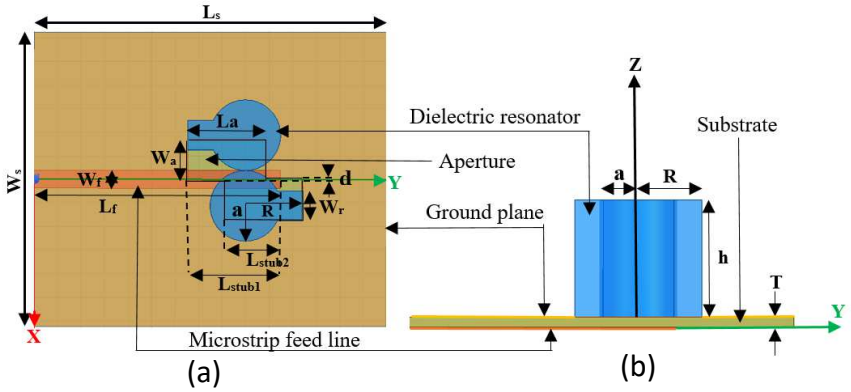

Figure 4.19: Proposed dielectric resonator antenna (a) Top view, (b) Side view, with parameters shown.

4.5.2 Results analysis and discussion

The simulated reflection coefficient (S_{11}) of the antenna presented in Figure 4.20, using two adjacent identical cylindrical dielectrics, gives a dual-band, a lower impedance bandwidth of 17.93%, covering the range from 6.09 to 7.29 GHz, the upper band possesses 66.86% relative bandwidth from 8.74 to 17.52 GHz.

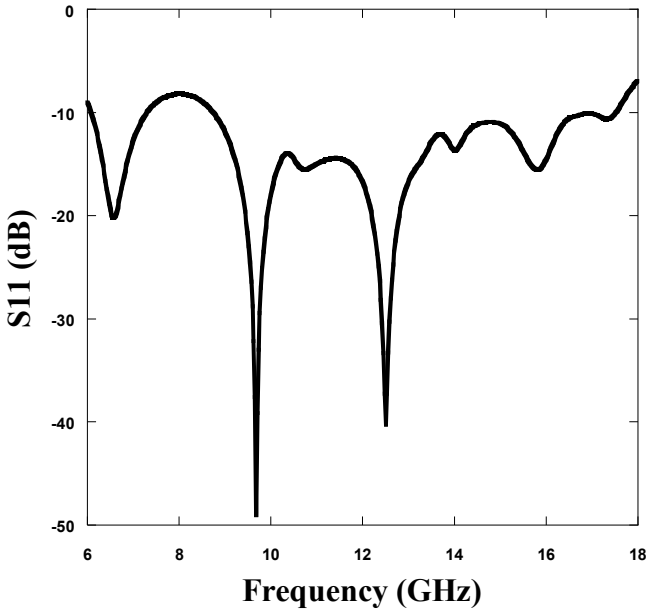

Figure 4.20: Simulated reflection coefficient (S_{11}) of dielectric resonator antenna, with two cylindrical only.

Figure 4.21 shows the four dielectric resonator antennas for different positions of a rectangular combined with a cylindrical and their effect on the reflection coefficient and bandwidth, which is depicted in Figure IV.22. Antennas A, C and D give three frequency bands and antenna B gives four frequency bands.

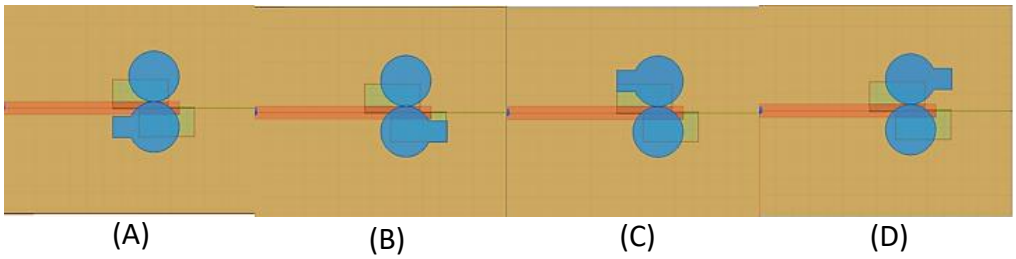

Figure 4.21: Top view of dielectric resonator antennas, position of the rectangular relative to the two cylindrical, (A) front left, (B) front right, (C) behind left, (D) behind right.

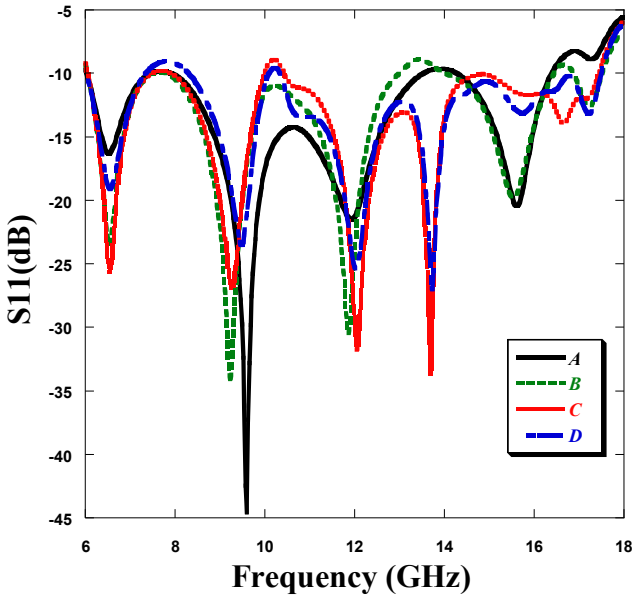

Figure 4.22: Simulated reflection coefficients (S_{11}) of four antennas shown in Figure 4.21.

Figure 4.23 shows the four dielectric resonator antennas for different positions of two rectangular combined with two cylindrical and their effect on the reflection coefficient and bandwidth, which is depicted in Figure 4.24. Antenna 1 operates in a single frequency band from 6.02 to 16.42 GHz. Antenna 2 operates in three frequency bands, antenna 3 works in dual band and antenna 4 presents our prototype. It is clearly visible the advantage of this compound structure of dielectric resonator.

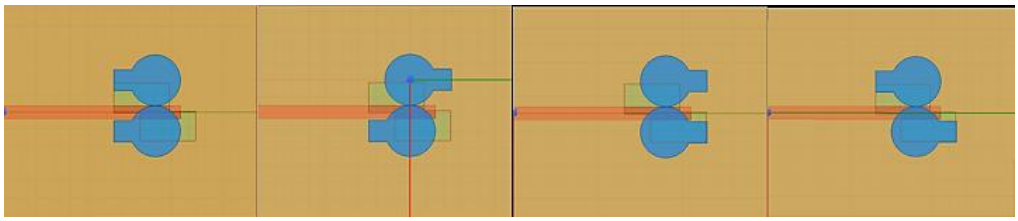

(1) (2) (3) (4)

Figure 4.23: Dielectric resonator antennas visible from above, position of the two rectangular relative to the two cylindrical, (1) both on the left, (2) one in front left and one in behind right, (3) both on the right, (4) one in front right and the other behind left**.**

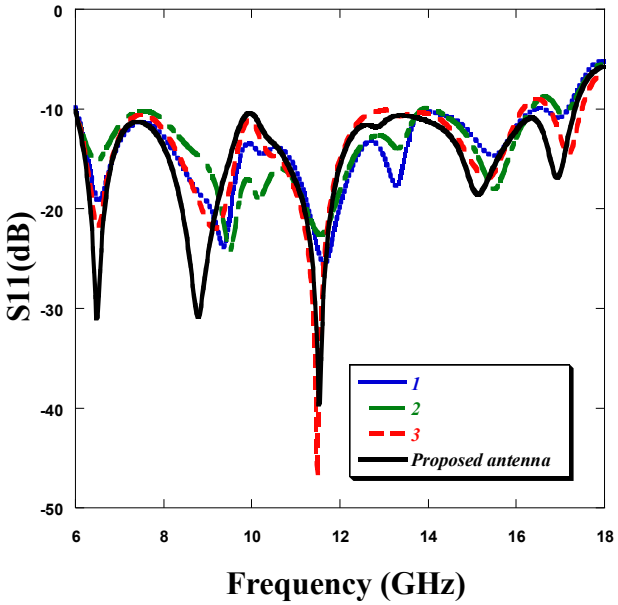

Figure 4.24: Simulated reflection coefficients (S_{11}) of four antennas shown in Figure 4.23.

By adding two rectangular to the two cylindrical as shown in Figure 4.19, appears other resonant frequencies and extends the bandwidth up to 97%. This structure of dielectric resonators has an important effect on the frequency. The creation of other resonance modes is also another important technique for extending the DRA bandwidth.

Using the coupling technique by an aperture formed by two rectangular slots with a large size and their offset positions. When combined with the hybrid shaped dielectric resonators shown in Figure 4.19 (the proposed antenna) generates orthogonal modes, that give rise to the dual-band circularly polarized (AR less than 3 dB), the lower band from 9.62 to 10.14 GHz and the upper band from 16.74 to 16.94 GHz shown in Figure 4.25.

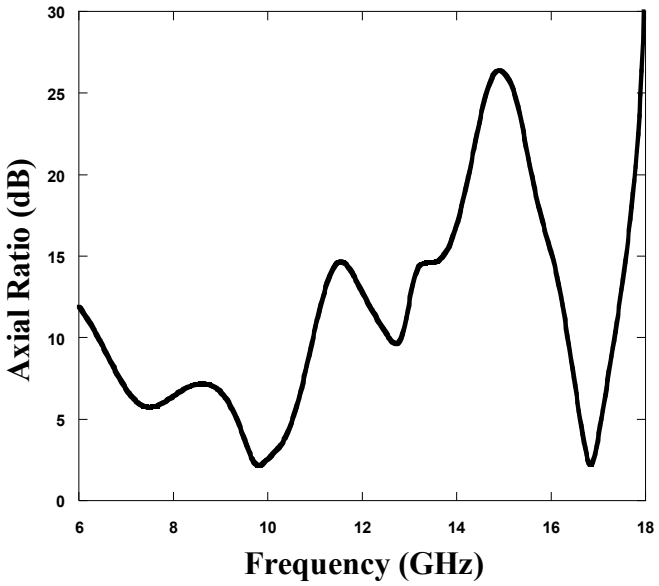

Figure 4.25: Simulated axial ratio at ($\theta = 0^{o}$) vs frequency.

The proposed antenna operates at ultra-wideband that covers the frequency band from 6 to 17.32 GHz, it has five resonance frequencies at 6.48, 8.8, 11.53, 15.14 and 16.92 GHz with maximum gains of 3.2, 4.94, 5.5, 5.52 and 3.3 dB respectively, as shown in Figure 4.26.

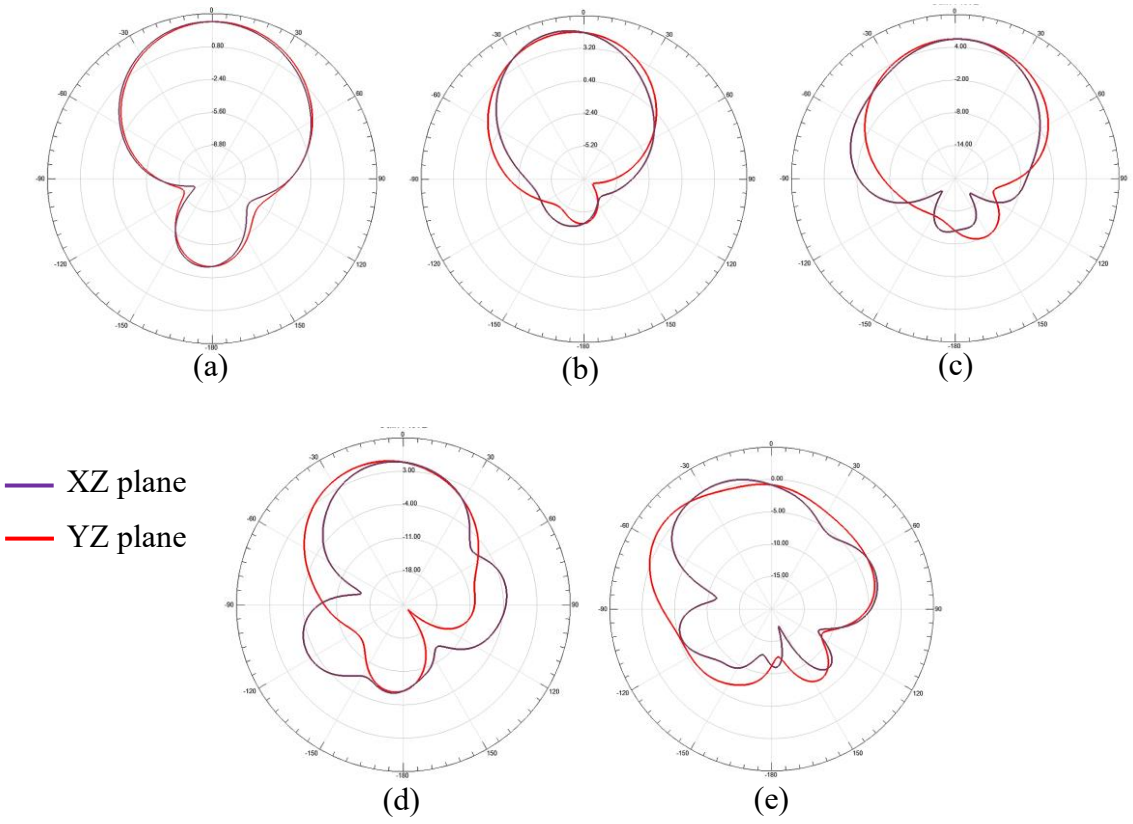

Figure IV.26: Simulated radiation patterns in XZ and YZ planes, (a) at 6.48 GHz. (b) at 8.8 GHz. (c) at 11.53 GHz. (d) at 15.14 GHz and (e) at 16.92 GHz.

To better estimate our proposed hybrid shaped dielectric resonator antenna, a comparison with previous studies in the literature is reported in the following table.

Table 4.7: Comparison between the hybrid shaped dielectric resonator antenna and previously published papers.

Reference, year	Antenna size (mm^3)	Dielectric resonator shape	Bandwidth (GHz)	BW (%)	Gain (dBi)
7, 2017	30 × 25 × 9.8	Two cylindrical	5.9–7.32/8.72–15	21/53	12
10, 2018	50 × 31 × 7.1	Ring	3.3–8.2	85.21	3
11, 2019	50 × 40 × 4.8	0M shaped	3.8–9.05	81.71	7.68
12, 2020	30 × 20 × 4.496	Perforated cylindrical	12.2–27.1	75.8	5.65
13, 2022	30 × 20 × 3.813	Stair shape half cylindrical	11.96–22.46	61.01	4.885
14, 2023	40 × 30 × 8.5	Rectangular	3.38–10.71	104	7.23
This work	30 × 25 × 9.8	Hybrid shaped	6–17.32	97	5.52

In particular, very good performances compared with the results of these references.

4.6 Conclusion

In this chapter, we studied four types of dielectric resonator antennas made from composite materials ($RE - BaTiO_3$) with low permittivity and low loss tangent.

In the first type, three antenna models were obtained based on their frequency bands: antennas operating in a single frequency band, dual-band antennas, and antennas covering three frequency bands. These antennas achieved peak gains ranging from 3.68 to 8.15 dB. Furthermore, the appearance of the three fundamental modes $HEM_{11\delta}$, $TE_{01\delta}$, and $TM_{01\delta}$, was observed, corresponding to an increase in the resonant frequency. These antennas operate over a frequency range covering the X-band (8 to 12.4 GHz), Ku-band (12.4 to 18 GHz), K-band (18 to 26 GHz), and Ka-band (26 to 40 GHz), making them suitable for satellite communication and 5th-generation (5G) applications.

The second type of antennas, the proposed antenna design, provides a dual-band. The first band exhibits an impedance bandwidth of 17.29%, covering the range from 6.76 to 8.04 GHz in the lower band. The second band is wide, with a relative bandwidth of 32.38% from 9.42 to 13.06 GHz in the upper band, with a peak gain of 5.85 dB. These frequency bands are suitable for utilization in radar systems (X-band radar) and satellite communication.

For the third type of antennas, the proposed design exhibits tri-band operation. The lower band covers the frequency range from 4.82 to 6.11 GHz, the middle band extends from 8.61 to 10.70 GHz, and the upper band covers the range from 13.54 to 14.19 GHz, achieving a maximum gain of 6.8 dB. The simulation results demonstrate the potential of this antenna for applications in the 5–6 GHz frequency band used by IEEE 802.11 standards and 5.8 GHz RFID systems in the SHF band, as well as at 10.5 GHz for police radar and in the 13.75–14 GHz range for fixed-satellite service (FSS) uplinks (earth-to-satellite).

For the fourth type of antennas, the proposed design offers ultra-wideband, with a relative bandwidth of 97%, covering the range from 6 to 17.32 GHz. It also exhibits a dual-band circular polarization, with the lower band extending from 9.62 to 10.14 GHz and the upper band from 16.74 to 16.94 GHz. The obtained findings cover parts of the C-band (4–8 GHz), X-band (8–12 GHz), and Ku-band (12–18 GHz), which are widely used in telecommunications, radar, and satellite applications. In this study, we demonstrate the benefits of integrating two or more dielectric material structures and employing multiple permittivities within the same antenna to achieve optimal performance.

References

[1] S. Long, M. McAllister, and L. Shen, "The resonant cylindrical dielectric cavity antenna", *IEEE Transactions on Antennas and Propagation*, vol. 31, no. 3, pp. 406-412, 1983.

[2] K. M. Luk and K. W. Leung, "*Dielectric Resonator Antennas*", Research Studies Press ltd, Baldock, Hertfordshire, England, 2003.

[3] Abolfazl Azari, Anja Skrivervik, Hadi Aliakbarian, and Ramezan Ali Sadeghzadeh, "A Super Wideband Dual-Polarized Vivaldi Antenna for 5G mmWave Applications", *IEEE Access,* vol. 11, pp. 80761-80768, 2023.

[4] Jie-Er Zhang, Qinfang Zhang, Wei Qin, Wen-Wen Yang, and Jian-Xin Chen, "Compact and Broadband Substrate Integrated Dielectric Resonator Antenna Suitable for 5G Millimeter-Wave Communications", *IEEE Open Journal of Antennas and Propagation*, vol. 4, pp. 982-989, 2023.

[5] L.X. Cui, X.H. Ding, W.W. Yang, L. Guo, L.H. Zhou, and J.X. Chen, "Communication Compact Dual-Band Hybrid Dielectric Resonator Antenna for 5G Millimeter-Wave Applications", *IEEE Transactions on Antennas and Propagation*, vol. 71, no. 1, pp. 1005-1010, 2023.

[6] A. H. Majeed, A. S. Abdullah, F. Elmegri, K. H. Sayidmarie, R. A. Abd-Alhameed, and J. M. Noras, "Aperture-coupled asymmetric dielectric resonators antenna for wideband applications", *IEEE Antennas and Wireless Propagation Letters*, vol. 13, pp. 927-930, 2014.

[7] C.E. Zebiri, M. Lashab, D. Sayad, I.T.E. Elfergani, K.H. Sayidmarie, F. Benabdelaziz, R. A. Abd-Alhameed, J. Rodriguez, and J.M. Noras, "Offset aperture-coupled double-cylinder dielectric resonator antenna with extended wideband", *IEEE Transactions on Antennas and Propagation*, vol. 65, no. 10, pp. 5617-5622, 2017.

[8] A. Petosa, S. Thirakoune, "Rectangular dielectric resonator antennas with enhanced gain", *IEEE Transactions on Antennas and Propagation*, vol. 59, no. 4, pp. 1385-1389, 2011.

[9] A. Petosa, "*Dielectric Resonator Antenna Handbook*", Norwood MA, USA: Artech House, 2007.

[10] G. Das, A. Sharma, and R. K. Gangwar, "Wideband self-complementary hybrid ring dielectric resonator antenna for MIMO applications", *IET Microwave, antenna & propagation*, vol. 12, no. 1, pp. 108-114, 2018.

[11] S. Kumar Yadav, A. Kaur, and R. Khanna, "An ultra-wideband 'OM' shaped DRA with a defected ground structure and dual polarization properties for 4G/5G wireless communications", *International Journal of RF Microwave Computer Aided Engineering*, vol. 30, e22327, 2020.

[12] I. Ahmad Zubir et al., "A low-profile hybrid multi-permittivity dielectric resonator antenna with perforated structure for Ku and K band applications", *IEEE Access*, 8, 151219, 2020.

[13] M. F. M. Omar, I. A. Zubir, S. Kamal, and M. F. Ain, "A tri-hybrid of Al2O3-SiO2-MgZrO3 stair shaped half-cylindrical dielectric resonator antenna (SHCDRA) for wideband wireless communication systems", *Engineering Science and Technology an International journal*, vol. 35, 101187, 2022.

[14] S. Huda, A. Saha, and A. Karmakar, "Ultra wideband (UWB) dielectric resonator antenna using fractal-inspired feeding mechanism" Int. J. Commun. Syst., 36, e5519 (2023).

Conclusion

Conclusion

The thesis investigated new techniques for designing and characterizing dielectric resonator antennas (DRAs) that utilize microwave dielectric materials. It focused on binary composite materials made from barium titanate ($BaTiO_3$) and epoxy resin (RE) to develop high-performance dielectric resonator antennas.

The research work presented in this thesis is divided into two parts. The first part focuses on the experimental investigation of the dielectric properties of the binary composite (RE -$BaTiO_3$), which was fabricated under ambient conditions (room temperature and atmospheric pressure) and characterized using the time domain spectroscopy method. The influence of barium titanate on the dielectric behavior was examined for several epoxy resin volume fractions ranging from 50% to 100% in steps of 5%.

The experimental results revealed the effect of barium titanate on both the dielectric constant and the dielectric losses of binary composites. The real part of the relative complex permittivity of the composite material increases significantly with increasing barium titanate content (volume fraction). The values of dielectric loss tangent show a strong change in behavior at a volume fraction of 20% of barium titanate, the same behavior was observed in the conductivity profile. The resonant frequency of the composite has also been studied, and it has been observed that this parameter tends to low frequency values as the concentration of the barium titanate increases.

The experimental results, presented in terms of the properties of the binary composites, demonstrate that the materials exhibit low permittivity values and low dielectric losses. These findings are expected to contribute to the development of new materials suitable for potential applications in the telecommunications domain, specifically focusing on microelectronic components utilized in telecommunication systems, such as resonators, substrates, cavities, PTC devices, filters, antennas, wave absorbers, pulse-generating devices, multilayer ceramic capacitors, ultrasonic transducers, and sensors.

In the second part, the design of four types of antennas and the study of their parameters are considered, using the properties of dielectric materials that we obtained experimentally. These antennas were designed, simulated, and optimized using the electromagnetic software Ansys HFSS.

The first type of designed antennas is based on the effect of dielectric properties of the binary composite materials on the performance parameters of the cylindrical dielectric resonator antennas

using all composite material samples. Three sets of designed antennas were obtained and classified by the number of frequency bands in which they operate: single-band, dual-band, and triple-band. Peak gain values between 3.68 and 8.15 dB are achieved.

In the second type of antennas, the influence of compound structures on the parameters of the dielectric resonator antennas was investigated. The structure consists of a combination of four dielectric resonator shapes: three identical rectangular joined with one cylindrical resonator of the same height, fabricated from a single binary composite sample composed of 60% of RE and 40% of $BaTiO_3$. This antenna provides a dual-band, with one of the bands being wideband, and achieves a peak gain of 5.85 dB.

In the third type of antennas, the influence of the multiple composite material structures on the parameters of the dielectric resonator antennas was studied. The structure consists of four adjacent, identical rectangular resonators, using two binary composite samples: one composed of 60% of RE and 40% of $BaTiO_3$, and the other composed of 50% of RE and 50% of $BaTiO_3$. The proposed antenna provides three frequency bands, with a maximum gain of 6.8 dB.

For the fourth type of antennas, the effect of combining several shapes (a hybrid structure) on the parameters of the dielectric resonator antenna was studied using a composite material sample composed of 60% of RE and 40% of $BaTiO_3$. The structure is coupled through an aperture formed by two large rectangular slots with offset positions. The antenna offers ultra-wideband, with a relative bandwidth of 97%, a dual-band circularly polarized, and a maximum gain of 5.52 dB. The proposed antenna is a good candidate for advanced communication systems that requires a high data rates.

The results in this thesis emphasize the attractive features of DRAs in applications requiring ultra-wideband performance with circular polarization or multiband operation in the frequency range corresponding to centimeter wavelengths, making them highly suitable for modern wireless communication systems.

Future prospective research on dielectric resonator antennas is expected to focus on optimizing their performance for next-generation wireless communication systems. Emphasis will be placed on improving parameters such as bandwidth, gain, efficiency, and miniaturization while maintaining compact and cost-effective designs. Studies will likely explore innovative materials, including ternary and quaternary dielectric materials with a wide range of enhanced properties.

List of publications

1. Journals

1. R. Chelghoum, Z. Messai, A. Brahimi, N. Bourouba, J.P. Martinez Jiménez and F. Bouttout, **"Dielectric Behavior Characterization of RE/BaTiO3 Using Time Domain Spec-troscopy: Application on high performance dielectric resonator antennas"**, *ECS Journal Solid State Science and Technology*, vol. 13, 043018, 2024.
   Link: https://iopscience.iop.org/article/10.1149/2162-8777/ad3f4e
2. A. Brahimi, R. Chelghoum, J.P. Martinez Jiménez, N. Bourouba, N. Bouzit, A. Yousfi, O. Saidani, and R. Zerrougui, " **A Compact Cylindrical Dielectric Resonator Antenna Using (RE-BaTiO3-ZnO) for 5G Wireless Communication Applications**", *ECS Journal Solid State Science and Technology*, vol. 14, 073003, 2025.
   Link: https://iopscience.iop.org/article/10.1149/2162-8777/ade915

2. International conferences

1. Rachid Chelghoum and Zitouni Messai, **"Compact Dual-Band And Wideband Aperture-Coupled Dielectric Resonator Antenna"**, *First International Conference on Advances in Electrical and Computer Engineering (ICAECE'2023)*, May 15-16, 2023, Larbi Tebessi University-Tebessa, Algeria.
   Link: https://books.aijr.org/index.php/press/catalog/book/163/chapter/2879
2. Rachid Chelghoum, Zitouni Messai and Abdelhalim Brahimi, **"Tri-band aperture-coupled dielectric resonator antenna using (RE-BaTiO3) composite materials"**, *The 6th International Conference on Electrical Engineering and Control Applications (ICEECA'24)*, November 19-21, 2024, University of Abbes Laghrour, Khenchela, Algeria.
   Link: https://link.springer.com/chapter/10.1007/978-981-95-1109-9_32